REPUBLIC OF NORTH MACEDONIA
SS. CYRIL AND METHODIUS UNIVERSITY IN SKOPJE
FACULTY OF CIVIL ENGINEERING

THERMO-MECHANICAL BEHAVIOUR AND STRUCTURAL DESIGN OF GEOTHERMALLY ACTIVE PILES

Doctoral thesis

Mentor
Prof. Dr. Josif Josifovski

Candidate
MSc. Guxim Rrudhani, grad. Civil Eng.

Skopje, January 2025

SS. CYRIL AND METHODIUS UNIVERSITY IN SKOPJE

FACULTY OF CIVIL ENGINEERING

THERMO-MECHANICAL BEHAVIOUR AND STRUCTURAL DESIGN OF GEOTHERMALLY ACTIVE PILES

Doctoral thesis

Mentor
Prof. Dr. Josif Josifovski

Candidate
MSc. Guxim Rrudhani, grad. Civil Eng.

Skopje, January 2025

Doctoral student:
GUXIM MUSTAFA RRUDHANI

Topic:
THERMO-MECHANICAL BEHAVIOUR AND STRUCTURAL DESIGN OF GEOTHERMALLY ACTIVE PILES

Mentor:
Ph.D. JOSIF JOSIFOVSKI,
Faculty of Civil Engineering Skopje
Ss. Cyril and Methodius University of Skopje

Defense Panel:

Prof. Dr. Todorka Samardzioska, Chair
Faculty of Civil Engineering Skopje
University Ss. Cyril and Methodius in Skopje

Ph.D. Hussein Mroueh, Member
Faculty of Civil Engineering
University of Lille

Ph.D. Florim Grajçevci
Faculty of Civil Engineering
University of Prishtina

Ph.D. Vlatko Sheshov
Institute of Earthquake Engineering and Engineering Seismology - IZIIS
Ss. Cyril and Methodius University in Skopje

Ph.D. Jovan Papic
Faculty of Civil Engineering Skopje
Ss. Cyril and Methodius University in Skopje

Scientific area:
ENERGY GEOSTRUCTURES

ABSTRACT

Geothermally active piles represent an efficient solution for integrating shallow geothermal energy systems with structural foundations, enabling sustainable heating and cooling of buildings while simultaneously carrying structural loads. Despite their increasing application, the design of energy piles remains challenging due to the complex interaction between mechanical loading and temperature-induced effects within the pile-soil system. In particular, thermal expansion and contraction of the pile may significantly influence stress transfer mechanisms, vertical displacements, and serviceability performance. This doctoral thesis investigates the thermo-mechanical behavior of geothermally active piles through a combined program of laboratory-scale experimental testing and numerical modeling. A controlled physical model of a single pile embedded in soil was subjected to staged mechanical loading, heating, cooling, combined thermo-mechanical actions, and recovery phases. The experimental setup was comprehensively instrumented to measure temperature evolution in the pile and surrounding soil, pile head vertical displacements, pore water pressure, total soil pressure, suction, and axial strains within the pile. The experimental results demonstrate that thermal effects are strongly concentrated near the pile shaft, with temperature variations attenuating rapidly in the surrounding soil. Heating induces pile expansion that can partially counteract mechanically induced settlements, whereas cooling leads to pile contraction and increased settlement. The most unfavorable displacement response was observed under combined mechanical loading and cooling, highlighting the importance of considering thermo-mechanical coupling in design. Recovery phases revealed partial reversibility of deformations, indicating stress redistribution within the pile-soil system. A finite element numerical model was developed to replicate the experimental conditions and loading sequence. The numerical simulations reproduced the measured temperature evolution and pile head displacements with close agreement across all loading phases, confirming the capability of the modelling approach to capture the governing thermo-mechanical mechanisms. Minor discrepancies were attributed to modelling idealizations and experimental uncertainties. Based on the validated experimental and numerical findings, the thesis provides design-oriented recommendations for geothermally active piles, including the treatment of thermal actions as variable loads, proposed partial and combination factors, and correlation assumptions between mechanical and thermal actions. The results contribute to improved understanding of energy pile behavior and support the rational integration of geothermal functionality into foundation engineering practice.

Keywords: Geothermally active piles; Thermo-mechanical behavior; Laboratory-scale experimental testing; Numerical modelling; Pile-soil interaction

Dedication

I dedicate this work to my parents, Mother Shpresa and Father Mustafa, whose support and help knew no bounds in terms of time and circumstances. Everything I have achieved is your merit. With love and gratitude!

Acknowledgement

My deepest appreciation goes to the professors of the doctoral program at the Faculty of Civil Engineering, Ss. Cyril and Methodius University in Skopje, as well as to the faculty management and entire staff, whose support has been instrumental throughout my doctoral journey.

I want to express my sincere gratitude to my mentor, Prof. Dr. Sc. Josif Josifovski, for his continuous guidance, constructive feedback, and invaluable support throughout my academic journey at the Faculty of Civil Engineering Skopje and during the development of this dissertation.

I would also like to extend my sincere thanks to the Department of Geotechnics, the Geotechnical Laboratory, and the Central Laboratory of the Faculty of Civil Engineering for their technical support and assistance throughout the experimental phase of this research.

I want to express my heartfelt gratitude to the Faculty of Civil Engineering at the University of Prishtina for their continuous encouragement and support. Special thanks are extended to the faculty management, academic staff, and colleagues whose collaboration, motivation, and assistance have greatly contributed to the successful realization of this research work.

Finally, I am deeply grateful to my family for their unwavering love, patience, and encouragement throughout every stage of this journey. Their constant support has been the foundation upon which this achievement was built.

Declaration

Herein, I provide my personal statement for the originality of the stated doctoral dissertation, that I duly provide a reference to the quoted sources, and that this paper is not used in any other university study for acquiring other knowledge.

Table of Contents

LIST OF SYMBOLS

λ	Thermal conductivity
Q	Heat amount
c	Heat capacity
c_s	Heat capacity of the solid phase
c_w	Heat capacity of the water
c_α	Heat capacity of the air
x_s	Solid material composition
x_w	Water contained in the pores
x_α	The percentage of pores filled with air
n	Porosity
S	Saturation degree
α	Thermal diffusion
ρ	Soil density
f_t	Tensile strength of the reinforcing steel
f_y	Yield strength of the reinforcing steel
ΔT	Temperature change
α_{EP}	Linear thermal conductivity coefficient
ΔL	Length change
L	Length
ε_f^{th}	Deformation caused by thermal actions
ψ_0	Combination factor
ψ_1	Frequent value factor
ψ_2	Quasi-permanent value factor
F_{cd}	Design axial load
R_{cd}	Design resistance value
R_{ck}	Characteristic resistance value
F_d	Design value of the mechanical action
γ_F	Partial factor
γ_t	Partial factor

ψ	Partial factor
F_{rep}	Representative value of the considered actions
F_k	Characteristic value of the considered actions
G_{rep}	Single permanent action
Q_{rep}	Single variable action
γ_G	Partial factor for permanent load
γ_Q	Partial factor for variable load
R_{sk}	Characteristic value of shaft friction resistance
R_{bk}	Characteristic value of base resistance
γ_s	Shaft friction resistance partial factor
γ_b	Base resistance partial factor
R_{cm}	Measured resistance value
ξ	Correlation factor
A_c	Cross-sectional area of the pile
$A_{r,\min}$	Minimum longitudinal reinforcement area

LIST OF FIGURES

LIST OF TABLES

Page left intentionally blank

1. INTRODUCTION

1.1. Motivation

In the context of global efforts to transition towards low-carbon energy systems and mitigate the impacts of climate change, the construction industry is increasingly required to adopt sustainable technologies and practices. Buildings account for a significant portion of total energy consumption worldwide, with a large share attributed to heating and cooling demands. As urban populations continue to grow and energy needs escalate, the pressure to find innovative solutions that reduce both operational energy use and greenhouse gas emissions has intensified. One such promising solution is the implementation of shallow geothermal systems, which harness the near-surface thermal energy of the ground for heating and cooling purposes.

Among the various shallow geothermal technologies, energy geostructures, particularly geothermally active piles, stand out as a dual-purpose innovation. These structural elements serve both as load-bearing foundations and as heat exchangers embedded within the ground. By integrating geothermal heat exchange systems directly into building foundations, energy piles provide an efficient and space-saving alternative to traditional borehole heat exchangers. This integration reduces the need for additional land, lowers installation costs, and aligns with the principle of multi-functionality in sustainable infrastructure design.

Despite their growing use in Europe, Asia, and North America, the widespread application of geothermally active piles is still limited by several factors. One of the primary challenges is the absence of standardized design methodologies that account for the complex interplay between thermal and mechanical loads. Unlike conventional piles, energy piles are subjected to daily and seasonal temperature fluctuations due to heat exchange with the ground. These thermal variations induce additional strains and stresses in the pile, which can potentially affect its structural integrity and serviceability. Traditional pile design methods, which assume isothermal conditions, may not adequately capture this coupled behavior, thereby raising concerns about long-term performance and safety.

Furthermore, existing guidelines and codes provide limited direction on how to incorporate thermal effects into geotechnical and structural analysis. Most designs rely heavily on simplified assumptions or empirical models that may not reflect the actual behavior of energy piles under real-world conditions. As a result, engineers face uncertainties in predicting settlements, axial and bending stresses, and overall system performance when deploying geothermally active piles. This knowledge gap undermines confidence in technology, especially for critical structures where conservative designs dominate.

Another motivational factor stems from the growing interest in hybrid and adaptive energy systems within the built environment. The integration of energy piles into building energy systems aligns with smart city concepts and supports efforts to decarbonize the heating and cooling sector. When combined with heat pump systems, energy piles offer a renewable and reliable energy source with low operating costs and minimal environmental impact. Their potential contribution to net-zero energy buildings and green certification schemes further increases their attractiveness to developers, engineers, and policymakers.

Yet, for geothermally active piles to become a mainstream solution, a deeper understanding of their thermo-mechanical behavior is essential. This includes understanding how factors such as pile geometry, material properties, soil conditions, load history, and thermal cycles interact to influence performance. High-quality experimental data and advanced numerical models are critical for developing design frameworks that ensure safety, durability, and efficiency.

In this context, the present doctoral research is motivated by the need to bridge the gap between the theoretical understanding, experimental observation, and practical design of geothermally active piles. By investigating the behavior of a single lab-scale energy pile under operational and mechanical loading conditions, this study seeks to provide valuable insights into the coupled thermal and structural phenomena that govern its performance. The outcomes aim not only to inform design practices but also to support the broader adoption of energy geostructures as a sustainable solution in Civil Engineering.

1.2. Objectives

This research aims to consolidate and critically synthesize the current state of knowledge on the thermo-mechanical behavior of energy piles, with particular emphasis on how observed mechanisms are represented in design and numerical modelling. By reviewing recent experimental, field, and modelling studies, the work establishes what is currently well understood (e.g., thermally induced axial strain development, redistribution of shaft resistance, pile-soil interaction under cyclic temperature variation) and, more importantly, identifies the remaining uncertainties that still limit confident prediction in engineering practice. The key gaps targeted in this thesis relate to the coupled nature of thermal and mechanical processes, the role of boundary conditions and soil state on cyclic response, the limited availability of well-instrumented physical datasets for validation, and the translation of research findings into safety format design choices suitable for structural design codes and geotechnical verification.

To address the gaps, a controlled laboratory-scale physical model test is designed and executed on a single geothermally active pile embedded in soil. The experimental programme is structured to reproduce the essential mechanisms governing thermo-mechanical pile behavior while retaining a high degree of control over loading paths and boundary conditions. A comprehensive instrumentation scheme is implemented to capture both thermal and mechanical response, including temperature in the pile and surrounding soil, pile head vertical displacement, and, where applicable to the experimental setup, additional measurements such as pore pressure, total pressure, suction, and strain response within the pile. This approach provides a coherent dataset capable of revealing the coupled response across loading stages and supporting direct comparison with numerical simulations.

The thermal response of the model pile is evaluated through analysis of the temperature evolution measured along the pile and within the surrounding soil. The heating and cooling cycles are applied to reproduce system operational conditions, enabling the thesis to characterize the transient and quasi-steady thermal behavior, quantify temperature gradients between the pile and soil, and assess the development of thermal equilibrium over time. A key objective is to define the extent and evolution of the thermal influence zone during cyclic operation, including how far temperature disturbances propagate into the ground and how this

zone differs between heating and cooling phases under the adopted boundary conditions and test durations.

In parallel, the mechanical response is evaluated by analyzing the vertical displacements of the pile head and their evolution through sequential loading stages. The testing programme distinguishes between purely mechanical loading, purely thermal loading, and combined thermo-mechanical loading to isolate the contribution of each action and to capture interaction effects. Special attention is given to the displacement trends during heating and cooling, the modification of settlement due to thermally induced pile expansion or contraction, and the extent of recovery upon unloading or thermal reversal. This objective will provide clear experimental evidence of how operational thermal cycles influence serviceability behavior, especially when superimposed on sustained mechanical loads.

Building on the experimental results, the thesis develops and validates a numerical modelling approach that can reproduce the observed thermo-mechanical response with acceptable accuracy. The modelling strategy is formulated to mirror the staged nature of the laboratory programme, enabling direct comparison of temperature evolution and pile-head displacement for each phase. Validation focuses on matching both the magnitude and time-dependence of the response, while also identifying which model components and parameters most strongly govern agreement, such as thermal properties of soil and pile, heat transfer assumptions at the pile-soil interface, stiffness and constitutive representation of the soil, interface conditions, drainage and pore pressure response where relevant, and boundary effects associated with laboratory scaling.

Finally, the work translates the experimental and numerical findings into design implications and practical recommendations for energy geostructures. The thesis recommends how thermal actions should be combined with mechanical loads in design situations, considering both serviceability and ultimate limit state perspectives, and recognizing the variable nature of thermal loading under operational cycles. In addition, it proposes recommendations for safety-format parameters, including partial factor selection and correlation assumptions for variable thermal actions, intending to support consistent and transparent verification within code-based design frameworks and improve the reliability of thermo-mechanical design procedures for geothermally active piles.

1.3. Thesis outline

This doctoral dissertation is structured to provide a coherent and design-oriented investigation of the thermo-mechanical behavior of geothermally active piles. The thesis progresses logically from the identification of research motivation and gaps in current knowledge, through theoretical background, experimental investigation, and numerical modelling, to synthesis of results and formulation of conclusions relevant to engineering design practice.

The introduction explains why the study is important and outlines its research goals, focusing on the growing use of energy geostructures in sustainable construction. A critical literature review is included, addressing existing analytical formulations, experimental investigations, and numerical approaches for energy piles. The text highlights challenges such as limited methods for modeling coupled thermo-mechanical behavior, few reliable experimental datasets

for validation, and unclear guidelines for integrating thermal effects into current geotechnical and structural design practices.

The theoretical background of geothermal energy utilization and energy-active structures is then presented, outlining the principles of shallow geothermal systems and their integration into civil engineering structures. Energy geostructures are introduced as multifunctional elements, with emphasis on geothermally active piles, while the energy walls and tunnels are discussed to provide a broader technological context.

The fundamental thermo-mechanical behavior of geothermally active piles is examined in detail, addressing temperature distribution along the pile, thermally induced vertical and radial deformations, shear stress redistribution, and variations in vertical stress under mechanical, thermal, and combined loading. The influence of system constraints and degrees of freedom is discussed, together with geotechnical challenges related to temperature variations in both the soil and the pile, which are directly relevant for serviceability performance and long-term operation.

Design considerations for geothermally active piles are subsequently addressed through a behavior-based framework. Relevant design parameters are introduced, including site conditions, material properties, pile and pipe characteristics, heat transfer fluid properties, and soil behavior. Behavior-based design methodologies are presented, followed by verification procedures for Ultimate Limit State and Serviceability Limit State conditions. The focus is on how thermal actions, like variable loads, interact with mechanical forces and affect displacement-controlled design.

The experimental programme forms the core of the research and is presented through the description of a laboratory-scale physical model of a single geothermally active pile. The experimental setup, materials, and testing procedures are detailed, establishing controlled boundary conditions for investigating coupled thermo-mechanical behavior. A comprehensive instrumentation scheme is adopted to capture temperature evolution in the pile and surrounding soil, pile head vertical displacements, pore pressure, total pressure, suction, and strain development within the pile.

The experimental results are presented and analyzed with a focus on the thermal response of the pile-soil system and the corresponding mechanical response under mechanical, thermal, and combined loading stages. The results provide direct insight into thermally induced displacement mechanisms, interaction effects, and recovery behavior, forming the experimental basis for subsequent modelling and design interpretation.

A numerical model is developed to replicate experimental results. Material models, material properties, and staged construction and loading phases are defined to reflect the laboratory conditions. Numerical outputs related to temperature distribution and vertical displacements are compared directly with experimental measurements, allowing assessment of model accuracy and identification of key parameters governing agreement.

The results and discussion section integrates experimental observations and numerical predictions. The governing thermo-mechanical mechanisms are identified, and the implications of modelling assumptions and parameter selection are critically examined. The findings are

discussed in relation to existing literature, highlighting the contribution of the present study to improved understanding of energy pile behavior under variable thermal loading.

The final chapter synthesizes the principal findings of the thesis and formulates design-oriented conclusions. Based on experimental and numerical evidence, recommendations are provided for the treatment of thermal actions in the design of geothermally active piles, including guidance on load combinations, correlation between mechanical and thermal actions, and the application of partial factors within a safety format consistent with Eurocode principles. The limitations of the present study are acknowledged, and directions for future research are proposed, particularly regarding long-term cyclic behavior, field-scale validation, and further refinement of design methodologies for energy geostructures.

1.4. Literature review

Geothermally active piles, also known as energy piles, combine the load-bearing function of deep foundations with the thermal exchange role of ground-source heat pump systems. Their integration into buildings reduces the need for separate geothermal boreholes, saving space and construction costs. As energy efficiency becomes increasingly critical in civil infrastructure, these systems offer a promising solution for heating and cooling demands. However, their design introduces complex coupled interactions between temperature, stress, and soil behavior, which are not adequately addressed by conventional pile design frameworks. Laboratory-scale testing has proven essential in investigating these interactions under controlled conditions and in validating analytical or numerical models. [1] [2]

An energy pile typically consists of a reinforced concrete or steel pile embedded with closed-loop heat exchanger pipes. These circulate a heat transfer fluid that exchanges energy with the surrounding soil. This dual-purpose design requires engineers to understand not only the structural response of the pile but also the impact of thermal cycling on deformation, stress redistribution, and long-term behavior. [3]

As the pile undergoes heating or cooling, it experiences thermal expansion or contraction. When mechanical loads are also present, such as axial forces from the superstructure, the combination of effects may lead to significant strain, movement, or stress concentration in the pile and adjacent soil. These complex behaviors necessitate experimental studies and coupled modelling strategies. [4]

Thermo-mechanical coupling in energy piles has been extensively studied over the last two decades. Laloui and Vöossoughi (2006) developed early analytical and numerical frameworks to model pile response under thermal loads, capturing key interactions between temperature and stress. [4] Bourne-Webb et al. (2009) conducted one of the first full-scale field tests in London, monitoring thermal effects on pile head displacements, stress redistribution, and axial strain. [5] Amatya et al. (2012) proposed a design framework based on thermo-hydro-mechanical behavior, emphasizing the significance of incorporating soil-structure interaction in numerical models. [3]

Although field studies offer real-world insights, they are logistically complex and site dependent. For this reason, controlled laboratory tests have become a crucial method for

systematically investigating how energy piles respond to cyclic thermal and mechanical loading.

Laboratory tests allow for a precise study of thermo-mechanical interactions under well-defined conditions. Their main purposes include:

- Investigating temperature-induced strain and displacement behavior,
- Validating numerical models using reproducible data,
- Assessing the influence of soil type, pile material, and load conditions on performance,
- Studying cyclic thermal effects that simulate seasonal use patterns. [2] [6]

Modern lab setups enable accurate measurement of thermal gradients, stress-strain development, and long-term plastic deformations, information that is often difficult to obtain in full-scale field studies.

Typical laboratory experiments use small-scale pile models installed in soil-filled containers. Heating is applied using embedded electrical cables or circulated fluid, and axial loading is imposed using dead weights or actuators. Data acquisition systems capture:

- Temperature distribution via thermocouples,
- Axial strain using strain gauges or fiber-optic sensors,
- Displacement using LVDTs,
- Load using calibrated load cells. [6] [7]

Stewart and McCartney (2014) developed a setup that applied cyclic heating and cooling to piles embedded in clay, revealing the accumulation of plastic strain and irrecoverable displacement over multiple cycles. [7] Murphy et al. (2015) conducted similar studies in sand beds and observed that heating generally resulted in pile uplift, while cooling led to settlement due to thermal contraction. [6] Abuel-Naga et al. (2015) tested energy piles in soft clay and highlighted how heating affected shaft resistance and pore water pressures. [8]

These and similar studies demonstrate that temperature variation leads to real, measurable structural and geotechnical consequences, even in small-scale models.

Table 1. Key observations from laboratory research

Authors	Pile type	Soil type	Key findings
Laloui & Vöossoughi (2006)	Concrete	Clay	Developed a coupled thermo-mechanical model; significant axial strains observed
Bourne-Webb et al. (2009)	Concrete	Sandy silt	Full-scale field test: temperature-induced axial stresses and displacements
Murphy et al. (2015)	Steel	Sand	Upward pile movement during heating; settlement during cooling
Stewart & McCartney (2014)	Concrete	Clay	Cyclic thermal loading caused plastic deformations; confinement effects were noted.
Abuel-Naga et al. (2015)	Steel	Soft clay	Shaft resistance affected by thermal cycles; pore pressure changes observed
Rafai et al. (2025)	Concrete	Sand	Long-term thermal cycles affect pile performance; the importance of considering cyclic loads.

Each study reinforces the conclusion that thermo-mechanical coupling cannot be ignored in energy pile design, particularly under repeated or seasonal temperature cycles.

Despite meaningful progress, several gaps remain:

- Lack of standardization in laboratory testing setups makes it difficult to compare findings or establish uniform design parameters. [2]
- Limited long-term testing, with most studies focusing on short durations. High-cycle experiments are needed to replicate annual heating and cooling patterns. [8]
- Boundary condition effects in soil containers, which do not fully replicate in-situ stress fields or hydrothermal gradients. [1]
- Most studies use uniform sands or clays, but actual sites often have stratified or mixed soils, raising concerns about soil type sensitivity.
- Lack of integration with renewable energy systems, such as hybrid testing setups combining energy piles with solar panels or thermal storage, remains rare. [1]

Energy piles are increasingly being used as sustainable solutions for integrated building support and energy exchange. Laboratory-scale testing has proven essential in characterizing their behavior under combined thermal and mechanical loading. The reviewed literature demonstrates that thermal loads can cause significant deformation and stress changes that should be incorporated into the design. While field tests are informative, lab-scale studies offer a level of control and detail that supports improved modeling, interpretation, and ultimately, safer and more efficient implementation.

Further standardization of test protocols, combined with an expanded focus on long-term cyclic behavior and soil-structure interface phenomena, needs to be addressed.

2. GEOTHERMAL ENERGY AND ENERGY ACTIVE STRUCTURES

2.1. General

Usually, energy geostructures are made of reinforced concrete. The pipe system is fixed along the reinforcing cage. For more, the placement of the fixed pipe system with reinforcement is preferable to enable their sufficient protective layer inside the ground. [9]

a) b) c)

Figure 1. Pipe system installed through reinforcement cage of a) energy slab, b) energy pile, and c) energy tunnel segmental lining

Placing the pipe system together with the reinforcement cage in geothermal structures can be done in the factory or on-site. This second one is more common. For each pipe system used in these structures, locking valves and a manometer are placed at their heads. This enables the tube circuit to be at a constant pressure of 5 to 8 bar for integrity control. It is preferable to test the pressure of the fluid inside this pipe 24 hours after the concreting process. The pressure in the pipes is applied again before their exploitation begins. [9]

Further, fluid is pumped through electrically driven machines and is used as a thermal energy carrier for the operation of energy geostructures in most shallow, closed-loop geothermal systems. The pipes are usually made of high-density polyethylene with a diameter of approximately 10 to 40 mm and a thickness of their walls of 2 to 4 mm. [9]

a) b)

Figure 2. Pipes, a) Connection of pipe edges in energy piles, b) Pipes storage in a construction site

The heat transfer medium (i.e., the heat carrier fluid) in the pipes consists of water, water with antifreeze, or a saline solution. Water with antifreeze is usually used to lower the freezing point. The usual antifreeze additives that are used are based on ethylene glycol and propylene glycol. These additives are poisonous to humans and animals and, as such, should be treated with special care.

2.2. Energy geostructures

Several geostructures, including geothermal piles, retaining walls, and tunnels, have been used or are under investigation for use as heat exchangers with the ground. These structures, besides the mechanical (bearing) function, have a thermal function working as heat exchanger systems.

2.2.1. Geothermal piles

Geothermal piles represent structural elements of double use. The main use is structural. When a system of geothermal energy is installed, it takes the role of the energy pile. The heat from geothermal energy is transferred by a fluid that circulates in tubes, and later, a certain temperature is regulated by using heat pumps. Tubes for geothermal energy absorption are typically attached to the reinforcement cage and properly arranged to take heat from soil in the most optimal way.

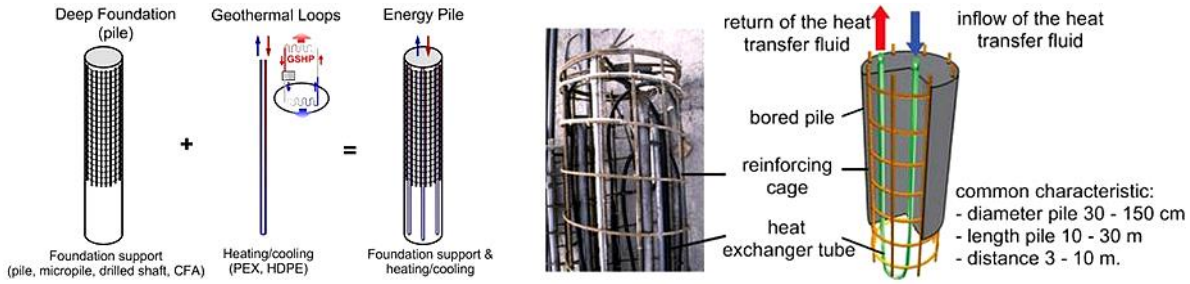

Figure 3. a) Energy pile (Guney, 2013), b) Typical energy pile arrangement (Laloui et al., 2013)

The relationship of the load transfer between the pile and the surrounding ground is essential to address the thermomechanical behavior of energy geostructure foundations. No matter how the energy pile is analyzed, in situ or in the laboratory, in both cases, they must be accompanied by numerical analysis, creating models in the software, and analyzing and comparing the output results. Very important parameters to evaluate the thermomechanical response of the pile during heating and cooling are the conditions of end constraints at the top and bottom of the pile [10].

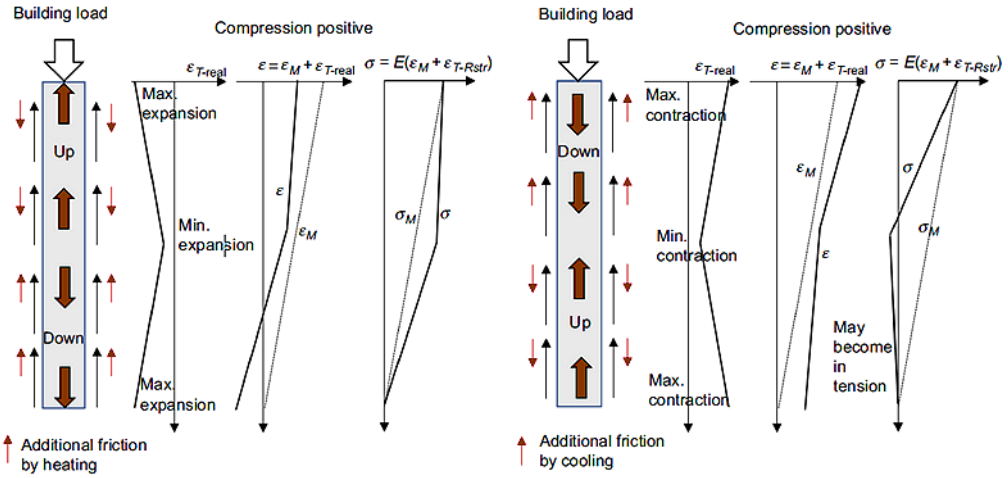

a) b)

Figure 4. Thermomechanical performance of friction pile. (a) Heating and (b) cooling [11]

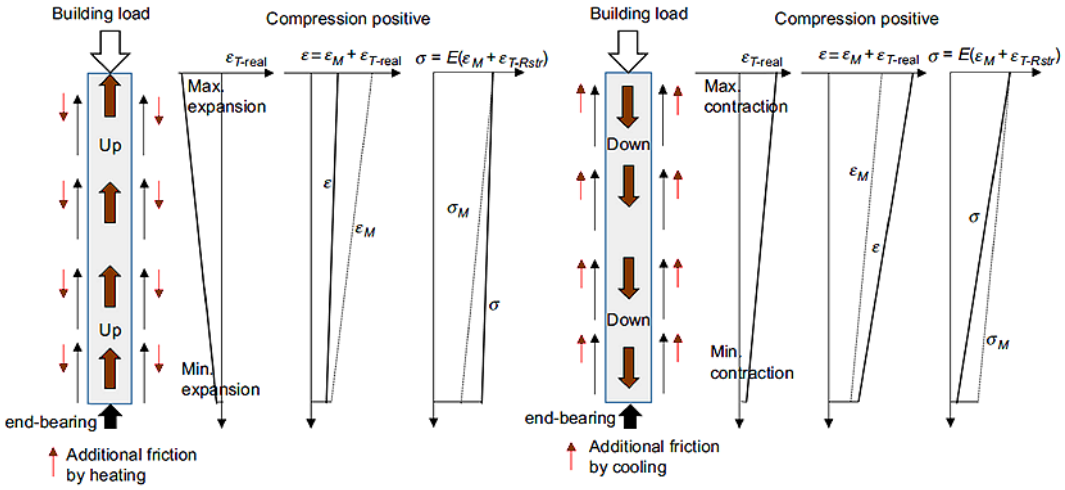

a) b)

Figure 5. Thermomechanical performance of end-bearing pile. (a) Heating and (b) cooling [11]

2.2.2. Energy walls

Compared to an energy pile system, potentially larger ground volume can be used for geothermal heat transfer in an energy wall system because of its larger structure. The pipes of the heat exchanger are fixed to the steel reinforcement cage, similar to an energy pile system. Usually, the position of the pipes within the concrete is close to the soil side, in order to reduce the thermal resistance of the concrete and, at the same time, to improve the overall thermal performance of the energy wall [12].

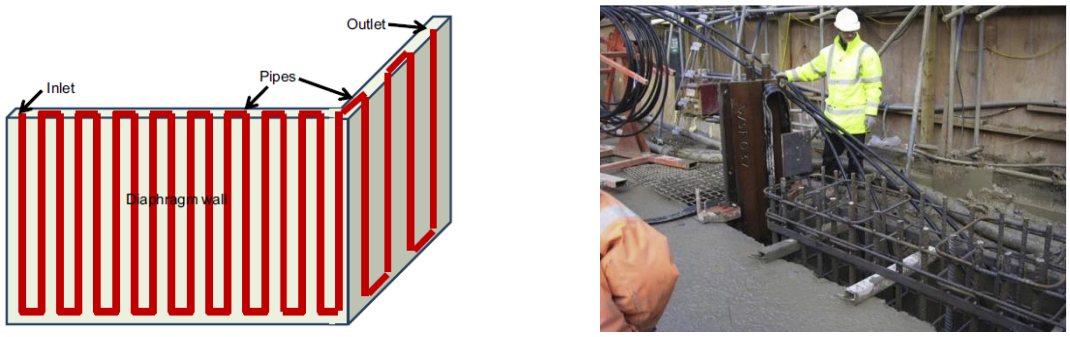

a) b)

Figure 6. a) A typical heat exchanger configuration in an energy wall, b) GSHP system in a diaphragm wall [11]

At the energy walls, there are two possible operating modes: both heating and cooling (Figure 7a) and heating only (Figure 7b).

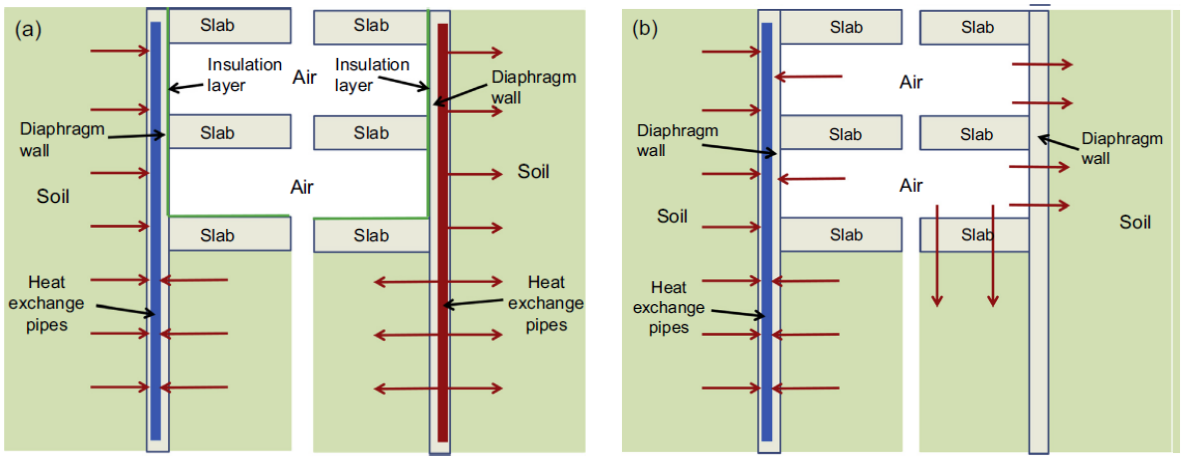

a) b)

Figure 7. Operating modes: a) Heating and cooling; b) Heating only [12]

In the case when pipes are embedded inside the wall, the temperature variation within the wall would induce additional bending movement inside the wall. So, the increased bending needs to be within the design bending moment envelope to ensure that the concrete structures do not deteriorate during their operation [13].

2.2.3. Energy tunnels

A large amount of heat can be provided by underground metro systems. The heat exchanger pipes are typically embedded in the tunnel linings to enable the tunnels to extract heat from the train operations for surrounding commercial and domestic needs. In the Figure 8 the concept of an energy tunnel system is presented. [14]

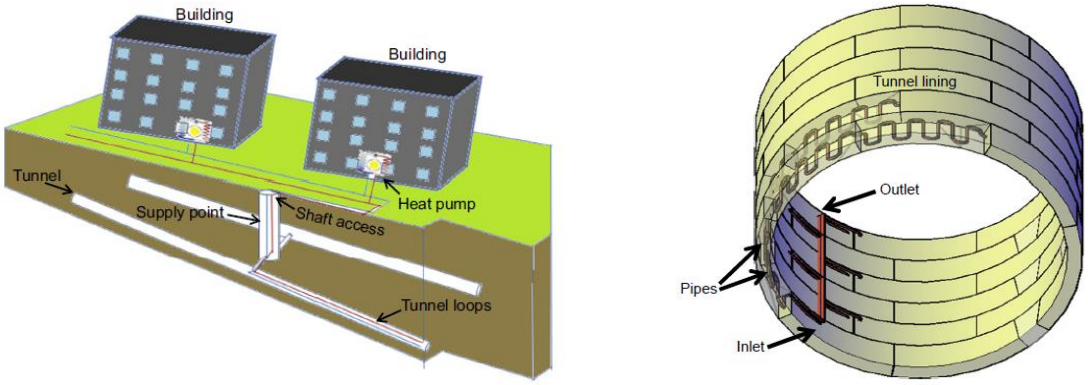

a) b)

Figure 8. a) Energy tunnel concept. b) Typical energy tunnel [11]

In most cases, for shield-driven tunnels, tunnel linings are pre-cased and installed on site. So, segmental lining with a pipe heat exchanger can be prepared in advance. The heat exchanger pipes are connected to the steel reinforcement cage of the tunnel linings (Figure 9a). Then, the ends of the pipes of each segment are connected to the ends of the next segments (Figure 9b). The tunnel construction process is not affected by this work, because the connecting work to the heat pump systems located above the ground is performed after the tunnel is constructed. [10]

a) b)

Figure 9. a) Pipes attached to a reinforcement cage, b) Pipe connections at the segmental joints. (Rehau and Zueblin) [11]

The effect of thermal expansion/contraction of the segments on the overall engineering performance of the tunnel is one of the most important design aspects to consider for an energy tunnel. It should be taken into consideration that all induced stresses caused by the temperature distribution within a segment are within the range of the design axial load and bending moment envelope of the tunnel lining. The local stresses at the joint sections need to be assessed because they may influence the water tightness of the lining as well as induce additional joint movements. In order to ensure structural integrity, the locations of heat exchange pipes within segments need to be decided carefully. Changes in the earth pressures applied to the tunnel can be induced by the expansion or shrinkage of the soil around the tunnel by temperature change (drying or freezing in extreme cases). This effect on the tunnel performance, as well as neighboring underground structures, needs to be assessed as well. [10]

3. THEORETICAL BACKGROUND

3.1. Thermo-mechanical behavior of geothermally active piles

The application of combined structural and thermal loads to geothermally active piles introduces a novel aspect to the mechanical response of these foundations, distinguishing them from conventional systems that are subjected solely to mechanical loading arising from their structural role. The interaction between heat transfer and material deformation results in thermal expansion and contraction within both the circuits and the surrounding soil, thereby altering the overall stress state. Therefore, investigating the effects of thermal loading, whether acting independently or in conjunction with mechanical loads, is essential for a comprehensive understanding of the thermo-mechanical behavior of an energy pile.

The materials composing energy geostructures, as well as the surrounding soils and rocks, are inherently heterogeneous. Nevertheless, in many practical analyses, an effective analytical approach allows these materials to be idealized as a continuous medium, often assumed to be homogeneous and isotropic. Such an approach is adopted in the present study for the subsequent interpretation of the thermo-mechanical behavior of energy piles.

Although in practice, piles rarely exhibit a perfectly cylindrical shape and the surrounding soil strata are seldom completely horizontal, the adopted assumptions considerably simplify the analysis of pile response under the considered conditions. These simplifications are taken into account in the subsequent improvements of the model.

Thermal and mechanical loading induce non-uniform variations in temperature, stress, strain, and displacement fields within and around energy piles (Abdelaziz and Ozudogru, 2016; Caulk et al., 2016; Rotta Loria and Laloui, 2017). In addition to analyzing the overall response of energy piles, it is also important to account for the inherently non-uniform nature of these fields. [9]

3.1.1. Temperature distribution along the pile

Significant temperature variations may develop within energy piles as a result of their geothermal operation. Under given boundary conditions, the magnitude of these temperature changes depends on the thermal power applied to the piles, as well as on the thermo-hydraulic properties of both the pile and the surrounding soil. For a specified thermal power input and thermal conductivity of the pile material, lower values of soil thermal conductivity and groundwater flow velocity lead to greater temperature variations within the pile. Moreover, variations in the boundary conditions at the ground surface can substantially influence the temperature field within the energy pile (Bidarmaghz et al., 2016), particularly in cases where the pile length is limited.

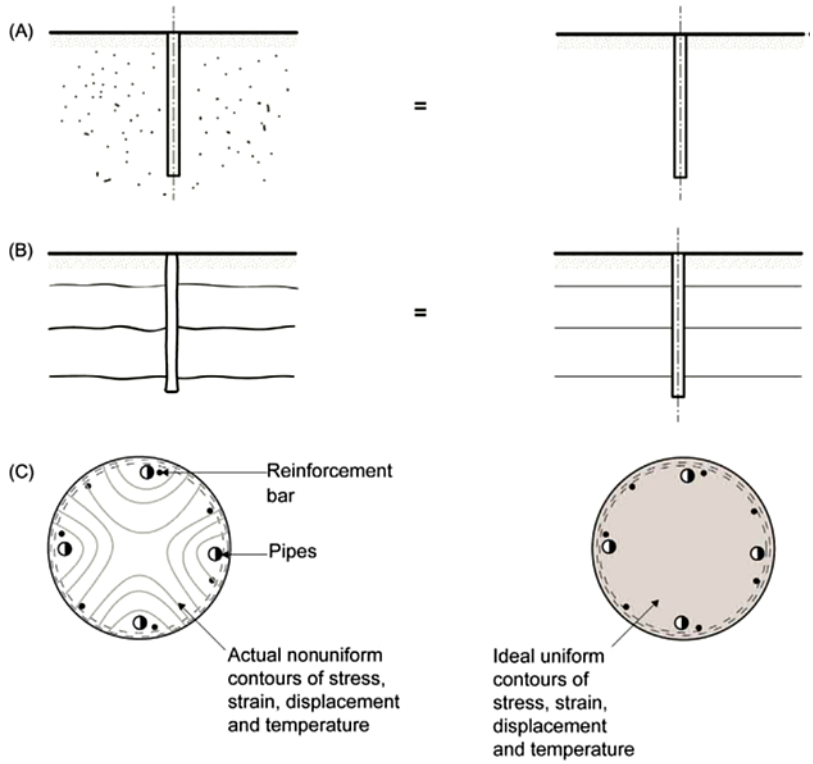

Figure 10. (A) Analytical approach for modeling non-homogeneous soil deposits; (B) approach for analyzing non-horizontal soil strata; and (C) idealized representation of stress, strain, displacement, and thermal fields within energy piles. [9]

Under typical operating conditions, the average temperature variations in energy piles can range from approximately $\Delta T = 15°C$ to $\Delta T = 30°C$. Figure 11 illustrates an example of temperature distribution along the pile length z for an energy pile that is free to expand vertically (Laloui et al., 2003a). In the analyzed case, heating the pile over 12 days resulted in an average temperature increase of $\Delta T = 22°C$ along its length.

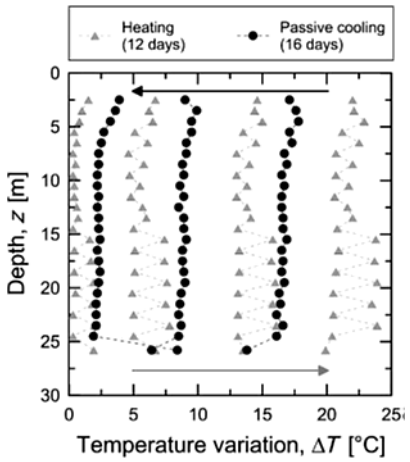

Figure 11. Temperature variations along the length of an energy pile during thermal cycles of heating and passive cooling. [15]

3.1.2. Thermal effects on vertical strain development

Thermal loads applied to energy piles induce elongation during heating and contraction during cooling. These thermally driven deformations are generally non-uniform along the pile length. Their development depends on the degree of restraint provided by both the surrounding soil and

the structural system. Specifically, the stiffer the soil in which the energy pile is embedded, the smaller the thermally induced deformations. The same principle applies to the structural elements connected to the pile head.

Typical values of average vertical strain induced by temperature variations in the range of $\Delta T = 15°C$ to $\Delta T = 30°C$ are approximately between $\Delta \varepsilon z = -100 \mu\varepsilon$ and $\Delta \varepsilon z = -250 \mu\varepsilon$. During the cooling phase, the opposite behavior is observed (Bourne-Webb et al., 2009). An example of thermally induced strain distribution along an energy pile that is free to expand vertically is shown in Figure 12, based on the results reported by Laloui et al. (2003). In this case, an average temperature increase of $\Delta T = 22°C$ along the pile length resulted in an average vertical strain of $\Delta \varepsilon z = -180 \mu\varepsilon$.

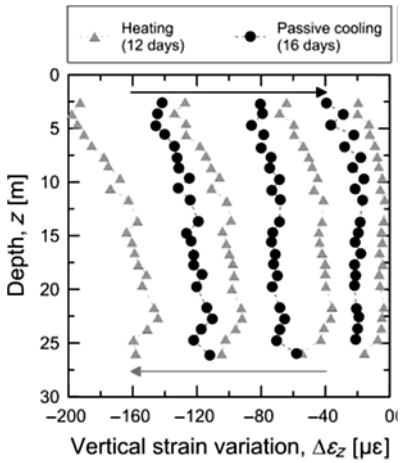

Figure 12. Vertical variations in dilation along the length of an energy pile during heating-cooling cycles. [15]

The vertical deformations observed in energy piles under thermal loading during heating are reversible, exhibiting thermoelastic behavior. This phenomenon was reported by Laloui et al. (2003) and is illustrated in Figure 13, which presents the evolution of vertical strain at various depths along the length of a floating energy pile that is free to expand vertically, under different applied temperature changes [15].

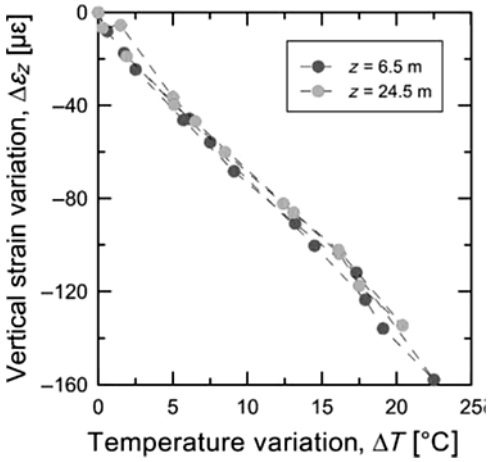

Figure 13. Development of thermal expansion in an energy pile following a heating-passive cooling cycle, at depths of z = 6.5 m (z/L = 0.25) and z = 24.5 m (z/L = 0.95). [15]

3.1.3. Radial deformations induced by thermal actions

In addition to the vertical deformations induced by thermal loading, radial deformations also develop. For the same temperature change applied to the energy piles, comparable magnitudes of vertical and radial strain may be observed. However, due to the distinct geometrical proportions characterizing the pile length and diameter, the resulting vertical and horizontal displacements differ significantly.

The observed variations in the radial deformation of energy piles can be attributed to a rebound effect (Mimouni and Laloui, 2015; Rotta Loria and Laloui, 2017). In other words, lateral contact between the energy pile and the surrounding ground is preserved after a complete thermal cycle. Figure 14 illustrates the evolution of radial deformation for an energy pile that is free to expand vertically (Laloui et al., 2006). In this example, the deformations do not return to their initial state at the end of the heating/cooling cycle, as the initial and final temperature values differ.

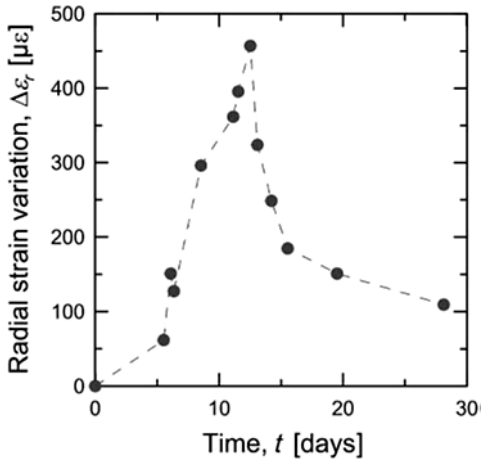

Figure 14. Evolution of radial dilation induced by thermal actions in an energy pile during a heating-passive cooling cycle. [4]

3.1.4. Vertical deformations induced by mechanical and thermal actions

The application of thermal actions to energy piles may result, in the ideal case, in a linear distribution of vertical displacements, whereas in more complex cases, a nonlinear distribution can develop, becoming increasingly pronounced with greater deformability and torsional effects of the pile (Rotta Loria et al., 2018). This assumption applies to both rigid and flexible piles, whether floating or end-bearing. In essence, heating causes an upward movement of the pile head, while cooling induces settlement. This behavior arises from the fact that thermal loading generates two regions within the pile that move in opposite directions relative to the so-called zero point of vertical displacement, located at a depth z (Laloui et al., 2003). The position of the zero point depends on the boundary conditions of the pile support (Mimouni and Laloui, 2014; Rotta Loria et al., 2015; Sutman et al., 2018). For an infinitely stiff foundation, the zero point coincides with the base, whereas for an infinitely stiff overlying plate, it is located at the pile head. In practice, the zero point lies along the pile shaft, closer to the location where the structural constraint is more pronounced.

In contrast to the previously described thermal behavior, the application of mechanical loads at the head of energy piles results in an approximately uniform distribution of vertical

displacements along the pile length, accompanied by a comparable distribution of shear stresses (Rotta Loria et al., 2018). Although this assumption is particularly relevant for the analysis of end-bearing piles with a predominantly frictional behavior, it is generally applicable to most pile types. Mechanical compression loads applied at the pile head induce settlements, whereas mechanical tension loads cause uplift. In practice, except in cases involving negative skin friction, mechanical loading typically produces displacements in a single direction, downwards under compression loads applied to the pile head.

From the above discussion, it can be concluded that the combined action of mechanical and thermal loads during cooling leads to an increase in pile head settlement, assuming a downward-acting mechanical load. Conversely, the combined effect of mechanical and thermal loads during heating reduces the magnitude of pile head displacement under the same loading conditions and even induces uplift of the foundation. This secondary phenomenon results from the opposing influence of downward mechanical loads and upward thermal expansion effects on the pile head behavior. Such conditions are typically observed in piles subjected to relatively low mechanical loads but significant thermal loads during heating. However, the described influence of thermal loading does not apply to energy piles embedded in normally consolidated soils, where thermal collapse of the soil matrix causes pile head settlement rather than uplift, irrespective of the pile's thermal expansion.

3.1.5. Shear stress variations induced by mechanical and thermal loads

As a result of the deformations induced by thermal actions in energy piles, shear stresses are mobilized along the pile shaft in the opposite direction to the pile settlement to maintain equilibrium with the surrounding soil. These stresses develop with respect to a so-called zero point of shear stress, generally located at a different depth z from that of the zero point of vertical displacement (Rotta Loria et al., 2018). The magnitude of the mobilized shear stresses depends primarily on the degree of soil confinement.

An example of mobilized bending and shear stresses induced by thermal actions along the length of a vertically free-to-deform energy pile subjected to heating is shown in Figure 15, based on the results of Laloui et al. (2003). Depending on the degree of constraint, different magnitudes of shear stress develop in correspondence with the various soil layers. Negative shear stresses are generated above the zero point under thermal heating (in the upper soil layers A1, A2, and B). In contrast, positive shear stresses occur below the zero point (in the deeper soil layer C). The opposite stress distribution is observed under thermal cooling conditions (Bourne-Webb et al., 2009).

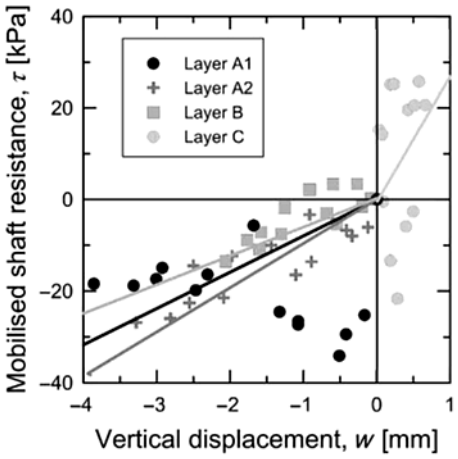

Figure 15. Mobilized frictional resistance induced by thermal heating along the length of an energy pile with a vertically free head. [15]

Under the action of mechanical loading, positive shear stresses develop near the head of the energy pile to maintain equilibrium with the surrounding soil. An example of the magnitude of mobilized frictional resistance resulting from mechanical loading applied to an energy pile restrained at the head by a plate is shown in Figure 16, based on the results of Laloui et al. (2003). Along the pile length, different values of mobilized frictional resistance are observed, depending on the increase in effective stress with depth and on the geotechnical characteristics of the surrounding soil.

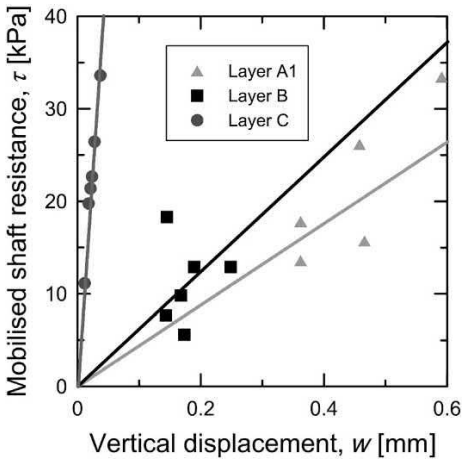

Figure 16. Relationship between mobilized frictional resistance and vertical displacement along the length of an energy pile restrained at its head, under mechanical loading. [15]

The direction of mobilized shear stresses induced by mechanical compression loads applied to energy piles is identical to that produced by thermal cooling above the zero point of shear stress, where it acts in the opposite direction to that caused by thermal heating. The reverse behavior occurs in the portion of the pile located below the zero point. An example of this phenomenon is presented in Figure 17, illustrating the combined effects of mechanical loading and thermal heating on an energy pile restrained at the head by a plate, in terms of the mobilized frictional resistance and corresponding vertical displacements, based on the results of Laloui et al. (2003).

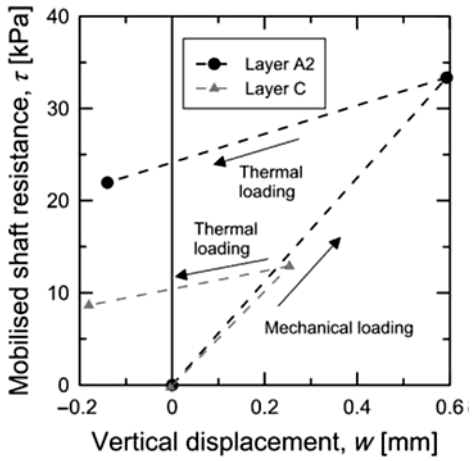

Figure 17. Mobilized frictional resistance and vertical displacement resulting from the combined mechanical and thermal heating actions in an energy pile restrained at its head, above the zero point of vertical displacement and shear stress. [15]

3.1.6. Vertical Stress under Thermal and Mechanical Loading

The thermal stresses develop in energy piles because the deformation induced by thermal loading is restrained by the interaction with the surrounding soil, the structural load transmitted at the pile head, and the resistance provided by the support at the pile base.

Compressive stresses induced by thermal loading can reach magnitudes comparable to those generated by structural mechanical loads. Consequently, the total variation in vertical stress resulting from the combined effects of mechanical loading and thermal heating may be up to twice as large as that produced by mechanical loading alone.

The influence of combined thermal and mechanical actions is illustrated in Figure 18 for an energy pile restrained at its head by a plate and subjected to a mechanical load of $P = 1300\ kN$ and a thermal heating load, resulting in an average temperature increase along the pile length of $\Delta T = 13.4\ °C$ (Laloui et al., 2003). The changes in vertical stress were derived from the experimentally measured deformations using a one-dimensional formulation expressed as:

$$\Delta\sigma_z = \Delta\sigma_{th} = E_{EP}\left(\Delta\varepsilon_{th} - \Delta\varepsilon_{free}\right) = E_{EP}\left(\Delta\varepsilon_z + \alpha_{EP}\Delta T\right)$$

where:

$\Delta\sigma_{th}$ - vertical stress induced by temperature,

E_{EP} - Young's modulus of the energy pile,

$\Delta\varepsilon_{th}$ - total thermally induced strain,

$\Delta\varepsilon_{free}$ - free (unrestrained) thermal strain,

α_{EP} - coefficient of thermal expansion of the pile material, and

$\Delta\varepsilon_z$ - measured axial strain along the pile.

The vertical stress profile was obtained as the difference between the total change in vertical stress measured along the pile length and that caused solely by mechanical loading. In this case, an increase in temperature of 1 °C led to an increase in vertical stress of approximately 165 kPa (equivalent to about 100 kN/°C).

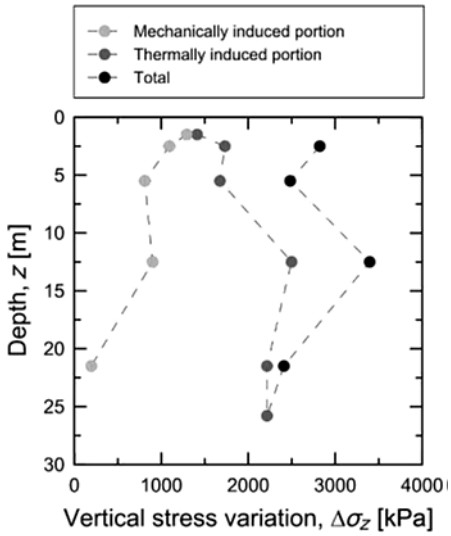

Figure 18. Vertical stress variations induced by mechanical loading and thermal heating in an energy pile restrained at its head. [15]

The variation in vertical stress induced by mechanical loading generally increases with depth. In contrast, under thermal cooling, the opposite trend can be observed in energy piles, as the reduction in compressive stress caused by thermal contraction may lead to the development of tensile stresses within the pile. This behavior is particularly evident in piles subjected to relatively low compressive loads at the head and significant cooling effects.

3.1.7. Variations in degrees of freedom

The support conditions at the head of energy piles are significantly influenced by the interaction between the imposed mechanical constraints and the thermally induced deformations (Mimouni and Laloui, 2014; Sutman et al., 2018). The greater the restraint provided by the surrounding soil and the superstructure, the smaller the allowable deformations and the higher the resulting thermal stresses along the pile (Bourne-Webb et al., 2011; Rotta Loria and Laloui, 2018). In this context, the *degree of freedom* (DOF) serves as an effective parameter to characterize the level of confinement of energy piles (Laloui et al., 2003). For instance, a DOF of 0.5 indicates that 50% of the thermally induced deformation associated with a given temperature change is restrained, thereby producing additional stresses.

An example illustrating the development of the degree of freedom along the length of an energy pile is presented in Figure 19, based on the results of Laloui et al. (2003). In the case of an energy pile initially free to deform vertically (test 1), the successive construction of building storeys leads to a progressive reduction in the pile's degree of freedom (tests 2 and 7). This phenomenon is attributed to the gradual increase in the overall stiffness of the pile-soil-structure system. The stiffness at the pile head varies locally depending on its position within the foundation. Consequently, energy piles subjected to identical thermal loading conditions within

the same soil environment but located at different positions in the foundation exhibit different degrees of freedom.

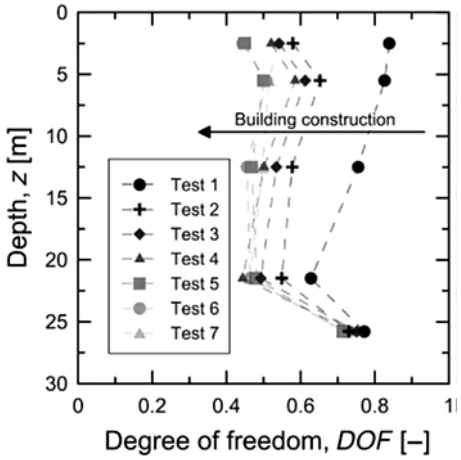

Figure 19. Variation in the degree of freedom along the length of an energy pile during the development of structural constraint conditions. [15]

In typical cases where the coefficient of thermal expansion of the soil is significantly smaller than, or theoretically equal to, that of the pile material, the degree of freedom ranges between $0 \leq DOF \leq 1$. However, due to the previously discussed influence of thermally induced deformations, in rare situations where the soil exhibits a higher coefficient of thermal expansion than the pile, geothermal operation may result in conditions where $DOF > 1$. [9]

3.1.8. Geotechnical challenges in the operation of energy piles

3.1.8.1. Temperature variations in the soil

The primary function of energy geostructures remains the transfer of structural loads to the ground; however, for safety and design reliability, temperature variations within the surrounding soil also should be considered.

Thermal processes within the soil induce the migration of water toward cooler zones (Brandl, 2006). In fine-grained soils, these processes may lead to cracking in warmer regions and swelling or expansion in cooler zones. Moreover, the thermal expansion of pore water increases pore pressure, thereby reducing the effective stress in the soil. As the temperature rises, the viscosity of pore water decreases, which in turn lowers the soil's shear strength. The presence of organic constituents further enhances the thermal sensitivity of soil, particularly in clays.

Field investigations have shown that properly designed and well-maintained energy foundations do not adversely affect load transfer mechanisms (Bourne-Webb et al., 2009; Murphy and McCartney, 2015; Faizal et al., 2018). In most cases, thermo-hydraulic interactions are negligible; however, they should be considered in structures that are highly sensitive to differential settlements. [16]

A decrease in groundwater temperature leads to an increase in viscosity and a corresponding reduction in hydraulic conductivity, which in turn results in lower groundwater flow velocities and smaller hydraulic gradients (Brandl, 2006). However, within the temperature range typically associated with the operation of energy geostructures (5-30 °C), these effects are generally negligible (SIA, 2005). A more significant consideration involves maintaining the

thermal balance of the soil, particularly in cases where the hydraulic gradient is below 1 m/day, as well as accounting for heat transfer processes when the hydraulic gradient reaches its higher values (SIA, 2005).

Excessive cooling of groundwater, resulting from excessive energy extraction, can lead to an increase in pH and a reduction in calcium solubility, thereby promoting pore clogging. Conversely, the increased solubility of gases such as CO_2 can enhance groundwater hardness (Brandl, 2006).

Temperature is one of the most influential environmental factors governing the activity of microorganisms in groundwater (Brandl, 2006). Most microbial species can survive only within a limited temperature range. In practice, microbial activity decreases at temperatures below 10 °C, whereas the growth of certain bacterial groups is enhanced at temperatures exceeding 35 °C (Fakharian and Evgin, 1997; Brandl, 2006).

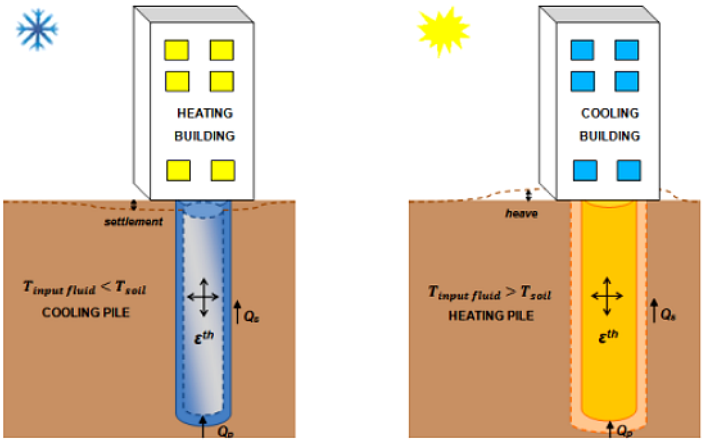

Figure 20. Illustration of the effects of thermal heating and cooling on energy piles. [15]

3.1.8.2. Temperature variations in energy piles

During heating/cooling cycles, temperature variations induce volumetric changes in both the pile and the surrounding soil. Thermal expansion alters the static behavior of energy foundations after multiple thermal cycles have been applied (Amatya et al., 2012). To prevent potential issues arising from temperature fluctuations in energy geostructures, it is essential to develop a thorough understanding of their thermo-mechanical response mechanisms. [16]

Assuming a simplified case of a homogeneous, linearly elastic, and laterally unsupported pile, the pile is expected to elongate during heating and contract during cooling. These deformations generate additional axial tensile stresses, thereby influencing the pile-soil interaction. The axial elongation of an unsupported pile depends solely on the coefficient of thermal expansion of the pile material and the applied temperature change, as expressed by:

$$\varepsilon_{obs} = \varepsilon_{free} = \alpha_c \Delta T$$

where ε_{obs} denotes the measured axial strain, ε_{free} represents the free axial strain of the pile under thermal loading, α_c is the coefficient of thermal expansion of the concrete, and ΔT denotes the applied temperature change.

The stress within the energy pile must remain below the allowable limits. Additional stress verification may be required in the case of supported energy piles, where thermal restraint can lead to increased stress development:

$$\sigma_T = \varepsilon_b E$$

where σ_T denotes the additional stress induced by thermal loading in the restrained pile, ε_b represents the prevented axial strain, and E is the Young's modulus of elasticity of the pile material.

In practice, the boundary conditions of energy piles lie between the two idealized cases of fully constrained and fully free elongation. Axial expansions induced by thermal loading do not occur under perfectly free conditions, and thermally induced stresses tend to increase along the pile length. Although the free elongation condition represents the upper limit of the pile deformation magnitude, the measured deformations are often significantly smaller, with the restrained portion of the deformation being converted into thermal axial stress.

$$\varepsilon_{free} = \varepsilon_{obs} + \varepsilon_b$$

where ε_{free} denotes the free axial expansion of the energy pile, ε_{obs} represents the measured axial expansion of the pile under thermal loading, and ε_b corresponds to the restrained (prevented) axial expansion resulting from thermal action.

To illustrate this behavior, the thermal response of a floating pile without structural loading during heating and cooling is presented in Figure 21 and Figure 22. As the stiffness and compressibility of the surrounding soil increase, the mobilized stiffness governing the pile-soil interaction also increases. During heating, expansion in the central portion of the pile becomes more constrained than at the pile ends, resulting in the development of additional axial compressive stresses. Conversely, during cooling, soil confinement leads to pile contraction, and tensile stress develops with increasing soil stiffness.

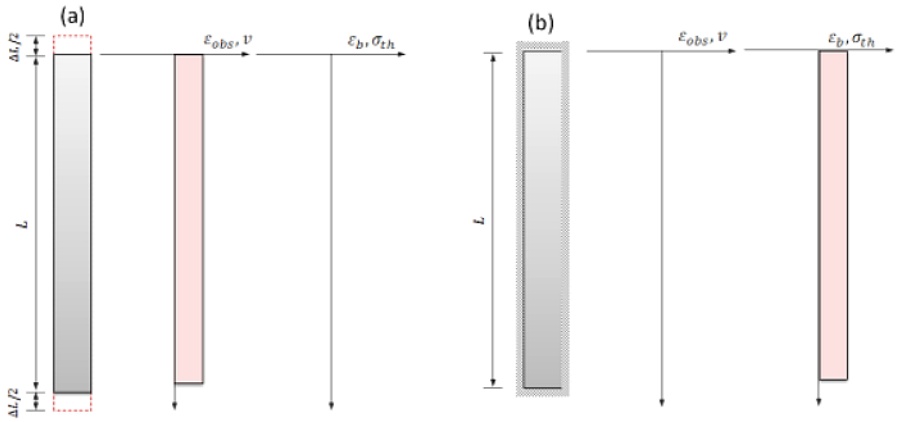

Figure 21. Thermal response of a free and a fully confined pile: (a) heating of a free pile; (b) heating of a confined pile (after Bourne-Webb et al., 2013).

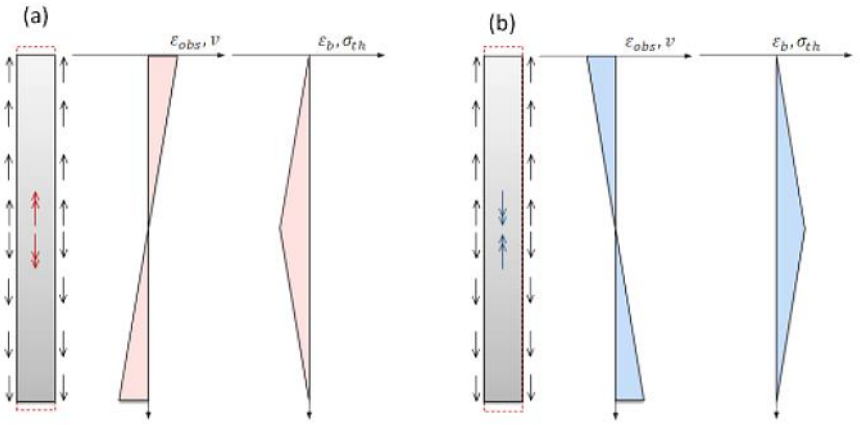

Figure 22. Effect of soil confinement on the response of energy piles during thermal loading: (a) heating; (b) cooling (after Bourne-Webb et al., 2013).

3.2. Design of geothermally active piles

3.2.1. Design parameters

Various input data are required for the analysis and design of energy geostructures. In order to determine the parameters needed for the analysis or design, it is necessary to conduct appropriate research. These researches are conducted as a function of the analysis or design and can be theoretical or empirical. The empirical approach includes experimental full-scale in situ tests, laboratory tests, and centrifugal tests. Theoretical approaches involve literature reviews and analytical calculations. In practice, no investigation can be considered comprehensive without parameters defined through detailed experimental studies.

3.2.1.1. Site condition characteristics

Each energy geostructure project has specific characteristics that define the multiphysical behavior of such systems. These must be considered in design and analysis. A modified and extended list of features based on Brandl (2006) includes:

- Geothermal site characteristics: thermal characteristics and in-situ temperature
- Aerothermal characteristics (if applicable): air flow in soil medium, velocity characteristics, and thermal boundary layers.
- Hydrogeological features: groundwater depth, seasonal fluctuations, flow direction, and velocity.
- Geotechnical characteristics: soil stratification, permeability, strength, deformability, and sensitivity to freeze-thaw cycles.
- Structural features: geometry, material strength, reinforcement details, installation method, reinforced concrete characteristics.
- Geothermal system: pipe configuration and layout, heat transfer fluid flow rate, heat transfer fluid composition, pipe thermal insulation length, heat pump specifications.
- Building physics aspects: Thickness of insulation on the roof, floors and walls (where applicable), size and quality of windows (where applicable), position and type of stairs

(closed/open), occurrence of thermal bridges, temperature conditions of the energy cycles, monthly heating or cooling demand and additional requirements, type of heating/cooling systems, type/mixture and speed circulation of the heat transfer fluid within of the energy system, operating plan, heating and cooling intervals.

Geotechnical, geothermal, aerothermal, and hydrogeological characteristics, together with the geothermal system and aspects related to construction physics, initially determine the thermohydraulic behavior, as well as the energy characteristics of geostructures. Accordingly, the geotechnical characteristics of the site and the structural characteristics of geostructures and facilities determine the thermomechanical behavior, as well as the geotechnical and structural characteristics of energy geostructures. However, due to the coupling between the phenomena involved in the operation of energy geostructures, a change in the previous characteristics can globally affect the thermo-hydro-mechanical behavior of energy geostructures. This change may require a change in all relevant analysis and design types of energy geostructures (for example, energy, geotechnical, and structural).

Typically, features 1) to 4) are given for any project, while features 5) to 7) may depend on the specific case. Knowledge of prior characteristics may become available at different stages of the project. However, successfully installed energy geostructures are associated with a remarkable amount of prior information available from the early stages of the analysis and design process.

3.2.1.2. Overview of the design parameters

Design parameters can be used for quantitative characterization of site characteristics and can be divided into categories depending on whether they are needed for energy, geotechnical, or structural design (or analysis) of energy geostructures. However, considering that the multiphysical behavior and phenomena that govern the energy geostructures are merged, the previous parameters may enter more projects and may have comparable impacts on the results.

Table 2 [9] summarizes the key parameters required for the design of energy geostructures, based on the work of Loveridge et al (2017). Thermal and hydraulic parameters are key to the energy design of energy geostructures. Mechanical parameters are crucial for the geotechnical and structural design of energy geostructures.

Table 2. Overview of design parameters for geothermal piles, according to the type of analysis

Analysis type	Project variable and corresponding parameters	Comment
Energy analysis	▪ Thermal characteristics of soils or rocks (thermal conductivity, specific heat) ▪ Thermal characteristics of reinforced concrete (thermal conductivity, specific heat) ▪ Undisturbed soils or rocks and geostructure temperature (initial temperature) ▪ Groundwater flow velocity (Darcy velocity)	▪ An average value of thermal conductivity is used in most design cases, although real conditions are anisotropic and heterogeneous.
Geotechnical analysis	▪ Soil/rock strength (shear strength, unconfined compressive strength)	▪ Total or effective stress conditions, respectively

	▪ Soil/rock compressibility (Young's Modulus of Elasticity, Poisson's coefficient) ▪ In situ stresses and pore pressure ▪ Stress history (over-consolidation ratio) ▪ Thermal expansion potential of rocks/soils (linear or volumetric coefficient of thermal expansion) ▪ Soil permeability	▪ An assessment of whether it is temperature-dependent should be included ▪ It should include an assessment of whether the dependency is complete
Structural analysis	▪ Strength of reinforced concrete (compressive and tensile strength, maximum allowable deformations) ▪ Compressibility of reinforced concrete (Young's modulus, Poisson's ratio) ▪ Thermal expansion potential of concrete (linear or volumetric coefficient of thermal expansion	

3.2.1.3. Geothermal pile design

Heat transfer efficiency improves with longer piles and larger diameter (Figure 23). The use of larger diameters has a positive impact, as it allows for the placement of more heat transfer tubes. It also reduces the thermal resistance of the pile and increases the heat flow. However, from a mechanical perspective, additional thermal loads, due to improved thermal characteristics, can increase axial stresses in the foundation. Therefore, any change in the design of the geothermal piles would have additional mechanical effects. [10]

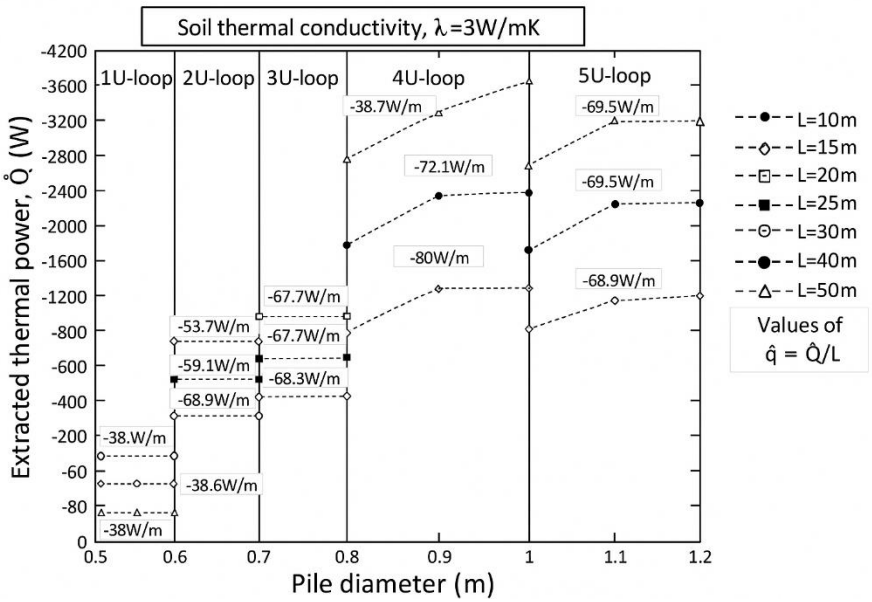

Figure 23. The effect of the diameter and length of the geothermal pile on its thermal. [9]

3.2.1.4. Pipe characteristics

Heat exchange pipes are commonly U-shaped due to ease of installation. Spiral pipes offer better thermal performance but are harder to install in smaller diameter piles. Pipes are usually made of polyethylene with diameters from 20 to 40 mm and wall thicknesses of 2 to 4 mm.

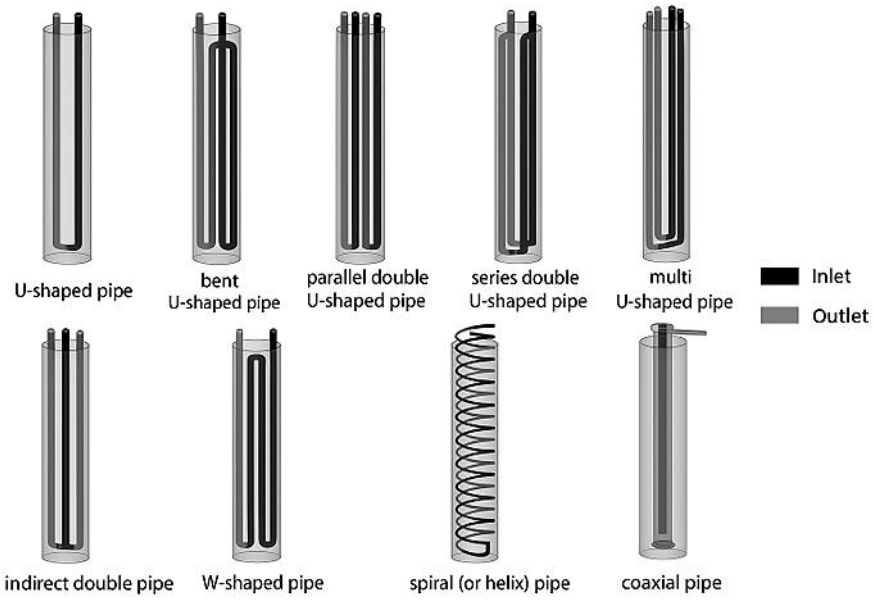

Figure 24. Pipe configuration in geothermal piles. [17]

The changes in the configuration of the pipes play an important role in the operation of the heating system. Basically, U-shaped, W-shaped, or spiral are connected to the reinforcement cage of the geothermal pile. For approximately thirty years, U-tubes have been the most used heat exchanger in geothermal piles, due to their simple design and ease of transportation and installation compared to other types of pipes. U and W-shaped pipes can be extended as double, triple, and more pipes to improve the efficiency of heat transfer. Spiral pipes, unlike others, have the best thermal characteristics, as they can produce heat 1.4 times more than the others. On the other hand, they have limited applications because they are more difficult to install and are not suitable for geothermal piles with a smaller diameter [18]. During their production, specific standards are applied to the application in geothermally active structures.

3.2.1.5. Concrete characteristics

Ensuring high mechanical properties of concrete is one of the main objectives to maintain the structural requirements for durability and strength. For geothermal piles, the thermal properties of concrete are quite important, due to their positive influence on the efficiency of heat transfer between heat exchange pipes and the surrounding soil. Concrete has thermal conductivity values in the range of 1 to 4 W/mK depending on the cement-to-aggregate ratio, the type of aggregate, and the water content. A large amount of aggregate improves the thermal conductivity of concrete, while the need for a large amount of cement to produce high-strength concrete mixtures can reduce thermal conductivity. The addition of additives such as fly ash to improve the behavior and durability of concrete can have an additional negative impact on thermal conductivity, i.e., a decrease of 20%. According to the results of Carotenuto et al., the thermal characteristics of geothermal piles increase by 42% with an increase in the thermal conductivity of concrete from 1.2 to 2.5 W/mK. Within the framework of a large number of studies, ways to improve this parameter have been proposed. Li et al. propose the addition of graphite powder to the cement paste. The results of laboratory tests and numerical analyses show a significant improvement in heat transfer with an increased amount of graphite at the

same temperature. Laing et al. show that mixing concrete with heat-transfer materials such as graphite or aluminum can provide heating and cooling needs with a smaller number of pipes or shorter lengths. Yang et al. propose combining graphite with PCM (Phase change material) in concrete, which allows for improved thermal conductivity and increased heat storage capacity. [18] Furthermore, other studies suggest adding materials with high strength and thermal conductivity, such as carbon fibers, copper fibers, or steel fibers. It can be concluded that the addition of conductive materials to the concrete mix is quite beneficial for improving the thermal properties of concrete. However, structural and economic feasibility studies are necessary to maintain the compressive strength of concrete and ensure the economy of the structure.

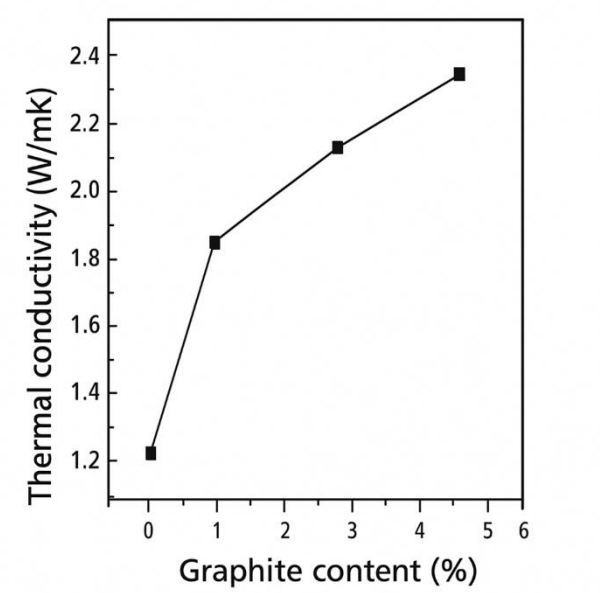

Figure 25. Relationship between heat transfer and percentage of graphite in concrete (Guo et al. 2010)

3.2.1.6. Heat transfer fluid characteristics

Fluid flow can be laminar or turbulent, which affects the efficiency of heat transfer between the fluid and the inner wall of the heat exchanger. It is characterized by the Reynolds number (Re), which increases with increasing tube diameter and fluid velocity or decreasing fluid viscosity. Reynolds' number values less than 2300 induce laminar flow, while values above 4000 induce turbulent flow. By applying turbulent flow, the heat transfer per meter between the pipe and the ground at the same time reduced heat transfer to the upper and lower part of the tubes, which limits the low circulation that occurs in low laminar conditions. However, according to Park et al., too fast flow during full turbulence does not provide enough contact time for heat transfer, which affects thermal efficiency. According to the recommendations of Kavanaugh and Rafferty, a fluid with a Reynolds number in the range of 2500 to 3000 is recommended.

Water is the primary fluid used in the operation of this system. It can be mixed with an antifreeze solution, such as propylene glycol and ethylene glycol, to prevent the fluid from freezing when the temperature drops below zero in the pipes themselves. It is important to choose the optimal mixture, which will improve the thermal characteristics and avoid increased viscosity.

3.2.1.7. Soil characteristics

The correct assessment of the thermal properties of the soil is of great importance for the design of geothermally active structures. These thermal properties can vary, depending on the water content, dry density, and structure of the material. According to Andersland and Ladanyi 2013, the basic thermal properties are:

Thermal conductivity: $\lambda \left[W/mK\right]$ is the ability of a material to transfer thermal energy. It is defined as the amount of heat Q that passes through a unit area A of the soil per unit time, with a temperature gradient set along the direction of the heat flow:

$$Q = \lambda A \frac{dT}{dx}$$

Heat capacity: $c \left[J/m^3K\right]$ is the ability of a material to store thermal energy. It is defined by the amount of heat required to increase the temperature by 1 K. It does not depend on the microstructure, so in most cases, it is considered acceptable to calculate the heat capacity of the soil through the values of the heat capacity of its components:

$$c = c_s x_s + c_w x_w + c_\alpha x_\alpha$$

Where $x_s = 1 - n$ is the percentage of solid material in the soil composition, n represents the porosity, $x_w = nS$ is the percentage of water contained in the pores, S is the saturation degree, and $x_\alpha = n\left(1 - S\right)$ is the percentage of pores filled with air.

Thermal diffusion: $\alpha \left[m^2/s\right]$ is the ability of a material to balance temperature differences and achieve thermal equilibrium in a non-steady state:

$$\alpha = \frac{\lambda}{c\rho}$$

Where λ is thermal conductivity, c represents heat capacity, and ρ is the soil density.

In the long term, consolidation or shrinkage processes of the soil (from external influences, its own weight, or heat extraction) can play a role in the thermal properties of the soil, due to changes in the volume ratios (Brandl 2006). The total heat capacity increases with water content and decreases in the case of freezing. The most important soil thermal parameter is the thermal conductivity. For a preliminary solution of complex energy foundations or for a detailed solution for simple projects, the value of λ can be adopted with sufficient certainty from diagrams that take into account water content, degree of saturation, and soil texture (SIA 2005).

For more complex cases, thermal characteristics should be determined from laboratory and/or field tests. [19]

3.2.2. Design of geothermally active piles

The dual action of thermal and mechanical loads on geothermal piles presents a challenge from the aspect of their multifunctional operation. From the aspect of design, such a challenge is primarily related to the fundamentally different nature of mechanical and thermal actions,

which leads to different effects on the mechanical response (stresses and deformations) of geothermal piles. These effects must be taken into account in the geotechnical and structural design of geothermal piles through a behavior design approach.

Thermal actions can be idealized as imposed deformations. These actions cause elongation and shortening of the geothermal piles and the surrounding soil. While geothermal piles elongate upon heating and shorten upon cooling, the soil can expand or contract upon heating and contract upon cooling. In most cases, part of the deformations caused by thermal actions are limited by the environment and cause thermal stress. The importance of the stresses and deformations caused by thermal actions depends on the support conditions and the relationship between the thermal conductivity coefficient of the soil and the circuit. Both aspects characterize the changes in vertical displacements and shear stresses in geothermal piles. These piles generally move in the opposite direction from the so-called zero point of vertical displacements and the mobilized shear strength of the pile to ensure equilibrium from the so-called zero point of shear stresses. The locations of the zero points mentioned are generally different and may vary under loading. The changes in stresses, strains, and displacements that characterize power circuits may vary critically due to the influence of group effects associated with temperature actions. These effects are responsible for a larger group deformation compared to a single isolated pile under the same average load.

Mechanical actions can be idealized as given influences on the structure. These loads usually cause changes in stresses and strains that decrease along the geothermal pile and the surrounding soil. In most cases, the evolution along the length of the changes caused by mechanical actions is more uniform than those caused by thermal actions, and is associated with changes in displacements in a single direction. In this context, the changes in strains, stresses, and displacements depend on the support conditions, together with the group effects caused by mechanical actions. [9]

A lot of theoretical and empirical background knowledge, as well as a large number of analyses, have been done to characterize the response of geothermal piles loaded with thermal and mechanical actions, as well as to address the geotechnical and structural behavior. In recent years, studies have been conducted to address performance-based approaches, which have also proposed recommendations for the design of this type of geostructures. In accordance with previous achievements and developments in the field, it is necessary to develop a methodology for the design of this type of structures.

3.2.2.1. Behavior-based design principles for geothermal piles

General

The principles and provisions for the behavior-based design approach for pile foundations can be found in EN 1997 (2004). Special attention is paid to the influence of axial loads on pile foundations in EN 1997-1 (2004). These guidelines apply primarily to driven or bored piles acting in end-bearing or frictional capacity. These provisions should not be applied to the design of piles intended to reduce settlement (application of piles with a pile cap).

According to Frank (2004), the reason for this is that the load-bearing function provided by the foundation slab, rather than by the piles, in those cases involves over-conservative partial

factors for the piles. Complementary information that may be useful in the design of this type of foundation can be found in EN 1992 (2004) for reinforced concrete piles, in EN 1536 (1999) for bored piles, in EN 12063 (1999) for diaphragms, in EN 12699 (2000) for movable piles, in EN 14199 (2005) for micro-pile and in EN 12794 (2005) for prefabricated piles. The information contained in the above-mentioned documents should be considered as the basis for designing the energy piles and their associated structural elements or systems. [20]

Relevant limit states

The most common limit states to be considered for pile design (EN 1997-1, 2004) include: (1) loss of overall stability of the pile foundation (2) loss of pile bearing capacity (3) uplift or insufficient tension strength of the pile (4) failure in the soil due to transverse loading of the pile structure (5) structural failure of the pile due to compression, tension, bending, shear or torsion (6) combined failure of the pile and the soil (7) combined failure of the soil and the structure (8) excessive settlement (9) excessive uplift (10) excessive lateral movement or (11) vibration. The limit states considered may affect the geotechnical or structural behavior of the structures. Phenomena (1-7) generally include the ultimate limit states. Phenomena (8-10) include the serviceability limit states for the geostructure or the ultimate limit states for the superstructure. Phenomenon (11) represents a serviceability limit state.

In the case of axially loaded piles, the design should show that the following limit states are unlikely to be exceeded (EN 1997 - 1, 2004):

- Ultimate limit states of loss of compressive or tensile strength of a single pile.
- Ultimate limit states of loss of compressive or tensile strength of the entire pile structure.
- Ultimate limit states of collapse or major damage to the structure caused by excessive displacement or differential displacements of the pile structure.
- Serviceability limit states of the structure caused by the displacement of piles.

Critical approaches and aspects to verify the behavior of geothermal piles using the considered boundary conditions are given in the following text.

3.2.2.2. Behavior-based design methodology

General

In essence, the geotechnical and structural behavior of geothermal piles can be verified without the influence of thermal actions, applied together with mechanical actions, for ultimate or serviceability limit states. In practice, according to Rotta Loria et al. (2019), the effects of thermal actions should be taken into account for the control of serviceability limit states because they are not expected to exceed the ultimate limit states. In other words, thermal actions include effects that can be neglected in the design approach with the behavior of energy circuits at ultimate limit states. Hence, the design and control of energy circuits at ultimate limit states can be considered as a conventional process. In contrast, the design and control of geothermal piles at serviceability limit states is a modified process in which the influence of mechanical and thermal actions must be considered. The previous approach is consistent with the Eurocodes (EN 1992, 2004), which state that "thermal effects may be considered as ultimate limit states

only where they are significant (e.g., fatigue conditions, secondary effects). In other cases, they need not be considered, provided that the ductility and rotation capacity of the elements are satisfied.

Typical characteristic values of temperature changes associated with thermal cooling actions applied to geothermal piles can be considered in the temperature range of $\Delta Tk = -5°C$ and $\Delta Tk = -10°C$. In the worst case, the value of $\Delta Tk = -15°C$ it can be considered in warm climates. Typical characteristic values of temperature changes associated with thermal heating actions applied to energy circuits are in the range of $\Delta Tk = 10°C$ and $20°C$. In the worst case, the value of $\Delta Tk = 30°C$ it can occur in cold climates.

Design criteria

The previous methodology, where the behavior of geothermal piles under thermal action is controlled only at serviceability limit states (not at ultimate limit states), can be considered appropriate if the following two design criteria are met, and is confirmed by the proposed arguments (Rotta Loria et al., 2019).

- It should be ensured that the design compressive strength of the concrete section (for example, in the case without applied moments) is at least equal to the bearing capacity of the pile (increasing the compressive strength of concrete sections can be achieved by increasing the concrete strength or the percentage of reinforcement. Special attention should be paid to the technical justification of using higher concrete classes, in relation to the quality of the concrete, especially for bored piles. When this approach is not applied, design actions supported from a geotechnical perspective may cause or exceed the ultimate limit states from a structural perspective. In contrast, the proposed approach guarantees a potential ductile failure mechanism associated with the initial overcoming of the ultimate limit states from a geotechnical perspective.
- The minimum reinforcement area of the concrete cross-section should be selected. When this approach is not applied, the requirements for durability and deformability (fracture) of the materials from which the designed structures are made will not be met. On the contrary, this approach guarantees durability and ductility.

Geotechnical aspects

From a geotechnical perspective, displacement and equilibrium control allow verification that ultimate limit states are not exceeded. Displacement control involves limiting the differential displacements occurring along the length of the piles in the soil to ensure that the superstructures are not affected by unacceptable stress changes that could be associated with failure or collapse mechanisms. Equilibrium control involves comparing the design values of the load acting on the pile and the load carried by the pile (load capacity) to ensure that failure or collapse mechanisms in the soil are not reached.

In this context, concerning displacement and equilibrium considerations, the worst-case predicted condition for the geotechnical behavior of energy piles involves foundations with fully mobilized base capacity and friction capacity caused by thermal cooling action and mechanical compression action (Rotta Loria et al., 2019). In this theoretical condition, where base capacity and friction capacity are fully mobilized and the soil behavior can be assumed to

be perfectly plastic, the zero point of the energy pile loaded by thermal cooling action is located at or towards the head, depending on whether there is an over-pile plate. Hence, the maximum possible displacement caused by thermal action occurs, in addition to the mechanical actions. This phenomenon has the potential to exceed the geotechnical ultimate limit state. In piles loaded by thermal heating actions, with fully mobilized capacities, no head displacements occur under such load cases. In this theoretical condition, where the basic capacity and the friction capacity are fully mobilized and the soil behavior can be taken as perfectly plastic, the zero point of the energy pile loaded by the thermal heating action is located at the head, regardless of whether or not there is an over-pile plate. This is the only way to ensure equilibrium. Otherwise, any other location of the zero point can cause an increase in the compressive force on the pile in the zone above the zero point (upward movement), which cannot be balanced because below the zero point, it will cause a downward movement (perfect plasticity). The application of the thermal heating action in all other cases where the full mobilization of the basic capacity and the friction capacity is not reached causes the head of the energy pile to move upwards. However, the considered phenomenon presents a serviceability limit state problem and is therefore not relevant for the considerations related to the ultimate limit states.

From a displacement perspective, thermal cooling actions are not expected to cause energy pile settlements (e.g., differential) that could generate a collapse mechanism (Rotta Loria et al., 2019). Typical orders of magnitude of energy pile displacements caused by thermal cooling actions after mechanical actions are from $0.10\%D-0.70\%D$ for pile slenderness ratios in the range of $L/D=20-50$ (where L and D are the pile length and its diameter, respectively) (Rotta Loria et al., 2019). Hence, from a displacement perspective, the effects of thermal actions can be neglected in favor of geotechnical verification of the ultimate limit states. Group effects caused by interactions between piles can increase the displacements. However, these effects should be considered at serviceability limit states, due to the magnitude of the phenomena involved. [9]

From the equilibrium point perspective, although in principle the full mobilization of the capacity of the energy circuits can be caused by the combined loading of thermal and mechanical actions, in practice the zero points always provide equilibrium, respecting the influence of thermal actions (Rotta Loria et al., 2019). For any magnitude of thermal action applied to the energy piles, the reactions provided by the soil below and above the zero point of shear stresses compensate each other and prevent the formation of a collapse mechanism Figure 26. The equilibrium of the geothermal piles will always be ensured, with the displacements caused by thermal actions equal to zero occurring respectively at the zero point of vertical displacements, which will prevent the occurrence of a collapse mechanism. Based on the above, thermal actions cannot cause a geotechnical collapse mechanism of the geothermal piles from the equilibrium point perspective, and therefore cannot include geotechnical ultimate limit states. [9]

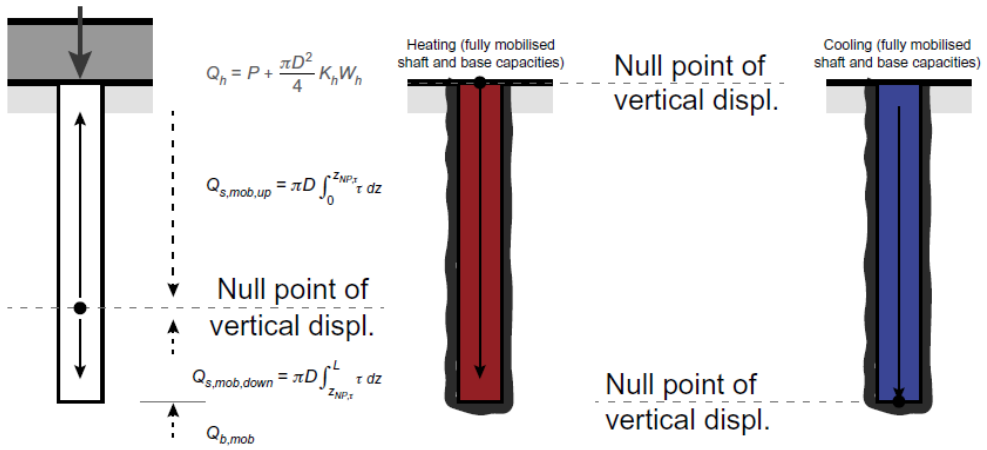

Figure 26. Vertical balance of the geothermal pile is ensured in any case of the presence of a zero point. [16]

Structural aspects

From a structural perspective, equilibrium considerations allow proof that ultimate limit states are not exceeded. Equilibrium considerations involve a comparison of the design values of the load acting on the pile and the load carried by the considered pile cross-section (or ratio) to ensure that failure mechanisms in the structure are not reached.

In this context, the worst-case predicted conditions for the structural behavior of geothermal piles include foundations with partially mobilized basic and frictional capacities, caused by significant thermal cooling actions and low mechanical pressure action or by significant thermal heating actions and high mechanical pressure action (Rotta Loria et al., 2019). Under these conditions, stresses from the applied actions occur, with the potential to exceed the structural ultimate limit state.

From a steady state perspective, thermal heating actions applied in combination with mechanical actions are unlikely to exceed the design compressive strength of the cross-sections of the geothermal piles, which are not expected to exceed the structural ultimate limit states (Rotta Loria et al., 2019). This result is ensured by the design criteria related to the design compressive strength of the cross-sections of the geothermal piles, proposed by Rotta Loria et al. (2019) and highlighted in the same study. Conversely, thermal cooling actions applied in combination with mechanical actions can exceed the design tensile strength of the cross-sections of the power circuits, which means that they can exceed the structural ultimate limit states. This result is confirmed by Rotta Loria et al. (2019), although it was underlined that it is unlikely to occur in practice due to the following arguments.

The actual behavior of reinforced concrete is nonlinear and is determined by the occurrence of cracks above specific strain levels. If the minimum percentage of reinforcement is sufficient to withstand the force at which cracks occur, the element does not experience failure at the first crack, and the occurrence of cracks leads to a redistribution of stress and a reduction in the load-bearing capacity of the structure. The load-bearing capacity involves lower values of stress compared to those associated with the compressibility of uncracked sections and linear stress-strain relationships. Hence, although the Eurocodes (EN 1992, 2004) [21] state that linear

stress-strain relationships and uncracked sections should be considered in behavior-based design, lower stresses can be expected once the crack-related strain levels are reached.

Once the nonlinear stress-strain relationship that characterizes reinforced concrete is taken into account, a design approach geared towards ductility is required. The reason for this is that when a displacement is applied to a structurally immovable member, equilibrium is only ensured when the ductility capacity is sufficient. Hence, tensile deformations caused by thermal actions can be accommodated by the structure, and the induced stresses are simply obtained from the constitutive model. To ensure adequate ductility capacity of reinforced concrete members, (1) the resisting axial force of the cross-sections should be greater than the axial force required to cause cracks, due to potential local effects of deformations, (2) the reinforcement should be characterized by a high deformation capacity, and (3) the ratio f_t/f_y should be within the lower limit (where f_t and f_y are the tensile strength and yield strength of the reinforcing steel). Condition (1) is achieved by providing a minimum percentage of reinforcement, determined by Rotta Loria et al. (2019). Condition (2) is related to the magnitude of the effects of the actions. Condition (3) is generally satisfied because the standards prescribe minimum values of the ratio f_t/f_y .

When choosing a design approach to ductility, a key aspect relies on understanding the level of deformation associated with a given load. This final assumption allows unsatisfactory proofs, such as those mentioned above, to be allowed. (Rotta Loria et al., 2019).

Based on the above, the following aspects can be highlighted for geothermal piles:

- The selection of an appropriate minimum percentage of reinforcement that ensures ductility (as proposed by Rotta Loria et al., 2019). Although cracking of concrete provides a change in axial resistance to deformation under load along the length of the piles may involve the phenomenon of deformation localization, the deformation caused by thermal actions remains in the cracked development phase for practical temperature changes. This result is qualitatively illustrated in Figure 27 in terms of the relationship between the design pullout force N_d and the normalized axial displacement $\triangle w/L$ that characterizes a reinforced concrete energy pile that has a minimum percentage of reinforcement. This relationship is compared with that of the same member characterized by simultaneous crack occurrence (which coincides with the response of a single cross-section), as well as with the connection with reinforcement.
- When comparing the imposed strain levels caused by thermal actions to the strain capacity of a properly designed cross-section, the structural ultimate limit states will not be exceeded by the influence of these actions, regardless of whether or not strain localization has developed. Cracking may occur in concrete due to the action of thermal cooling actions. However, sufficient ductility capacity is provided by the proposed design approach, and structural ultimate limit states will not occur. Cracking of concrete is a common phenomenon that needs to be controlled.

Based on the above, thermal actions do not include the structural failure of the geothermal piles, which means they do not exceed the structural ultimate limit states.

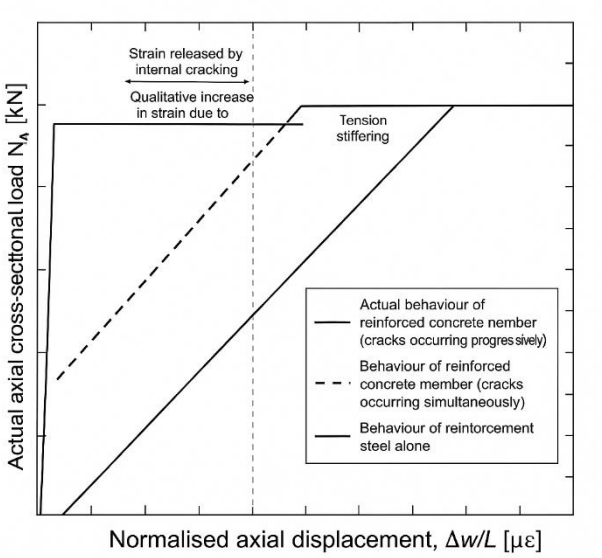

Figure 27. Relationships between axial shear load and normalized axial displacement for geothermal piles. [22]

Typical design cases

Two typical problems can arise when designing piles (Rotta et al., 2019):

- Constant mechanical action and change in pile length - the pile length can be defined for each pile of the foundation structure to accommodate the applied mechanical action. The considered length can be increased as needed. As a result, the value of the design bearing capacity of the pile will be greater than the required value.
- Change in applied mechanical action and constant pile length - a design mechanical action can be taken for all piles of the foundation structure based on the maximum load applied to one or more piles. However, not all piles in the foundation structure need to accept this action. As a result, the pile length will be increased compared to the required value.

If we have a length of geothermal piles greater than the design length, which are loaded with a given mechanical action, the axial bearing capacity increases, and the effects caused by temperature actions become more burdensome for the same applied temperature change. From a geotechnical perspective, the previous aspect is related to the fact that for the same applied temperature change ΔT and linear thermal conductivity coefficient α_{EP}, longer piles involve proportionally larger changes in length $\Delta L = \alpha_{EP}\Delta TL$, even though the deformation caused by thermal actions under free elongation conditions is independent of their length $\varepsilon_f^{th} = -\alpha_{EP}\Delta TL$. From a structural perspective, the previous aspect can be emphasized by taking into account that longer geothermal piles loaded with the same intensity of mechanical actions are characterized by greater stress caused by thermal actions. Based on the previous considerations, the oversize geothermal piles should be avoided, i.e., they should be appropriately dimensioned. In essence, if the aim is to limit the vertical displacement of geothermal piles caused by thermal actions, larger diameters of geothermal piles should be applied, and longer circuit lengths should be avoided (Rotta Loria et al., 2019). The previous statement is contrary to the belief

that longer piles provide greater safety against thermal actions. It should also be distinguished from the justified reasoning that the design that takes into account longer piles provides greater safety against mechanical actions.[9]

Investigation methodology

Two aspects need to be considered to demonstrate the structural and geotechnical behavior of energy piles (Rotta Loria et al., 2019).

1. The vertical stress variations induced by mechanical and thermal actions must be taken into account along the entire length of the energy pile, and the most critical cross-section should be verified.
2. The vertical displacement variations induced by mechanical and thermal actions must be taken into consideration, particularly at the head of the energy piles.

The variations in vertical stresses and displacements induced by mechanical and thermal actions differ along the length of the energy piles. However, while the most critical cross-section along the energy pile must be examined to ensure adequate performance, which might otherwise not be satisfied, only the displacements at the pile head need to be considered in cases where the structural response (along with the connected structural elements) is primarily governed by the displacements at that location.

Partial factors for thermal actions affecting energy piles

To account for the effects of thermal actions in serviceability limit state combinations, the following factors should be applied to the combination, frequent, and quasi-permanent values of the variable actions, respectively (Rotta Loria et al., 2019): $\psi_0 = 0.60$, $\psi_1 = 0.50$, and $\psi_2 = 0.50$. [22]

3.2.2.3. Design according to the Ultimate Limit State

General

The fundamental inequality that needs to be verified for all combinations of actions in the ultimate limit states for a single pile or a group of piles subjected to axial mechanical actions is. [20]

$$F_{cd} \leq R_{cd}$$

Where F_{cd} is the design axial load acting on a single pile or a group of piles, while R_{cd} is the design value of the ground resistance associated with the single pile or group of piles. The design load is typically determined from combinations of actions following the general format of the partial factor method. The design ground resistance is usually determined through three approaches: (1) results from pile load tests (static or dynamic), (2) calculations based on soil profile data from boreholes, and (3) calculations based on shear strength parameters of the soil.

To verify the ultimate limit states, the following considerations should be taken into account:

- A displacement of the pile head equal to or greater than 10% of the pile diameter should be considered as a failure criterion. (EN 1997, 2004)

- When pile foundations exhibit significant upward or downward movement with negligible increase or decrease in resistance, safety against compressive or tensile failure must be considered during design.
- The ultimate limit state of piles is considered reached only when a significant number of piles experience failure simultaneously, or when the structure connected to the piles fails. Until one of these failure mechanisms occurs, the ultimate limit state is not deemed to have been reached. (EN 1997, 2004)
- Two failure mechanisms should be considered for a group of piles (EN 1997, 2004):
  a) Compressive or pull-out failure of the individual piles, and
  b) Compressive or pull-out failure of the piles together with the soil between them acting as a block.
- Design resistance should be taken as the lower value associated with these two failure mechanisms.
- To determine the design strength of individual piles, the actions should be assessed considering (EN 1992, 2004):
  - Pile-to-pile interaction, (2) The pile head, and (3) The bearing soil.
  - When piles are arranged in multiple rows, the actions on each pile should be evaluated considering pile-to-pile interaction (EN 1992, 2004). This interaction may be ignored when the clear spacing between piles exceeds twice the pile diameter (EN 1992, 2004).
  - The pull-out resistance of individual piles must be verified in accordance with Eurocodes using the geotechnical (GEO) set of partial factors and the relevant inequality (EN 1997, 2004). Failure of a pile group in uplift may be accounted for using the block strength of the soil containing the piles, and should be verified using the uplift (UPL) set of partial factors and the corresponding inequality (EN 1997, 2004).

The main difference between the methods for determining the basic resistance of piles in tension and in compression is that the base resistance is always negligible in tension, unlike in compression.

Calculation of the design actions

The design value of the mechanical action on a single pile or a group of piles, F_d, can be calculated directly through the combination of relevant actions, or it can be derived from representative values of actions:

$$F_d = \gamma_F F_{rep}, \text{ where}$$

$$F_{rep} = \psi F_k$$

Where γ_F and ψ are partial factors, and F_{rep}, F_k are the representative and characteristic values of the considered actions, respectively.

In situations where a single permanent action G_{rep} and a single variable action Q_{rep} are considered, the combination of actions allows the definition of the design axial compressive load F_{cd} as the product of the representative permanent and variable actions with their corresponding partial factors γ_G and γ_Q:

$$F_{cd} = \gamma_G G_{rep} + \gamma_Q Q_{rep}$$

Two sets of recommended partial factors for actions and their effects are presented in Table 3, in accordance with EN 1997 (2004). The self-weight of the pile should be included in the calculation of the design axial load F_{cd} . However, the assumption that the pile's self-weight is balanced by the surcharge allows this contribution to be excluded from both F_{cd} and R_{cd}. The self-weight of the pile may not cancel out the surcharge if settlement is significant, the soil is lightweight, or the pile extends above the ground surface (EN 1997, 2004).

Table 3. Recommended Partial Factors for Actions and Effects of Actions

Action	Symbol	Set	
		A1	A2
Permanent			
Unfavorable	γ_G	1.35	1.0
Favorable		1.0	1.0
Variable			
Unfavorable	γ_Q	1.5	1.3
Favorable		0	0

Source: EN 1997:2004, Eurocode 7: Geotechnical Design, London, United Kingdom, p. 171.

Design ground resistance calculation

The design value of compressive soil resistance can be obtained in two ways: by treating the resistance as a total resistance, or by dividing it into a shaft friction component and a base resistance component, developed along the length of the pile. In the first case, the design value of such resistance is obtained by dividing the total characteristic resistance R_{ck} by the corresponding partial factor γ_t.

$$R_{cd} = \frac{R_{ck}}{\gamma_t}$$

In the second case, the design value of the compressive ground resistance is obtained by dividing the characteristic values of shaft friction and base resistance, R_{sk} and R_{bk}, by their corresponding partial factors γ_s and γ_b, respectively.

$$R_{cd} = \frac{R_{sk}}{\gamma_s} + \frac{R_{bk}}{\gamma_b}$$

Different sets of partial factors should be considered for driven, bored, and CFA piles [12] EN 1997-1 (2004). Four sets of proposed values for these factors are presented in Table 4 in

accordance with EN 1997 (2004). The following aspects should be taken into account when applying the partial factors:

- The values of the partial factors R1, which are greater than 1.0 for bored and CFA piles under compression, and equal to 1.0 for driven piles;
- The partial factors R2 are the same for all three types of piles;
- The partial factors R3 are all equal to 1.0 for all three types of piles.
- The partial factors R4 are greater than 1.0 and higher than the values of the partial factors R2.
- For tension piles, only the shaft friction resistance factor is relevant, and it has the same value for all three types of piles.

In the following section, aspects related to the definition of the design value of compressive ground resistance are presented. For this purpose, the three commonly used approaches, static pile load testing, results derived from the soil profile, and strength parameters, may be considered for design purposes.

Table 4. Recommended Partial Resistance Factors for Driven, Bored, and CFA Piles

Resistance	**Symbol**	**Set**			
		R1	**R2**	**R3**	**R4**
Partial Resistance Factors for Driven Piles					
Base Resistance	γ_b	1.0	1.1	1.0	1.3
Shaft resistance	γ_s	1.0	1.1	1.0	1.3
Total resistance	γ_t	1.0	1.1	1.0	1.3
Shaft Friction in Tension	$\gamma_{s,t}$	1.25	1.15	1.1	1.6
Partial Resistance Factors for Bored Piles					
Base Resistance	γ_b	1.25	1.1	1.0	1.6
Shaft resistance	γ_s	1.0	1.1	1.0	1.3
Total resistance	γ_t	1.15	1.1	1.0	1.3
Shaft Friction in Tension	$\gamma_{s,t}$	1.25	1.25	1.1	1.6
Partial Resistance Factors for CFA Piles					
Base Resistance	γ_b	1.1	1.1	1.0	1.45
Shaft resistance	γ_s	1.0	1.1	1.0	1.3
Total resistance	γ_t	1.1	1.1	1.0	1.4
Shaft Friction in Tension	$\gamma_{s,t}$	1.25	1.15	1.1	1.6

Source: EN 1997:2004, Eurocode 7: Geotechnical Design, London, United Kingdom, p. 171.

- **Calculation of bearing capacity based on static load test**

Load tests directly allow the determination of the characteristic ground resistance R_{ck} from the measured resistance values R_{cm} associated with the ultimate limit state, through the application

of correlation factors ξ_1 and ξ_2 to the mean and minimum values of the measured actions, as shown below:

$$R_{ck} = \min\left\{\frac{(R_{cm})_{mean}}{\xi_1}; \frac{(R_{cm})_{min}}{\xi_2}\right\}$$

The recommended values for ξ_1 and ξ_2 , depending on the number of load tests performed, are provided in Table 5 in accordance with EN 1997 (2004). The discussed values of ξ_1 and ξ_2 illustrate the advantage of conducting a higher number of load tests, as the correlation factors decrease with the increasing number of tests, resulting in higher values of R_{ck} . For structures that have sufficient deformation resistance under load transfer from weaker to stronger piles, the values of ξ_i may be divided by 1.1 (EN 1997, 2004).

For compressive piles, it is often difficult to identify the load value corresponding to the expected achievement of the ultimate limit state from the results of static load testing, as the load-settlement curve of the pile typically exhibits continuous curvature. Particularly in such cases, a pile head settlement equal to 10% of the pile diameter should generally be taken as the failure criterion (EN 1997, 2004). [21]

Table 5. Recommended Correlation Factors for Determining the Characteristic Pile Resistance from Static Load Test Results

Number of Tests	1	2	3	4	≥5
ξ_1	1.4	1.3	1.2	1.1	1.0
ξ_2	1.4	1.2	1.05	1.0	1.0

Source: EN 1997:2004, Eurocode 7: Geotechnical Design, London, United Kingdom, p. 171.

- **Calculation of bearing capacity based on data from borehole samples**

Geotechnical test profiles obtained from in situ investigations, such as the cone penetration test (CPT) or the standard penetration test (SPT), directly allow for the determination of the characteristic design ground resistance R_{ck} from the measured resistance values R_{cm} associated with the ultimate limit state, by applying the correlation factors ξ_3 and ξ_4 to the mean and minimum values of the measured actions, as follows:

$$R_{ck} = \min\left\{\frac{(R_{cm})_{mean}}{\xi_3}; \frac{(R_{cm})_{\min}}{\xi_4}\right\}$$

The recommended values for ξ_3 and ξ_4, depending on the pile investigations, are provided in Table 6 in accordance with EN 1997 (2004).

Table 6. Recommended Correlation Factors for Determining the Characteristic Pile Resistance from Borehole Samples

Number of Tests	1	2	3	4	5	7	10
ξ_3	1.4	1.35	1.33	1.31	.29	1.27	1.25
ξ_4	1.4	1.27	1.23	1.2	1.15	1.12	1.08

Source: EN 1997:2004, Eurocode 7: Geotechnical Design, London, United Kingdom, p. 171.

- **Calculation Based on Shear Strength Parameters of the Soil**

Soil shear strength parameters allow for the indirect determination of the shaft and base components of the characteristic ground resistance, R_{sk} and R_{bk}, through appropriate bearing capacity expressions. Since the soil absorbs all actions through the piles, the selection of characteristic values of the geotechnical parameters should take the following into account (EN 1997, 2004):

- Geological and other background information, such as data from previous projects;
- The variability of the measured values and other relevant information, for example, from existing knowledge;
- Type and Number of Samples
- Extent of Fieldwork and Laboratory Investigation;
- Extent of the soil zone that governs the behavior of the geotechnical structure;
- Consideration of the limit states;
- The ability of the geotechnical structure to transfer actions from weaker to stronger zones in the soil.

To obtain the design value of ground resistance using the presented approach, the partial factors γ_M may be applied either to the characteristic soil properties X_k, to the characteristic resistance values R_k, or to both. Two sets of proposed partial factors for the soil properties γ_M are presented in Table 7 in accordance with EN 1997 (2004).

Table 7. Partial Factors for Soil Parameters

Soil Parameter	Symbol	Set	
		M1	M2
Internal friction angle*	$\gamma_{\varphi'}$	1.0	1.25
Effective Cohesion	$\gamma_{c'}$	1.0	1.25
Undrained Shear Strength	γ_{c_u}	1.0	1.4
Uniaxial Compressive Strength	γ_{UCS}	1.0	1.4
Unit weight	γ	1.0	1.0

*This factor is applied to $\tan\phi$

Source: EN 1997:2004, Eurocode 7: Geotechnical Design, London, United Kingdom, p. 171.

3.2.2.4. Design according to the Serviceability Limit State

General

The geotechnical and structural behavior of energy piles, as well as the structural performance of the connected superstructure at the serviceability limit states, can be verified for the effects of thermal actions, applied either independently or in combination with mechanical actions (Rotta Loria et al., 2019). The following aspects should be taken into account when analyzing energy piles:

Limitation of individual or group vertical displacements (e.g., differential and average), taking into account group effects;

- Control of deflection and distortion angle;
- Limitation of Compressive Stresses;
- Limitation of Tensile Stresses;
- Crack Control

Control of vertical displacements, deflections, and distortion angle

The limitation of vertical displacements of energy piles is closely related to the control of deflection and angular distortion that characterize these foundations, representing a fundamental step in ensuring the required geotechnical serviceability performance. This outcome can be achieved by ensuring that only a relatively small portion of the soil strength is mobilized in order to keep deformations within the specified limits.

Foundation displacements are critical, and any differential settlements leading to structural deformations must be limited to ensure that they do not result in the attainment of a limit state in the structure (EN 1997, 2004). The selection of design values for allowable displacements and deformations depends on a wide range of parameters, and the calculation of differential settlements should take into account: (1) the occurrence and magnitude of vertical displacements and ground movements; (2) random and systematic variations in soil properties; and (3) the structural resistance to deformation under loading during and after construction, among others. These aspects should be considered as key criteria for evaluating vertical displacements of energy piles caused by mechanical and thermal actions. The imposed limitations should be defined and justified by the designer. In essence, it is practically impossible to establish general recommendations that apply to all design situations: vertical displacements that are acceptable in some projects may be unacceptable in others due to the structural concept and detailing, the intended function of the structure, and the response of the users.

The critical condition related to the displacement of the head of energy piles may be associated with the combined effect of downward-directed mechanical action and negative temperature changes applied to the piles, which counteract the settlement caused by the downward mechanical load. Contrary to this considered action, assuming that the energy piles are unrestrained provides a conservative estimate of the vertical displacement of the pile head that is expected to occur in practice (Rotta Loria et al., 2019).

Assuming a balanced temperature field at the surface over time, an increase in the settlement of the head of individual energy piles may occur due to the following aspects:

- Group effects;
- Irreversible phenomena;
- Changes in soil properties;
- Negative skin friction;

- Time-Dependent Effects

In essence, accounting for all the aspects requires the execution of comprehensive analyses (e.g., numerical), including appropriate mathematical formulations. In practice, however, such comprehensive analyses are often impractical; therefore, simplified calculations are typically performed, incorporating the following aspects to validate the obtained results or to draw conclusions for design justification (Rotta Loria, 2018):

- Along the length of energy piles, group effects and interactions arise due to the presence of mechanical and thermal actions from neighboring piles located in proximity (Jeong et al., 2014; Mimouni and Laloui, 2015; Salciarini et al., 2015; Saggu and Chakraborty, 2016; Salciarini et al., 2017; Rotta Loria and Laloui, 2017, 2018). These phenomena lead to different responses in piles within a group compared to single, isolated piles. The analysis of deformations in individual energy piles is not exhaustive and cannot accurately represent the actual behavior of energy piles operating within a closed group (Rotta Loria and Laloui, 2018). In contrast, analyses of stress development in individual energy piles are considered useful because they offer conservative estimates, even for piles arranged in a closed group (Rotta Loria and Laloui, 2018).
- Irreversible phenomena in the soil surrounding energy piles may be induced by the cyclic influence of thermal actions, applied either independently or in combination with mechanical actions (Dupray et al., 2014; Rotta Loria et al., 2015; Saggu and Chakraborty, 2015; Ozudogru et al., 2015; Salciarini et al., 2015, 2017; Suryatriyastuti et al., 2015; Gawecka et al., 2016; Ng et al., 2016; Adinolfi et al., 2018). The significance of these phenomena depends on: (1) the level of mechanical loading applied before the thermal action, (2) the amplitude of the thermal cycles, (3) the number of thermal cycles, and (4) the characteristics of the soil. Limiting the magnitude of the applied mechanical actions to approximately 30% of the value associated with 'failure' is often the most effective approach to prevent the intensification of irreversible soil phenomena, and this effect may be neglected in cases where more detailed information is not available.
- Changes in soil properties may be induced, for example, by the phenomenon of mechanical degradation and by effects caused by thermal actions (Cekerevac and Laloui, 2004; McCartney and Rosenberg, 2011; Vieira and Maranha, 2016; Eslami et al., 2017). The changes under consideration may result in irreversible phenomena, although the physical processes that characterize these changes differ from those previously mentioned and highlighted in (2).

Mechanical degradation of the pile-soil interface due to repeated shearing caused by mechanical and thermal loading and unloading may be considered, particularly under two loading scenarios: (1) significant magnitudes of mechanical actions applied before thermal cyclic loading, or (2) significant thermal cyclic actions gradually applied to a limiting mechanical action. However, this phenomenon is generally treated as temperature-independent and considered negligible under most boundary conditions that define energy piles, provided that the intensity of thermal and mechanical actions is previously limited to

avoid the amplification of irreversible phenomena in the soil. Neglecting the reduction in interface shear strength due to cyclic loading of energy piles is consistent with French recommendations (CFMS - SYNTEC - SOFFONS - FNTP, 2017).

The effects of thermal actions should be taken into account due to changes in the strength and deformation characteristics of the soil. In practice: (1) the effect of temperature on the shear strength properties of soils and the soil-concrete interface, such as the angle of shear strength under constant volume conditions can be neglected within the typical temperature range of 2°C to 60°C relevant to current energy pile applications; and (2) the effect of temperature on the deformation characteristics of the soil, such as the Young's modulus of elasticity, may be neglected for coarse-grained soils, whereas it becomes relevant for fine-grained soils within the same temperature range. However, this temperature sensitivity is limited in magnitude and is therefore typically disregarded in design, except in cases involving foundations on temperature-sensitive soils.

- Negative skin friction or the degradation phenomenon may be induced by the influence of thermal actions, applied either independently or in combination with mechanical actions, particularly in energy piles installed in lightly over-consolidated to normally consolidated soils. To address negative skin friction and the degradation phenomenon caused by body forces, as discussed in the previous scenarios, it is commonly assumed that the neutral point lies at the interface between the stiff and soft layers. Negative skin friction is then calculated as a fraction (depending on the soil type) of effective vertical stress. Negative skin friction and degradation phenomena may also arise due to thermal actions and the thermal collapse of soils subjected to positive temperature changes (Bourne-Webb et al., 2016). Soil-induced actions should be considered in design by using their maximum expected values, defined by the upper-bound compressibility and strength of the soil (EN 1997-1, 2004). In this context, one of the following two approaches should be adopted: (1) ground movement is treated as an action in the design calculations and an interaction analysis is conducted; or (2) the action exerted on the pile as a result of ground movement is treated directly as the design action.
- Time-dependent effects, such as consolidation or creep, may characterize the behavior of energy piles subjected to mechanical or thermal actions. For piles subjected solely to mechanical actions, imperceptible settlements due to creep may occur when the load level is approximately 30% of the failure load. A further increase of 10% beyond this estimate may be attributed to consolidation in fine-grained soils (Poulos and Davis, 1980). Creep may be accelerated by rising temperatures (Leroueil and Soares Marques, 1996; Mitchell and Soga, 2005; Laloui et al., 2008), potentially resulting in greater long-term settlement. Although there is no conclusive evidence of unacceptable displacements caused by thermally induced cracking, limiting the level of mechanical actions may help ensure appropriate performance, similar to that expected for piles subjected to mechanical actions alone.

In the assessment of vertical deformations of energy piles, considering the temperature sensitivity of the volumetric behavior of soils may be important when the thermal conductivity of the soil exceeds that of the pile. The rationale for this aspect is that, during successive phases of geothermal loading in energy piles, the corresponding deformation may be governed by that of the soil, and such a phenomenon could be unforeseen. [23]

Limit stress and crack control

The limitation of compressive and tensile stresses occurring in energy piles as a result of thermal and mechanical actions is closely linked to crack control in such foundations and represents a fundamental step in ensuring the required structural serviceability of these elements. This challenge can be effectively addressed by applying the verification procedures outlined within the Eurocode framework (EN 1992, 2004) and by providing a minimum area of longitudinal reinforcement in accordance with the specified standards.

Attention should also be given to the development of stresses in energy piles founded in soils characterized by a higher thermal conductivity coefficient. The reason for this is that tensile stresses may be induced during the heating of energy piles, while compressive stresses may occur during cooling. Regardless of the ratio between the thermal conductivity of the soil and that of the energy pile, assuming that the energy piles are restrained at the head by an infinitely rigid structural element (e.g., a slab) provides a conservative estimate of the stress variation induced by thermal actions that are expected to occur in practice (Rotta Loria et al., 2019).

Concrete cover and reinforcement

To calculate the minimum concrete cover and the minimum reinforcement area of energy piles, the provisions outlined in EN 1992 (2004) should be taken into account. Adequate concrete cover, defined as the distance from the surface of the reinforcement to the outer edge of the concrete, is required to ensure durability.

Bored energy piles with a diameter of up to 600 mm are characterized by a concrete cover of 50 mm, while for larger diameters, a cover of 60 mm is applied (EN 1992, 2004). The concrete cover may be reduced to 40 mm when a permanent casing is provided on the outer side (EN 1992, 2004). The minimum cover should be increased to 75 mm if: (1) the piles are constructed in sandy soils without casing; (2) they are located in an exposure class characterized by freeze-thaw cycles (Class 5 according to DD ENV 206 (1992)); (3) concrete placement is carried out under water conditions and the maximum aggregate size is outdated; and (4) the reinforcement is placed subsequently after the concrete has been cast (EN 1992, 2004). A minimum cover of 80 mm is required for high-density concrete, although a greater cover is generally recommended (BS 8004, 2015).

Bored piles may be reinforced with the recommended values for minimum longitudinal reinforcement area $A_{r,\min}$, depending on the cross-sectional area of the concrete A_c. Table 8 presents proposed values for the minimum reinforcement area in accordance with EN 1992 (2004). It must be ensured that these provisions provide adequate ductility (Rotta Loria et al., 2019). The minimum diameter of the longitudinal bars should not be less than 16 mm, and at least six longitudinal bars must be provided (EN 1992, 2004). The clear spacing between bars, measured along the pile circumference, should not exceed 200 mm (EN 1992, 2004). The

arrangement of longitudinal bars must allow for proper concrete flow, but the spacing should not exceed 400 mm [12] [13] (EN 1992, 2004).

A minimum diameter of 6 mm [12] [13] should be considered for transverse reinforcement provided in the form of links, stirrups, or spiral reinforcement, while a diameter of 5 mm should be applied for welded wire mesh (EN 1992, 2004).

Table 8. Recommended Values for Minimum Longitudinal Reinforcement Area in Bored Piles

Pile Cross-Sectional Area, A_c	**Minimum Longitudinal Reinforcement Area,** $A_{r,\min}$
$A_c \leq 0.5\ m^2$	$A_r \geq 0.005\ A_c$
$0.5\ m^2 \leq A_c \leq 1.0\ m^2$	$A_r \geq 25\ cm^2$
$A_c > 1.0\ m^2$	$A_r \geq 0.0025\ A_c$

Source: EN 1992:2004, Design of Concrete Structures - Part 1-1: General rules for building

4. PHYSICAL MODELLING

4.1. Experimental modelling

A circular model tank with dimensions of 200 x 150 cm (diameter x height) was used in the model tests. Figure 28 and Figure 29 show the lab-scale model setup and the instrument layout. The pile was 110 cm long with a diameter of 15 cm. The embedded length (L) of the pile in the soil was 100 cm. The toe of the energy pile prototype was 50 cm distant from the bottom of the tank (3.33D), which was longer than the distance in Goode et al. (2014) and McCartney and Rosenberg (2011); therefore, the results would not be affected according to the boundary conditions.

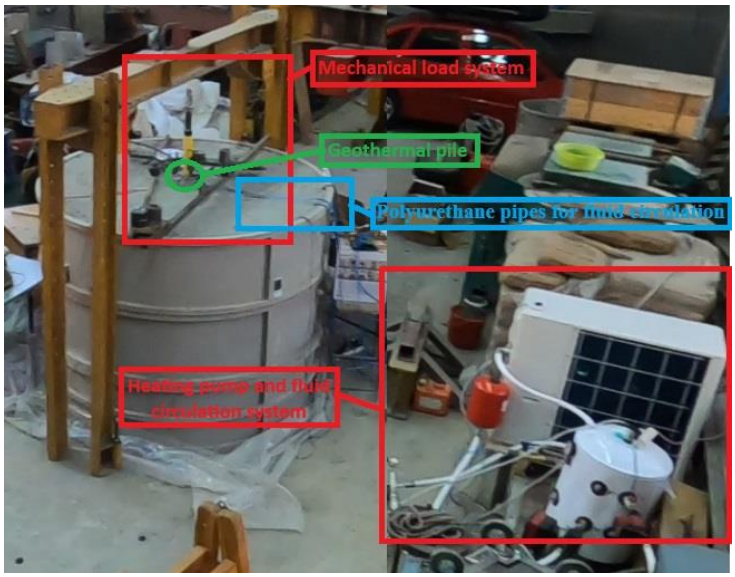

a)

b)

Figure 28. a) Lab-scale model setup of geothermal pile; b) Reinforcement cage and arranged pipe

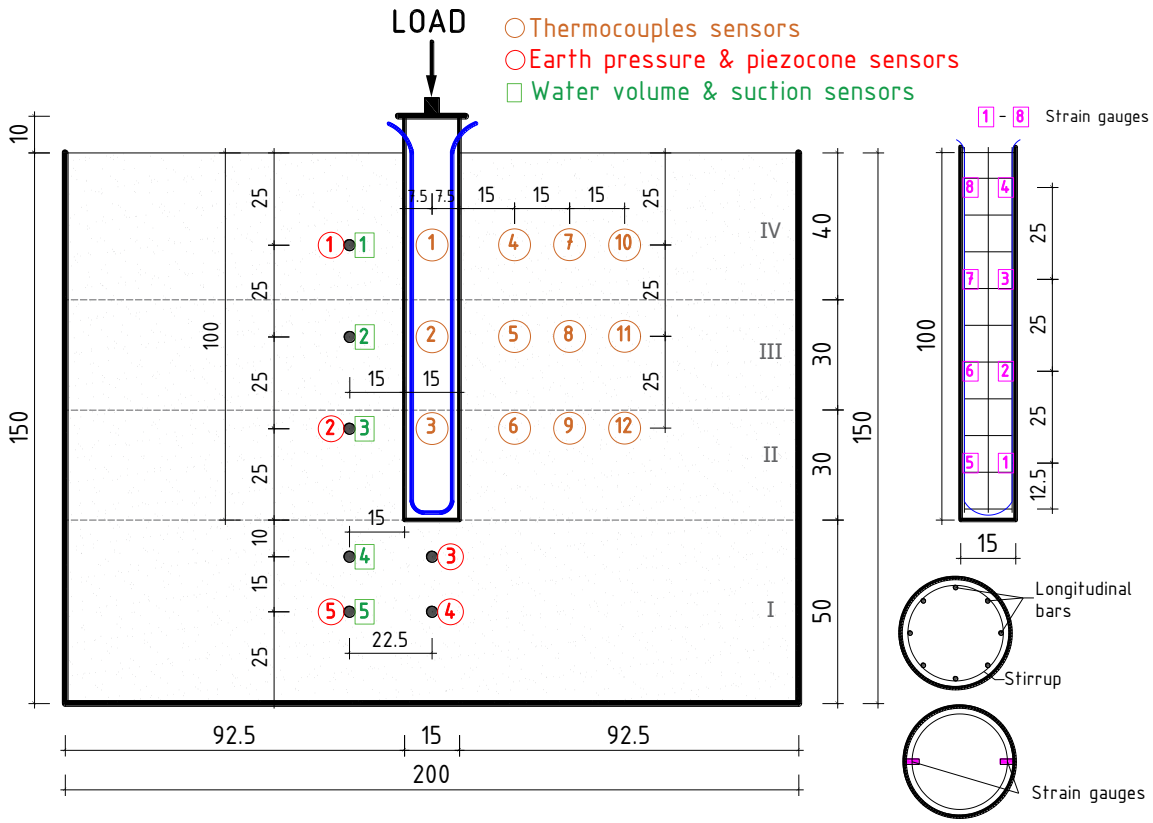

Figure 29. Lab-scale model setup scheme - Instrumentation layout and cross-section of geothermal pile

Six types of sensors, 40 sensors in total, were utilized in the monitoring data:

- thermocouple sensors
- pressure transducer sensors,
- piezocone sensors (pore pressure cells)
- suction sensors,
- volumetric water content sensors, and
- Strain gauges

As illustrated in the figure above, the left-hand side shows, with dark green color, the positions of sensors numbered 1, 2, and 3, which are positioned 15 cm from the pile axis, while position 4 is located 15 cm from the pile axis horizontally and 10 cm below the pile shaft. Position 5 is 15 cm away from the pile axis horizontally and 25 cm vertically. These positions contain water volume and suction sensors. Red color marks show the sensors of earth pressure and piezocone sensors. Positions 1 and 2 are positioned 15 cm from the pile horizontally, and 50 cm vertically between them. Positions 3 and 4 are on the same line of the pile axis, below the pile, 10 cm and 25 cm respectively. Position 5 is located 25 cm vertically below the pile and 15 cm horizontally from the pile.

Inside the pile body, three thermocouples were installed (T1-T3) on three different levels starting from 25 cm from the top of the pile and keeping this distance between the other two thermocouples. Furthermore, inside the pile body, 8 strain gauges are in four levels, 2 pieces for measuring strain inside the pile. On the right-hand side of the diagram, nine thermocouples

(T4-T12) are shown, installed in the surrounding soil in a three-row arrangement across three levels. In the horizontal direction, these thermocouples are positioned 15 cm from the pile shaft and are spaced 15 cm apart. Vertically, they are located 25 cm below ground level and are also spaced 25 cm apart, as shown in the figure above.

4.1.1. Materials

4.1.1.1. Concrete

The concrete mix for the pile was formulated using a mass ratio of 0.44:1:1.79:3 for water, cement, fine aggregate, and coarse aggregate, respectively. The compressive strength of the concrete was measured at 30.9 MPa. In addition, the thermal conductivity of the samples extracted from the test pile was determined using the Transient Plane Source (TPS) method.

Figure 30. Measurement of thermal conductivity using the Transient Plane Source (TPS) method

The thermal conductivity of the concrete was evaluated through three separate measurements, yielding values of 1.964, 1.844, and 2.059 W/m·K. These results indicate a relatively consistent thermal behavior of the material. Accordingly, the average thermal conductivity value of 1.96 W/m·K is considered representative for the concrete used in this study.

4.1.1.2. Pipes and heat pump system

The experimental model of the energy pile was instrumented with two U-shaped heat exchange pipes, which were carefully integrated within the steel reinforcement cage, as illustrated in Figure 31a. These pipes were fabricated from polyurethane, with an internal diameter of 4 mm

and an external diameter of 6 mm, selected for their flexibility and thermal stability. Thermal loads were applied by means of a heat pump system that circulated heated/cooled water with a flow rate of 1.6 m^3/h through a closed-loop network of polyurethane pipes embedded within the pile. The system utilized a high-efficiency DC Inverter air-to-water heat pump with a nominal thermal output capacity of 8 kW (Figure 31b). This setup enabled controlled thermal activation of the energy pile, simulating realistic operational conditions typically encountered in ground source heat exchange systems. The precise temperature control provided by the inverter technology ensured stable and gradual thermal loading throughout the heating and cooling phases of the experiment.

a) b)

Figure 31. a) Polyurethane pipes arranged with a reinforcement cage b) Heat pump system

During the heating phase, the circulating water reached a maximum temperature of approximately 45°C, while during cooling, the minimum temperature dropped to around 10°C. The entire experiment was conducted within a closed laboratory environment, where ambient temperatures were relatively stable, ranging between 16°C and 19°C, as monitored by a digital thermometer. This setup allowed for the controlled assessment of heat transfer behavior between the internal fluid and the surrounding soil medium, thereby simulating the real-world performance of geothermal piles under seasonal thermal loads.

4.1.1.3. Soil

Fine sand with a small silt content was used in the model test. The maximum dry density is equal to 1.55 gr/cm^3. The uniformity coefficient (C_u) and curvature coefficient (C_c) are 4.29 and 1.51, respectively.

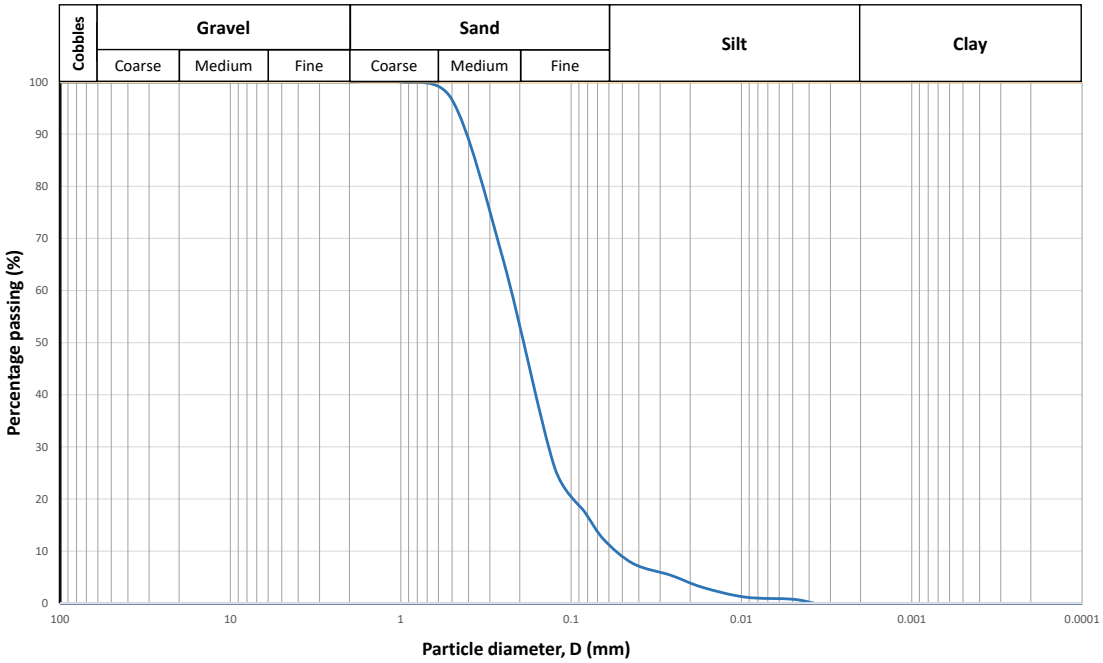

Figure 32. Granulometric curve (Susinov & Josifovski, 2018)

Table 9. Physical-mechanical soil characteristics (Susinov and Josifovski, 2018)

Characteristic	Unit	Value
Sand	%	82.5
Silt	%	17.5
C_u	/	4.29
C_c	/	1.51
Specific gravity G_s	/	2.72
USCS classification	/	Zone 1C (SM)
AASHTO classification	/	A-2-4

Due to the shape of the grains and the granulometric composition, the soil has very little plasticity, which cannot be precisely determined by the standard procedure for determining the Atterberg limits. The soil test fill was prepared using a controlled sand raining technique.

To evaluate the thermal behavior of soils under varying moisture conditions, a series of controlled laboratory tests was designed and implemented. The primary objective was to determine the thermal conductivity of soil in both dry and saturated states using a comparative experimental approach. Understanding the thermal response of soils under various moisture regimes is crucial for applications such as energy geostructures, where heat transfer through the surrounding soil significantly impacts overall system performance.

Two dedicated experimental schemes were developed to simulate realistic heat flow scenarios under laboratory-controlled conditions. These setups were specifically designed to isolate the effect of soil moisture content on heat propagation by ensuring consistent geometry, boundary conditions, and instrumentation across both test environments.

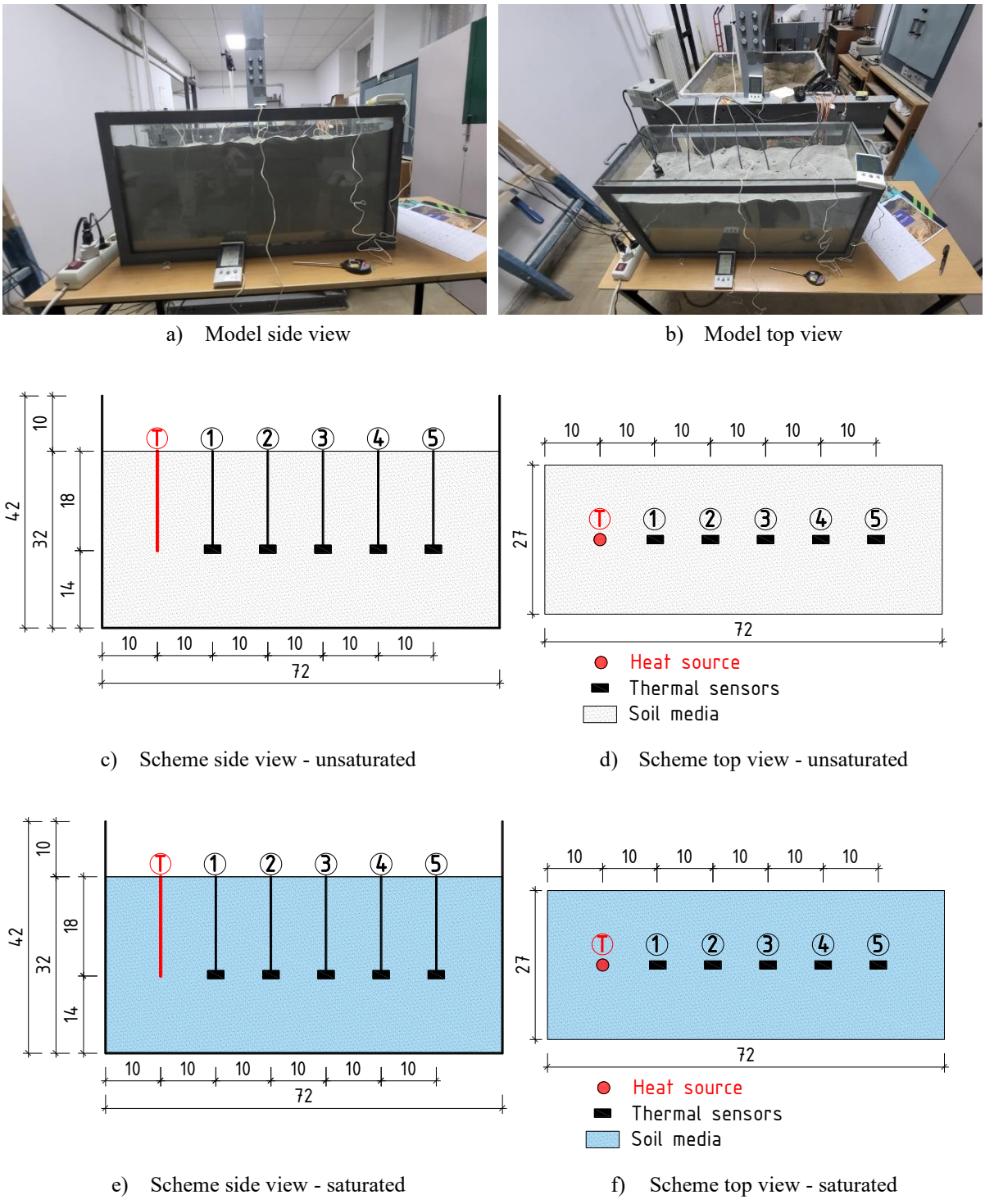

a) Model side view

b) Model top view

c) Scheme side view - unsaturated

d) Scheme top view - unsaturated

e) Scheme side view - saturated

f) Scheme top view - saturated

Figure 33. Model setup for determining the thermal conductivity of soil in dry and saturated soil media

Figure 33a-Figure *33*f presents the schematic representations of the two configurations used: one with a dry soil medium and the other with a saturated soil medium. The setup includes a centrally placed heat source, along with temperature sensors arranged at various locations to monitor the thermal field. The collected data served as the basis for determining the thermal conductivity of the soil under the specified conditions.

The experimental procedure was conducted on both soil models under constant temperature conditions, with each test running continuously for a total duration of 21 hours. This controlled

timeframe was selected to ensure sufficient thermal propagation through the soil medium and to allow the system to reach a quasi-steady-state thermal response. Maintaining a consistent temperature throughout the testing period was essential for accurately evaluating the thermal conductivity and heat transfer behavior of the soil in both dry and saturated conditions.

Table 10. Geometric parameters of the test box

Test box	
Height	H=0.32 [m]
Width	B=0.27 [m]
Area	0.086 [m^2]

Table 11. Heat source characteristics

Dry soil medium	
Heat flux	Q=25 [W]
Temperature	T=56 [°C]
Saturated soil medium	
Heat flux	Q=25 [W]
Temperature	T=33 [°C]

- **Dry soil medium**

As shown in Figure 33c and Figure 33d, the first setup represents the thermal conductivity test performed in a dry soil medium. A controlled rectangular tank was filled with dry, homogeneous soil to a 32 cm depth. The central element of this configuration is a cylindrical heat source, marked with the symbol T, vertically embedded into the soil at 18 cm depth. Adjacent to this source, five digital thermometers (labeled “a” to “e”) and five thermal sensors (labeled “1” to “5”) spaced 10 cm horizontally, were installed. This sensor layout allows for precise recording of the temperature gradient as a function of both distance and time during the heating process. The dry condition simulates soil with negligible moisture content, typical of arid or laboratory-dried samples.

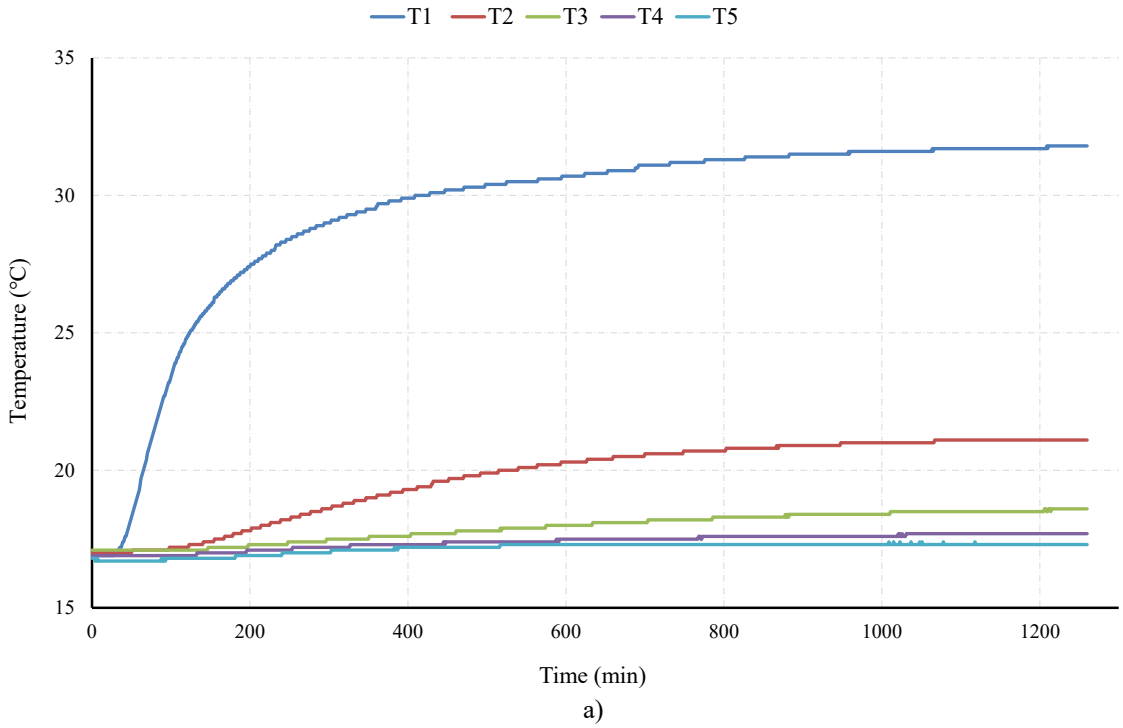

a)

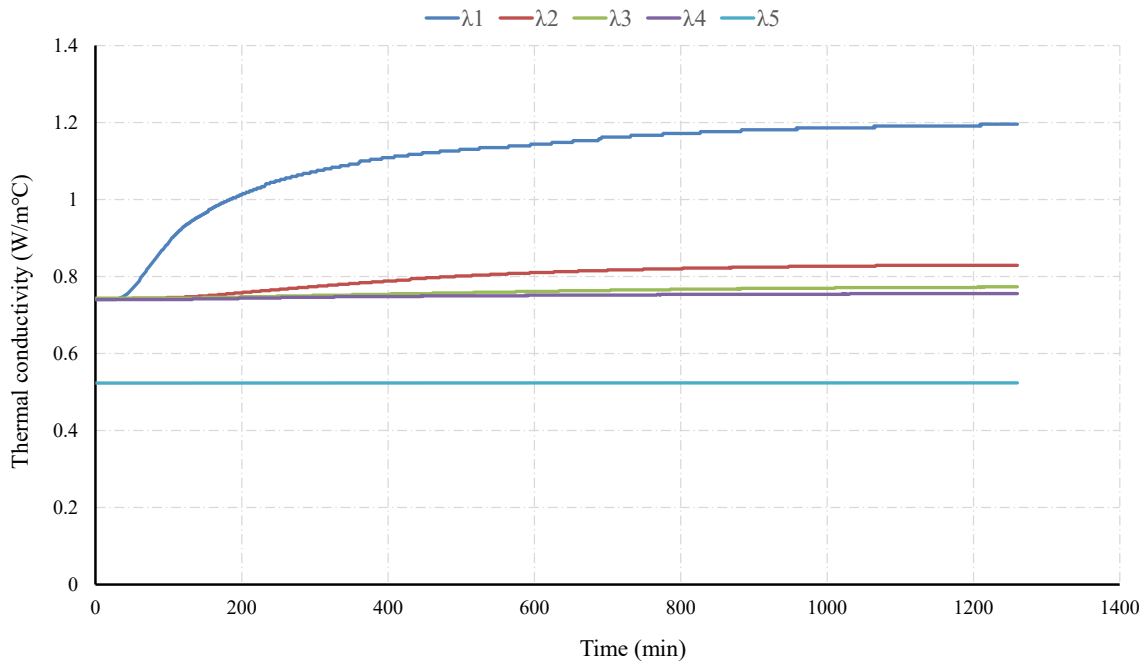

b)

Figure 34. Dry soil medium, a) Diagram of temperature changes; b) Diagram of thermal conductivity

The temperature-time graph (T1-T5) shows a clear gradient in thermal response among the five sensors (Figure 34a). Sensor T1, located closest to the heat source, experiences a rapid temperature rise, reaching approximately 32.5°C, while sensors farther from the source show progressively lower temperatures, with T5 stabilizing near 17.0°C. This trend confirms the radial dissipation of heat energy through the dry soil medium, with clear attenuation as distance increases.

The calculated thermal conductivity values (λ1-λ5) over time indicate that Sensor λ1, located nearest to the source, reaches a peak value of approximately 1.20 W/m·°C, while the remaining sensors exhibit lower values that stabilize between 0.50 and 0.85 W/m·°C (Figure 34b). These differences reflect both the thermal gradient and the soil's limited ability to conduct heat in unsaturated conditions. The average thermal conductivity for the dry soil, based on stabilized values of λ1-λ5, is approximately 0.75 W/m·°C.

This value aligns with literature-reported values for granular soils in dry states, which are typically lower due to the dominance of air voids reducing effective heat transfer.

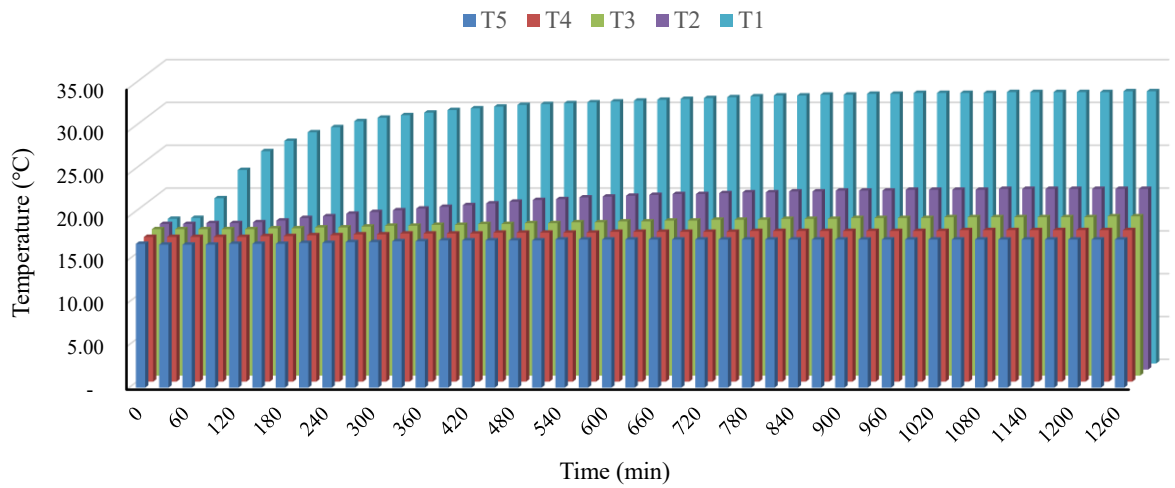

Figure 35. Diagram of temperature changes through time in five thermal sensors - Dry soil medium

The diagram shown in Figure 35, representing temperature variation across five distances (0.1 m to 0.5 m) over time, shows a consistent increase in temperature, particularly at the nearest distance (0.1 m), reaching values over 34°C. With increasing depth, the recorded temperatures decrease progressively, demonstrating the horizontal damping effect of heat in the dry soil. Even at the largest sensor (0.5 m), however, a noticeable temperature increase is observed, indicating that the heat was effectively transmitted across the entire column over the test duration.

- **Saturated soil medium**

Figure 33e and Figure *33*f present the configuration for testing the thermal conductivity in a saturated soil medium. The setup closely replicates the dry condition in terms of geometry and sensor placement, but differs in the medium: the soil was fully saturated with water before testing. The presence of water significantly alters the heat transfer characteristics due to the higher thermal conductivity of water compared to air-filled pore spaces. The same type of heat source (T) and identical arrays of digital thermometers (“a” to “e”) and thermal sensors (1 to 5) were utilized to ensure comparability between both test conditions.

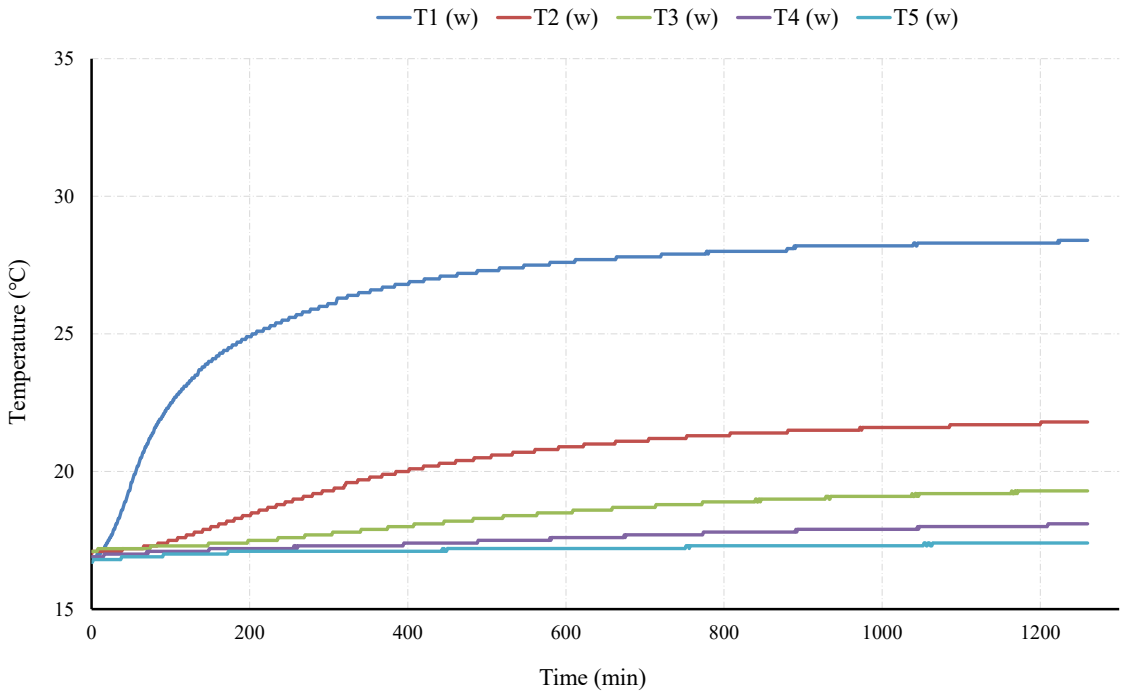

a)

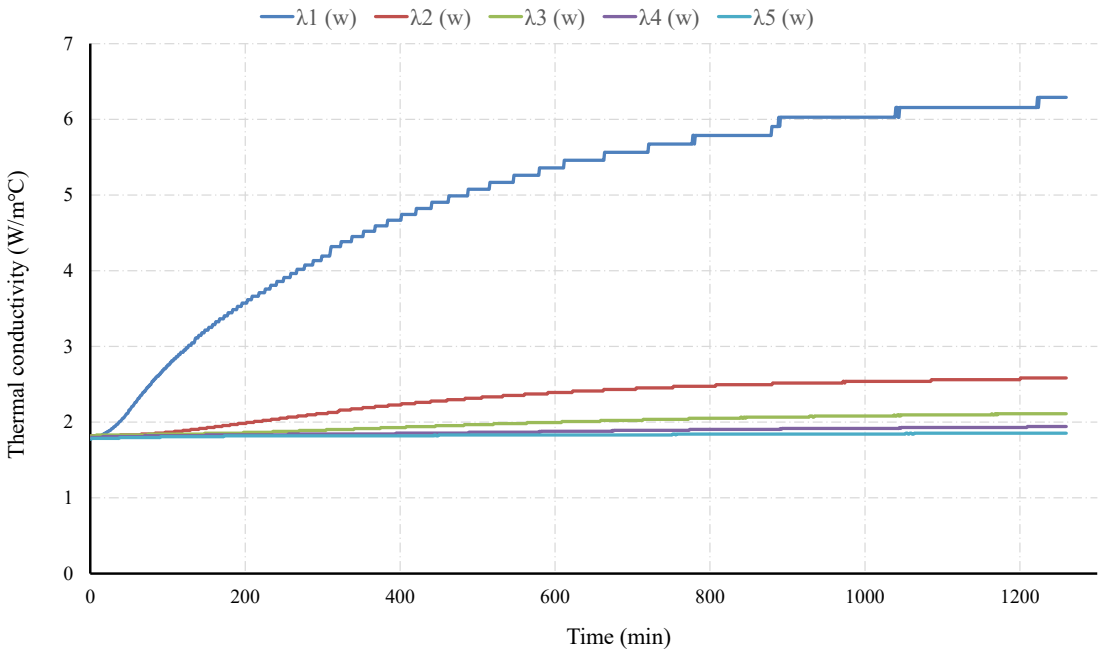

b)

Figure 36. Saturated soil medium, a) Diagram of temperature changes; b) Diagram of thermal conductivity

The temperature-time plot (Figure 36a) for thermal sensors TS-1 to TS-5 shows a clear gradient of thermal increase corresponds to the distance from the heat source. Sensor TS-1 (closest to the heat source) records a sharp rise in temperature up to approximately 28.5°C, while TS-5 (farthest) stabilizes at around 18.0°C. Compared to the dry condition, the temperature increase in saturated soil is more gradual and uniformly distributed, indicating a more efficient thermal propagation due to the presence of water in pore spaces.

The graph depicting calculated thermal conductivity values (λ1(w) to λ5(w)) reveals a notable improvement in thermal transfer capabilities (Figure 36b). Sensor λ1(w) shows the highest

value, stabilizing around 6.4 W/m·°C, while the remaining sensors show values ranging from approximately 1.80 to 2.8 W/m·°C. These elevated values reflect the increased thermal bridging effect in water-saturated pores. The average thermal conductivity for the saturated soil, based on the stabilized values of all five sensors, is approximately 3.24 W/m·°C.

This result is consistent with the expected enhancement of thermal conductivity in saturated granular materials and supports the key role of pore water in facilitating heat transfer.

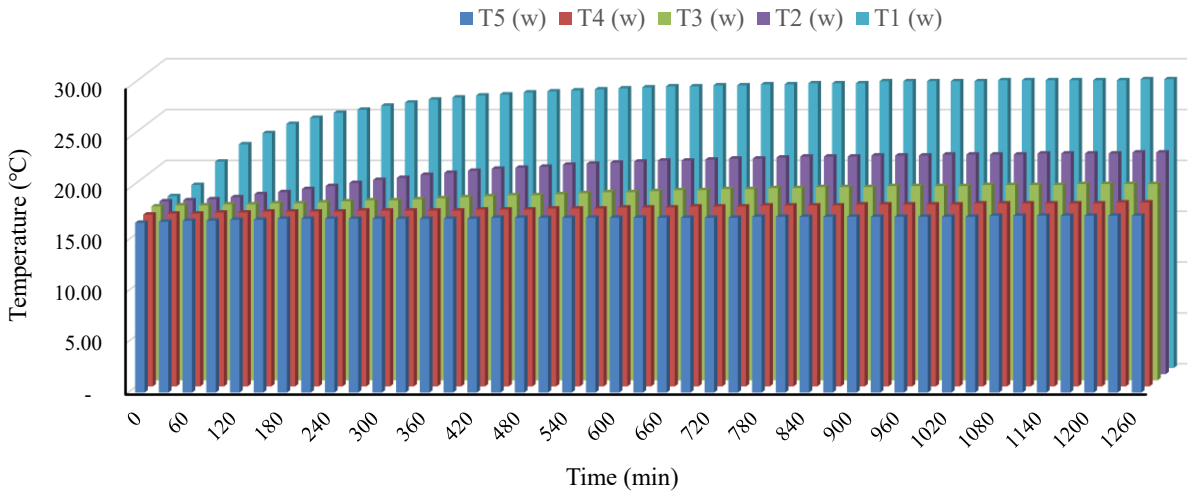

Figure 37. Diagram of temperature changes through time in five thermal sensors - Saturated soil medium

The diagram shown in Figure 37 presents the temperature evolution at distances ranging from 0.1 m to 0.5 m over time. A steady increase in temperature is observed across all sensors, with the nearest sensor (0.1 m) reaching values over 30°C. Even at larger distances, temperatures remain elevated, demonstrating homogeneous and effective thermal diffusion through the saturated soil profile.

Figure 38 presents a comparative analysis of the temperature evolution over time in both dry and saturated soil media, based on readings from five thermal sensors (T1 to T5 for dry soil, and T1(w) to T5(w) for saturated soil). The graph captures the dynamic thermal response of each medium over a testing period of approximately 1500 minutes under identical heating conditions.

The sensors labeled T1 to T5 correspond to temperature measurements in dry soil, while T1(w) to T5(w) represent the same measurements in saturated soil. Sensor 1 in both cases (T1, T1(w)) is located closest to the heat source and thus records the highest temperature increases. A clear trend of decreasing temperature magnitude is observed with increasing distance from the heat source, consistent for both soil types. Across all sensors, the temperature in the dry soil (darker lines) rises more sharply and reaches higher values compared to the corresponding sensors in saturated soil (lighter lines).

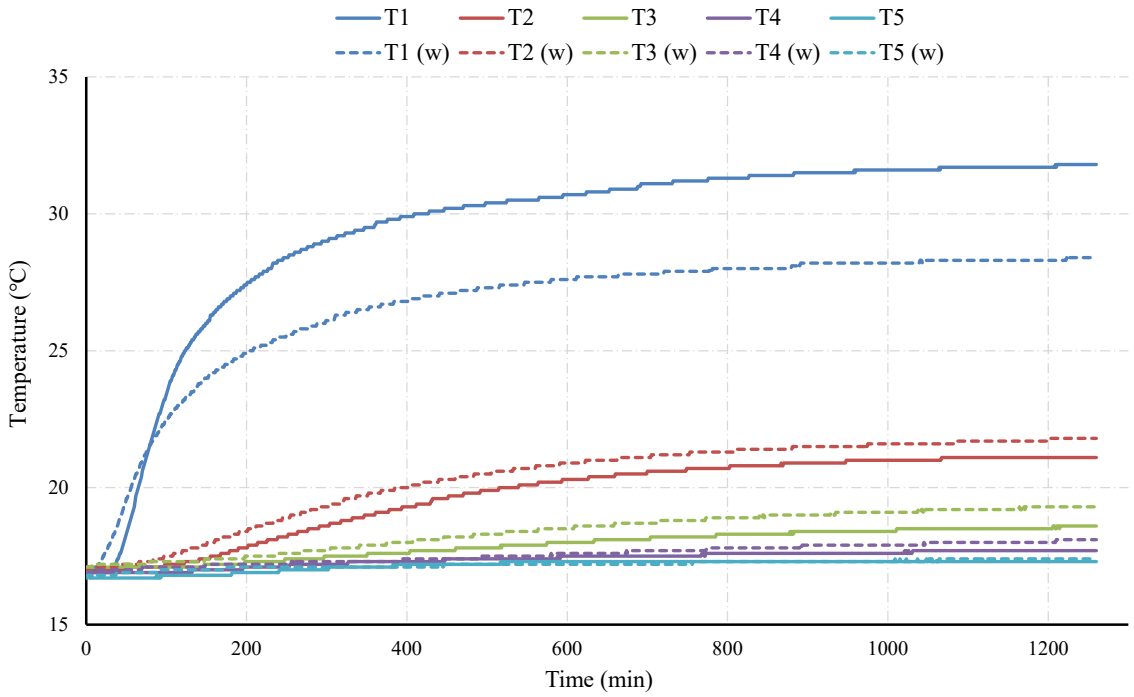

Figure 38. Diagram of temperature changes through time in five thermal sensors - Dry and Saturated Soil Medium

The steeper temperature rise in dry soil, especially evident in T1, indicates a more localized and concentrated heat accumulation near the heat source. This behavior is characteristic of materials with lower thermal conductivity, where heat is less efficiently distributed through the medium. In contrast, the temperature rise in saturated soil is slower, and the values are slightly lower at each corresponding sensor, suggesting more efficient heat dissipation. The presence of water increases the thermal conductivity of the medium, allowing heat to be more rapidly and evenly distributed away from the source. Despite the lower peak temperatures in the saturated medium, the overall heat transfer is more effective, as the medium avoids overheating near the source and delivers more uniform temperature increases across the entire profile. At the farthest sensor (T5 and T5(w)), temperature values converge, confirming that at greater distances the influence of the soil's moisture content becomes less pronounced, though still distinguishable.

This comparative graph highlights a fundamental difference in heat transfer mechanisms. In dry soil, thermal energy tends to accumulate near the source, resulting in steeper local gradients and less efficient distribution. In saturated soil, the higher thermal conductivity of water allows for broader spatial heat distribution, resulting in smoother gradients and more thermally responsive behavior. These observations underscore the importance of soil moisture content in the thermal design of energy geostructures, such as geothermal piles, where optimizing heat exchange with the surrounding soil is critical for long-term performance.

Figure 39 presents the variation of thermal conductivity (λ) over time for both dry and saturated soil media, as measured by five sensors placed at different locations from the heat source (λ1-λ5 for dry soil and λ1(w) - λ5(w) for saturated soil). The objective of this comparative analysis is to highlight the influence of moisture content on the heat transfer capacity of the soil.

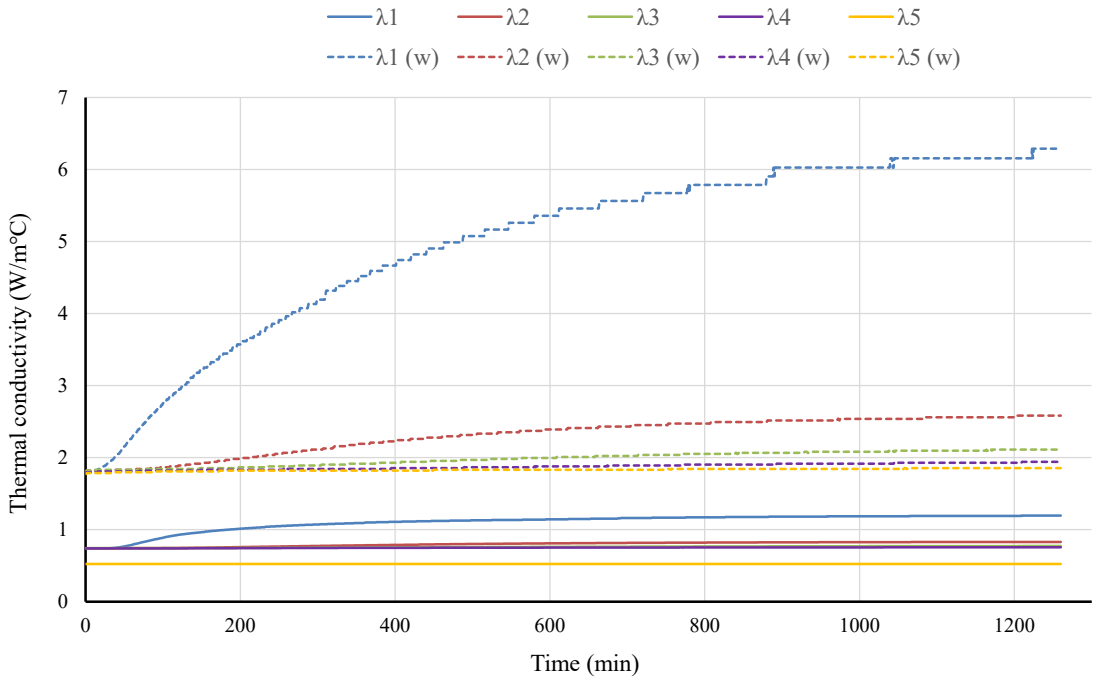

Figure 39. Diagram of thermal conductivity changes through time in five thermal sensors - Dry and Saturated Soil Medium

The vertical axis represents thermal conductivity in units of W/m·°C, while the horizontal axis shows time in minutes, spanning the entire 1500-minute test duration. For both dry and saturated conditions, sensor 1 (λ1, λ1(w)), located closest to the heat source, records the highest thermal conductivity values due to the steepest thermal gradients at this location. Across all sensors, the saturated soil curves (dashed lines) consistently register higher conductivity values compared to their dry soil counterparts (full lines). The thermal conductivity values tend to stabilize after approximately 1000 minutes, indicating that a quasi-steady thermal state has been reached.

The results clearly demonstrate that saturation significantly enhances the thermal conductivity of soil. This effect is most pronounced near the heat source, where λ1(w) reaches values above 6.4 W/m·°C, compared to λ1 in the dry soil, which stabilizes around 1.28 W/m·°C. For sensors located farther from the heat source (e.g., λ5 and λ5(w)), the difference is still notable, with saturated soil exhibiting values around 1.9-2.1 W/m·°C, while dry soil remains below 0.9 W/m·°C. This enhancement is attributed to the higher thermal conductivity of water compared to air. In saturated conditions, water fills the soil pores, forming continuous thermal bridges between soil particles, thus enabling more efficient heat conduction. In contrast, air-filled pores in dry soil reduce the effective thermal contact area and introduce thermal resistance. The smoother and faster rise in λ values for saturated soil also indicates a more stable and efficient heat transfer regime, which is particularly beneficial for energy geostructure applications like geothermal piles and ground heat exchangers.

The average thermal conductivity of saturated soil was found to be approximately 3.24 W/m·°C, significantly higher than the dry soil average of 0.88 W/m·°C. The time required for conductivity values to stabilize is shorter in saturated conditions, implying quicker thermal equilibrium due to the better heat conduction pathways. The results validate the critical role of

moisture in soil thermal behavior and emphasize the need to account for saturation levels when modeling or designing thermally active geostructures.

4.2. Testing procedure

The application of thermo-mechanical loads during testing is systematically organized into six distinct phases. These phases are carefully designed to ensure a comprehensive evaluation of the material's response under varying thermal and mechanical conditions. A detailed diagram illustrating the sequence of these phases is provided in the figures below, offering a visual representation of the testing process.

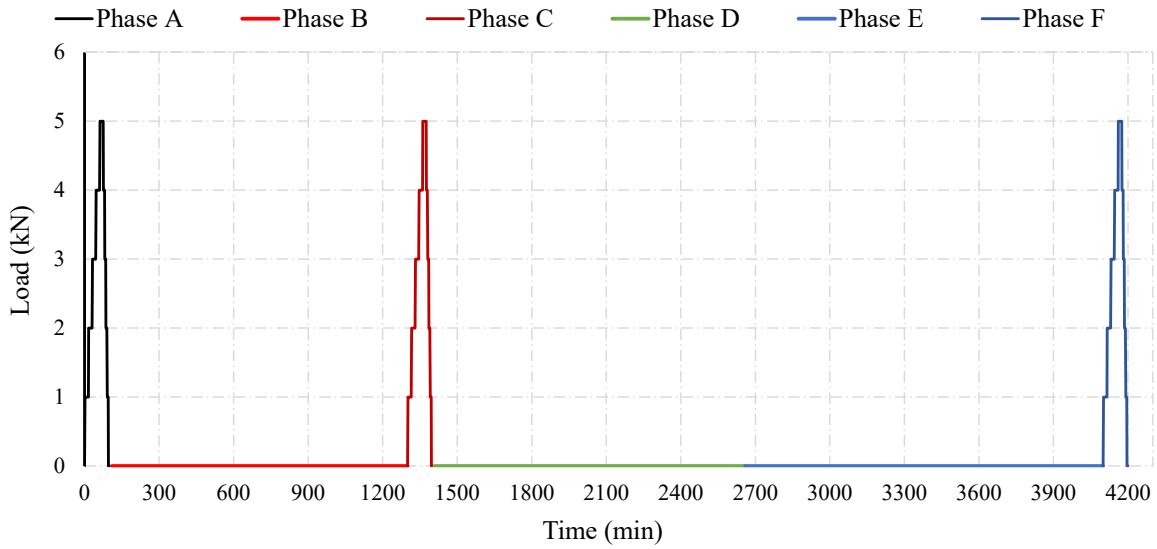

Figure 40. Loading phases during the testing

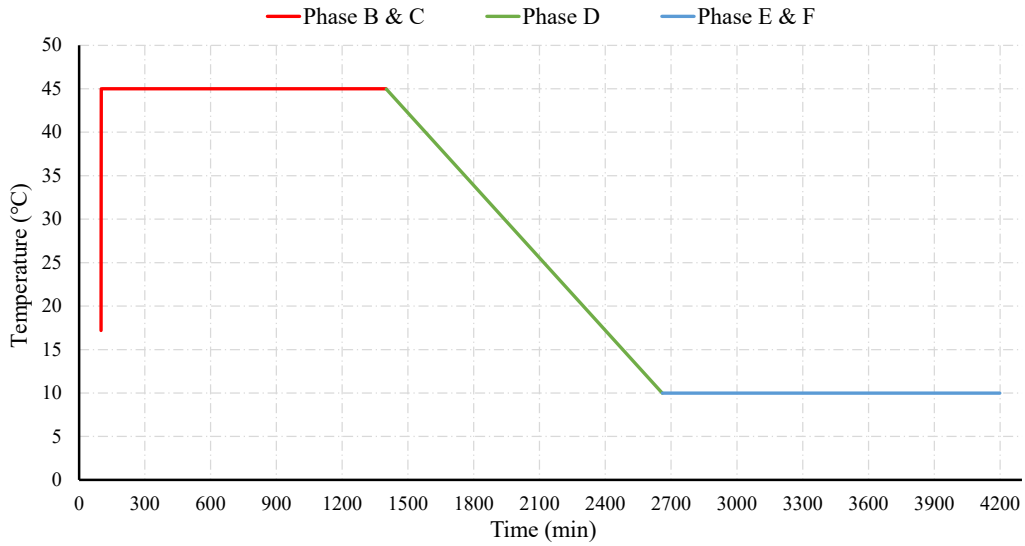

Figure 41. Thermal loads applied to the pile as per the loading phases scheme

The application of thermo-mechanical loads during testing is systematically organized into six distinct phases, each designed to evaluate the response of the pile under various loading conditions. A diagram illustrating the sequence of these phases is presented in the figures below.

Phase A: involves the application of a mechanical load, with a maximum load of up to 5 kN, representing 50% of the pile's ultimate bearing capacity. This capacity has been determined through prior software calculations specific to this model. The load is applied incrementally, with a 1 kN increase every 15 minutes during the loading phase, while the unloading phase is performed in increments of 1 kN, but at shorter intervals of 5 minutes. The duration of this phase is 100 minutes (1.66 hours).

Phase B: follows the completion of the first phase and involves the application of a thermal load in the pile. The pile is subjected to heating, with a constant fluid temperature of 45°C, which flows through the pipes installed inside the pile. This thermal load is applied for a continuous period of 1200 minutes (20 hours).

Phase C: combines both thermal and mechanical loads. The thermal load remains unchanged, with the fluid temperature maintaining a constant 45°C, while a mechanical load similar to the one applied in Phase A is introduced. This phase ensures the simultaneous effect of both loading types on the pile.

Phase D: represents the relaxation or recovery period. During this phase, which lasts for 1260 minutes (21 hours), the pile is not subjected to any mechanical or thermal load. All actions are halted to allow the pilot to relax and its internal temperature to return to its initial state, before the application of the next thermal load. This period is crucial for simulating a natural recovery phase before applying the thermal-cooling load.

Phase E: involves the application of a thermal-cooling load, during which the fluid temperature is reduced to a constant 10°C. The pile is subjected to this cooling load for a duration of 1440 minutes (24 hours). This phase assesses the response of the pile to cooling conditions following the recovery phase.

Phase F: is the final phase, in which the pile continues to experience the thermal-cooling load, with the fluid temperature maintained at 10°C. A mechanical load, identical to that applied in Phase A, is reintroduced. The load is applied incrementally, with 1 kN every 15 minutes during the loading phase, up to a maximum of 5 kN. The unloading phase follows a similar pattern, with increments of 1 kN every 5 minutes.

Each of these six phases is carefully designed to simulate different environmental and load conditions, enabling a thorough evaluation of the pile’s behavior under thermo-mechanical loads.

4.3. Experimental results

Various parameters were recorded during the test, including the temperature of the pile and surrounding soil, soil pressure at the pile tip, horizontal soil pressure, strain distribution, thermal stress, mobilized side shear stress, axial load, and pile head settlement. Figure 42 shows the measured temperatures of both the pile body and the surrounding soil. During the heating phase, both the pile and soil temperatures increased, while during the cooling phase, they decreased accordingly. As previously mentioned, the water was heated to 45°C for a duration of 1200 minutes (20 hours) and then cooled to 10°C for 1440 minutes (24 hours), following a recovery phase (Phase D) lasting 1200 minutes (20 hours).

4.3.1. Temperature in the pile and surrounding soil

Thermocouples T1, T2, and T3 were installed at three different levels within the pile body, while other thermocouples were positioned in the surrounding soil. These thermocouples were arranged in three rows at varying depths. In the first row, thermocouples T4, T5, and T6 were located 15 cm from the pile and spaced 25 cm apart vertically. In the second row, thermocouples T7, T8, and T9 were placed 30 cm from the pile shaft, with a vertical distance of 25 cm from each other, and 15 cm horizontally from the first row. The third row, consisting of thermocouples T10, T11, and T12, was positioned 45 cm from the pile shaft, with a vertical spacing of 25 cm, and 15 cm horizontally from the second row.

Under no applied load on the pile, the initial temperatures in the pile were measured as 17.25°C, 17.24°C, and 17.1°C (at T1, T2, and T3, respectively). In the surrounding soil, the temperatures were recorded as 17.1°C, 16.95°C, and 16.65°C (at T3, T4, and T6, respectively) in the first row; 16.75°C, 16.65°C, and 16.35°C (at T7, T8, and T9) in the second row; and 16.85°C, 16.55°C, and 16.4°C (at T10, T11, and T12) in the third row.

The temperature profiles of both the pile and the surrounding soil exhibited slight variations, depending on whether a vertical load was applied or not. This variation can be attributed to the influence of the ambient air temperature on the upper part of the pile and surrounding soil, as well as the differing rates at which the temperature recovered along the pile's length.

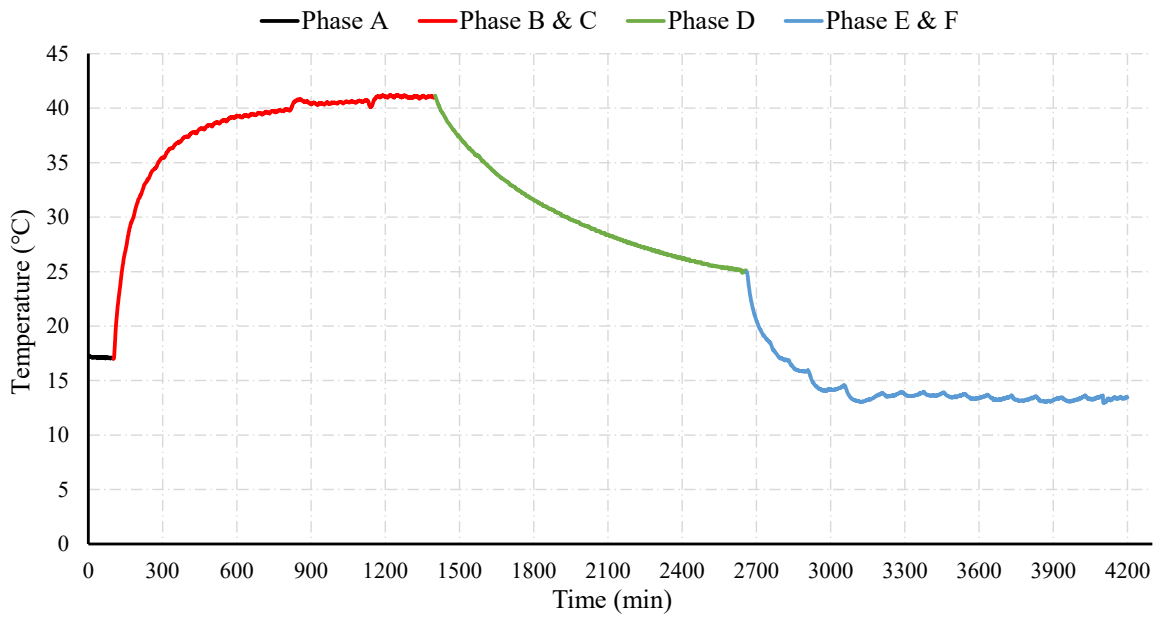
Phase A
Phase B & C
Phase D
Phase E & F
Temperature (°C)
0
5
10
15
20
25
30
35
40
45
0
300
600
900
1200
1500
1800
2100
2400
2700
3000
3300
3600
3900
4200
Time (min)

a)

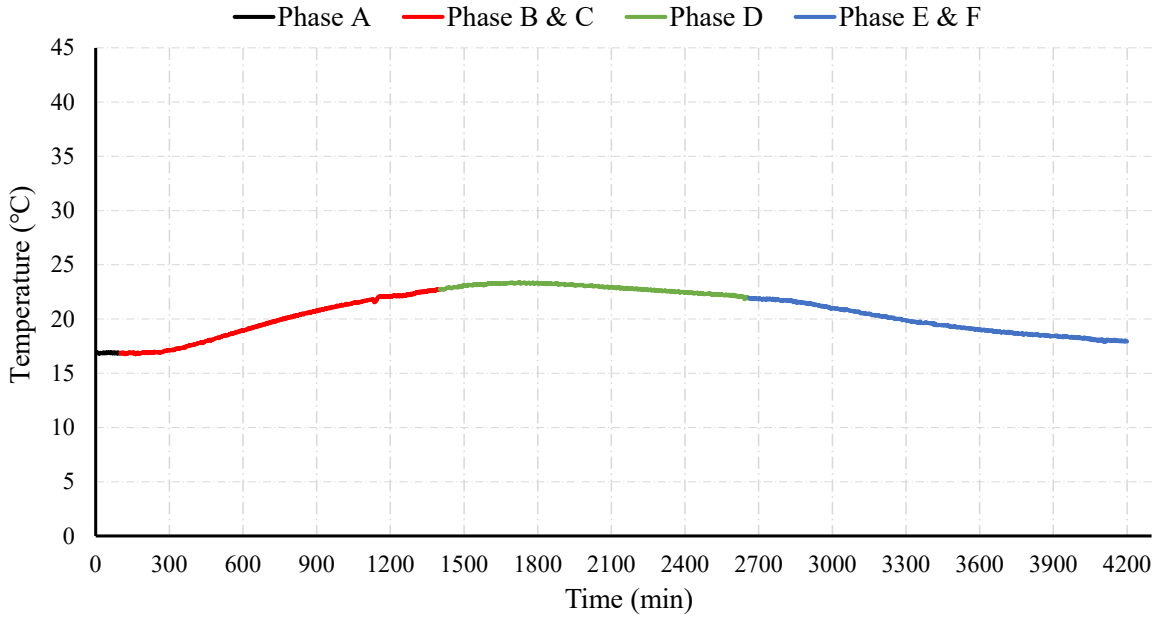
Phase A
Phase B & C
Phase D
Phase E & F
Temperature (°C)
0
5
10
15
20
25
30
35
40
45
0
300
600
900
1200
1500
1800
2100
2400
2700
3000
3300
3600
3900
4200
Time (min)

b)

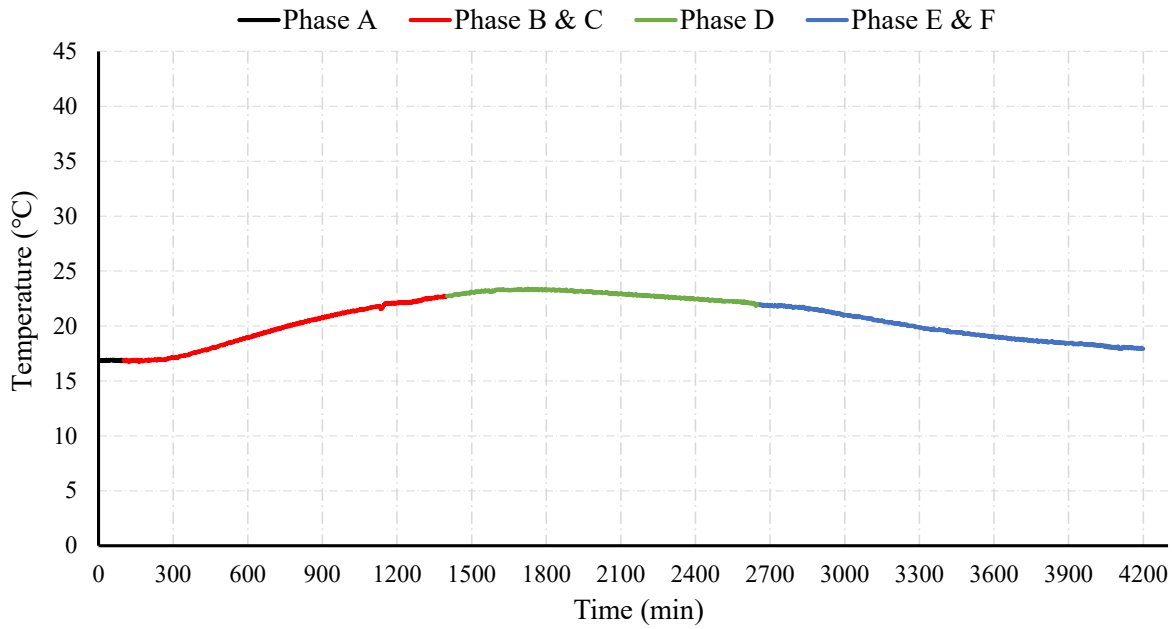
Phase A
Phase B & C
Phase D
Phase E & F
Temperature (°C)
0
5
10
15
20
25
30
35
40
45
0
300
600
900
1200
1500
1800
2100
2400
2700
3000
3300
3600
3900
4200
Time (min)

c)

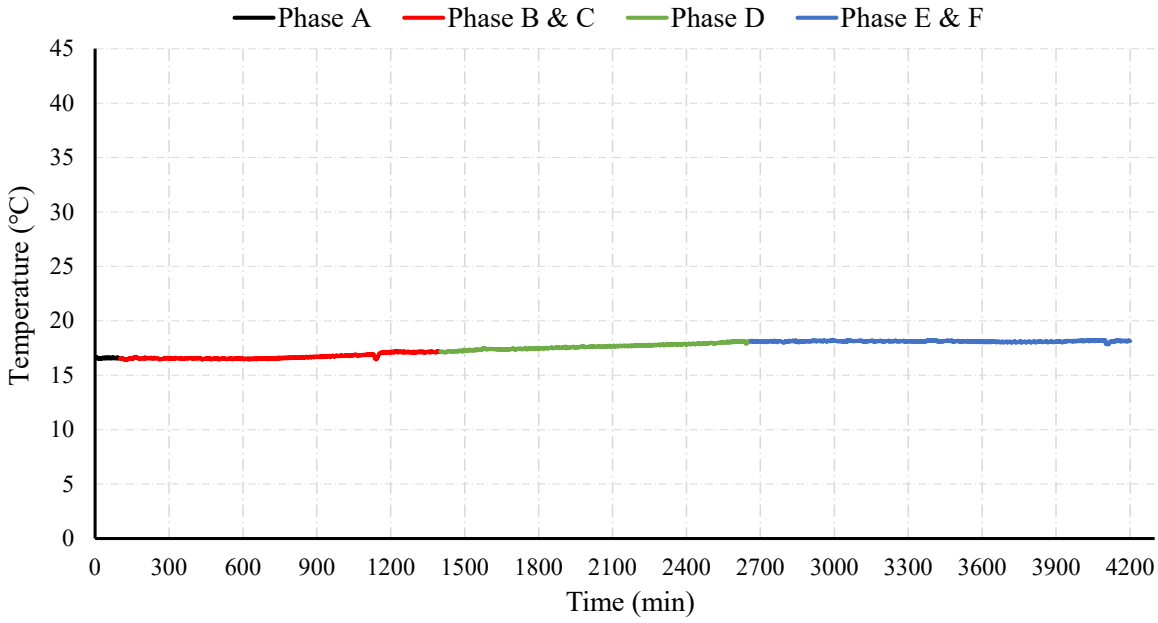
Phase A
Phase B & C
Phase D
Phase E & F
Temperature (°C)
0
5
10
15
20
25
30
35
40
45
0
300
600
900
1200
1500
1800
2100
2400
2700
3000
3300
3600
3900
4200
Time (min)

d)

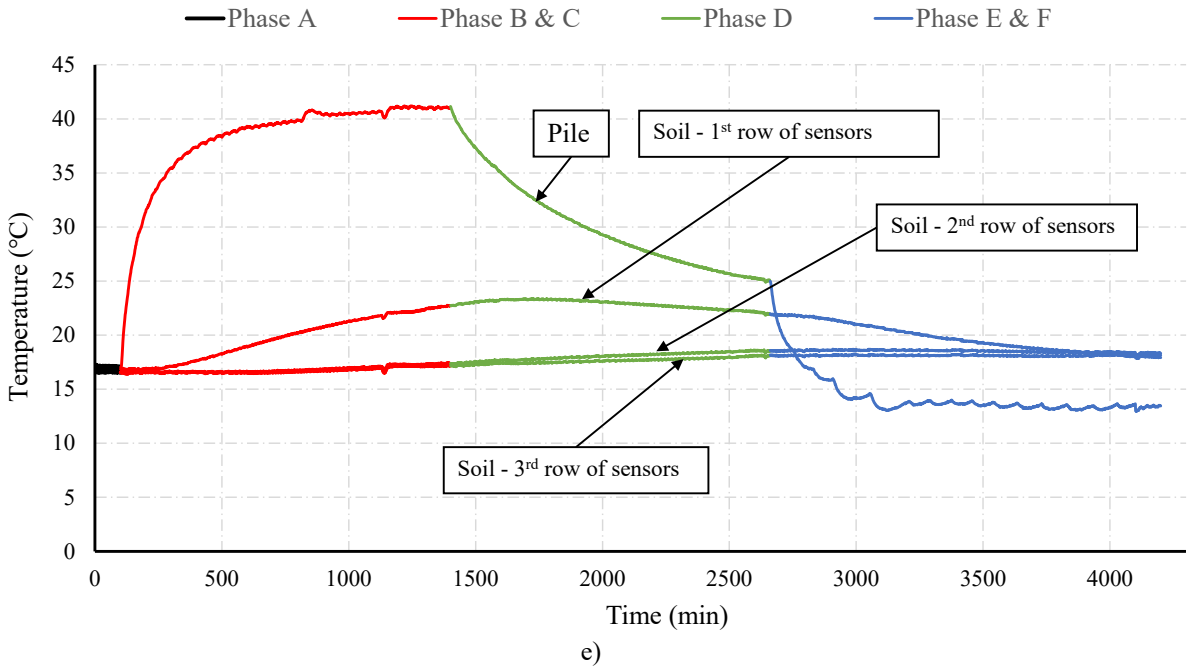

e)

Figure 42. Temperature changes in the pile and the surrounding soil due to thermal effects applied to the pile. a) Pile; b) 1st row of sensors in the soil; c) 2nd row of sensors in the soil; d) 3rd row of sensors in the soil, and e) pile and surrounding soil

Under the action of thermal load heating during phases B and C, the maximum average temperatures recorded were as follows: in the pile, 41.2°C (T1, T2, T3); in the first row of sensors, 23.4°C (T4, T5, T6); in the second row, 18.7°C (T7, T8, T9); and in the third row, 18.27°C (T10, T11, T12). It is noteworthy that the temperature in the first row of sensors within the surrounding soil began to rise only after more than three hours of thermal load application to the pile.

At the conclusion of the relaxation or recovery phase (Phase D), before the application of the thermal cooling load, the average temperatures were recorded as follows: in the pile, 24.9°C (T1, T2, T3); in the first row of sensors, 21.9°C (T4, T5, T6); in the second row, 18.52°C (T7, T8, T9); and in the third row, 18.1°C (T10, T11, T12). It is important to note that the recovery phase is designed to allow the pile and surrounding soil to return to temperatures similar to those before the application of thermal heating. However, full recovery was not achieved within the expected time frame, as the temperature reduction during the recovery phase occurred at a very slow rate over time. As mentioned in the testing procedure section, the recovery phase lasted 24 hours, and the pile temperature dropped to approximately 24.9°C, compared to the initial temperature of 17.2°C before the testing began.

During the cooling load phases E and F, the minimum average temperatures were as follows: in the pile, 12.95°C (T1, T2, T3); in the first row of sensors, 16.73°C (T4, T5, T6); in the second row, 16.42°C (T7, T8, T9); and in the third row, 16.38°C (T10, T11, T12).

4.3.2. Vertical displacements

The initial phase (Phase A) of the experimental campaign involved a purely mechanical loading-unloading cycle applied to the geothermal pile, intending to establish the reference mechanical response of the system under isothermal conditions. The load was increased in

discrete steps of 1 kN every 15 minutes, up to a maximum of 5 kN, followed by a symmetric unloading in steps of 1 kN every 5 minutes, as defined in the loading protocol (see Figure 40).

Following the initial mechanical loading cycle, the second phase (Phase B) of the experimental campaign was designed to evaluate the thermal response of the geothermal pile under controlled heating conditions. During this phase, a constant temperature of 45 °C was maintained through the circulation of heated fluid inside the pile's embedded pipe system, simulating the operation of a geothermal energy exchange system. The heating phase lasted for 1,200 minutes (20 hours), and no mechanical load was applied concurrently.

Phase C of the testing program was designed to investigate the thermo-mechanical behavior of the geothermal pile under the simultaneous influence of mechanical and thermal loads. In this phase, the pile was subjected to a stepwise mechanical loading-unloading cycle, identical to that in Phase A, while the elevated temperature of 45 °C, established during the prior heating phase (Phase B), was continuously maintained throughout the test.

Phase D represents the recovery phase during which the geothermal pile was allowed to stabilize without the influence of any external loading. Specifically, both mechanical and thermal loads were entirely removed, allowing the system to evolve under natural stress redistribution and environmental equilibrium. This phase lasted for 1,260 minutes (21 hours) and served to capture the time-dependent recovery behavior of the pile and surrounding soil mass.

Phase E was conducted to assess the displacement behavior of the geothermal pile during a thermal loading phase characterized by cooling. After the completion of the recovery phase (Phase D), the pile was subjected to a constant temperature of 10 °C for a total duration of 1,440 minutes (24 hours). No mechanical load was applied during this phase. The objective was to evaluate the impact of thermal contraction on the axial displacement of the pile and the surrounding soil.

Phase F was the final stage of the experimental program and involved applying mechanical loading to the geothermal pile while it was thermally conditioned at a constant cooling temperature of 10 °C, as established during Phase E. This phase aimed to evaluate the pile's response to mechanical loading under low-temperature conditions, which could reflect seasonal cold periods in real-life geothermal systems. The same loading pattern from Phases A and C was applied: the load increased incrementally up to 5 kN, held briefly, and then symmetrically unloaded.

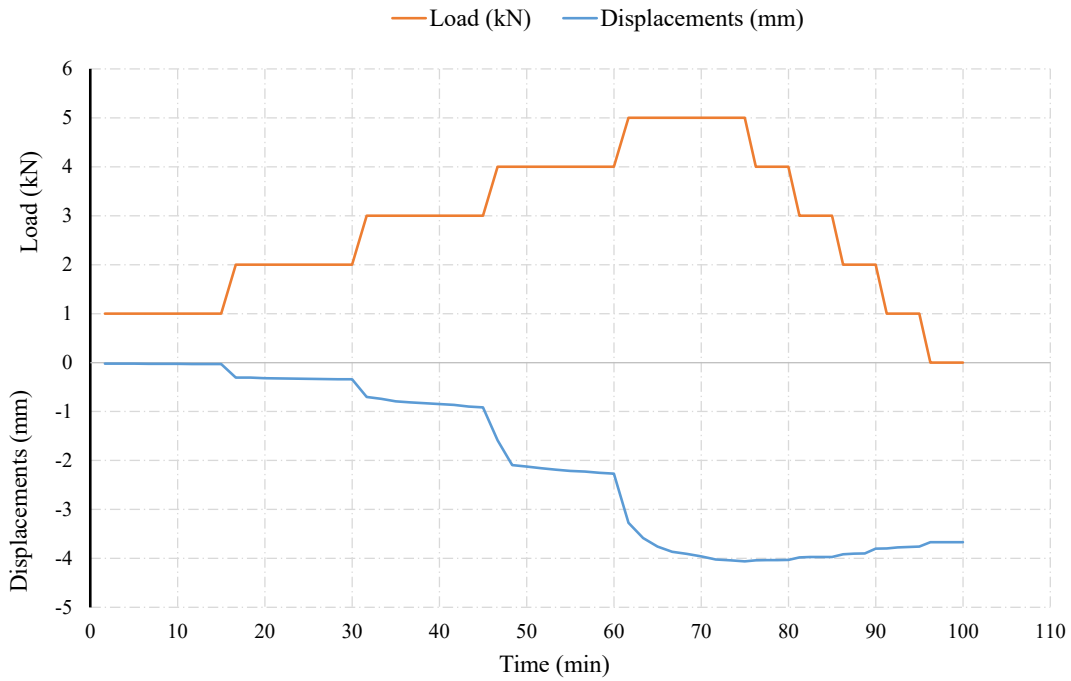
Load (kN)
Displacements (mm)
Load (kN)
Displacements (mm)
6
5
4
3
2
1
0
-1
-2
-3
-4
-5
0
10
20
30
40
50
60
70
80
90
100
110
Time (min)

a)

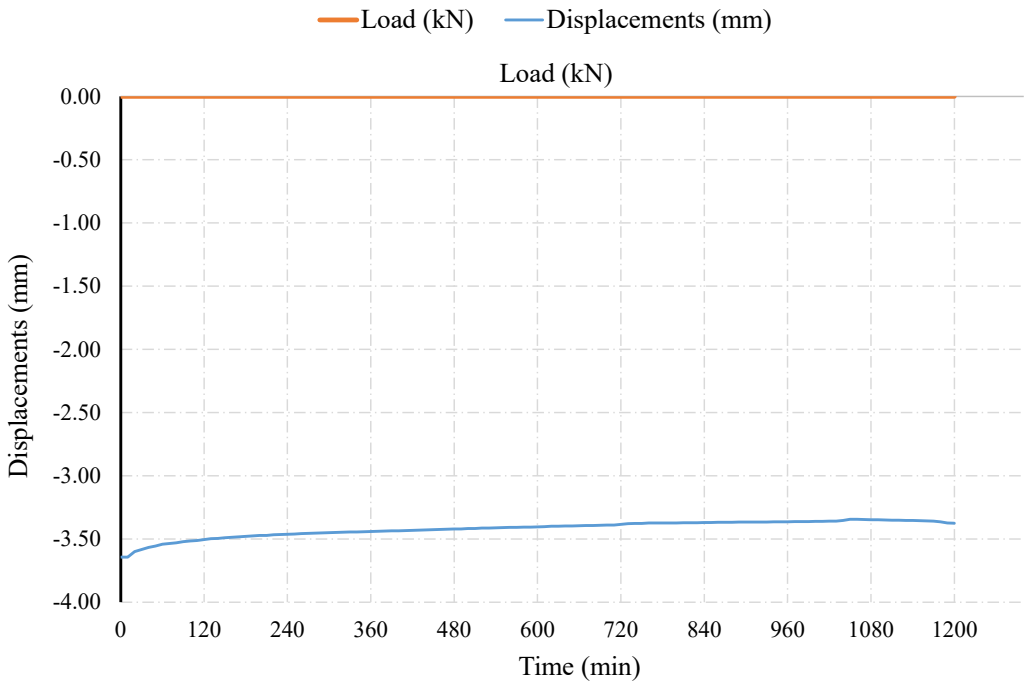
Load (kN)
Displacements (mm)
Load (kN)
Displacements (mm)
0.00
-0.50
-1.00
-1.50
-2.00
-2.50
-3.00
-3.50
-4.00
0
120
240
360
480
600
720
840
960
1080
1200
Time (min)

b)

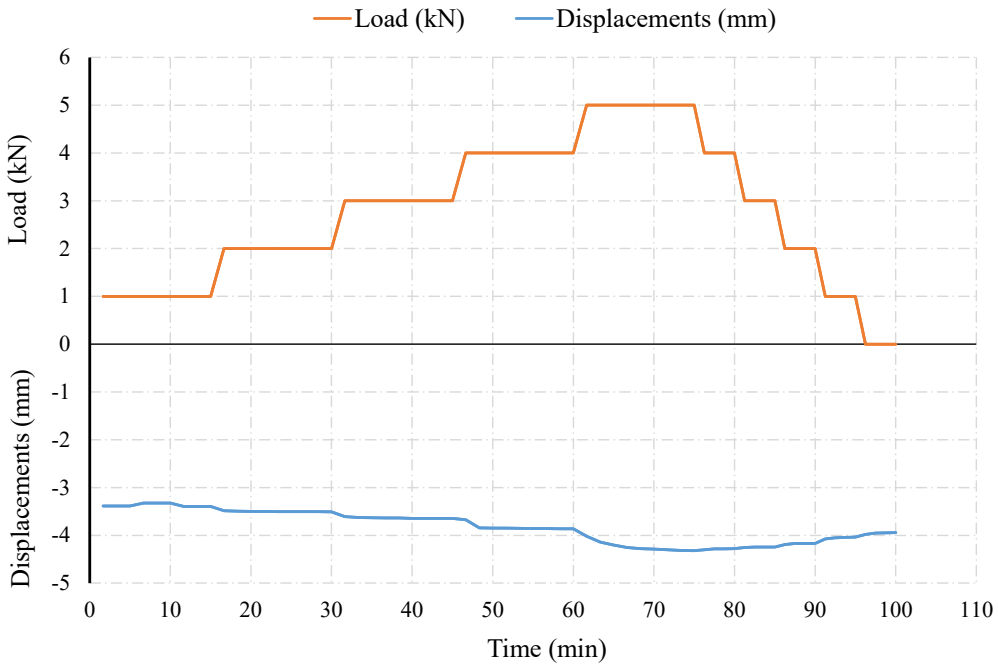
Load (kN)
Displacements (mm)
Load (kN)
Displacements (mm)
6
5
4
3
2
1
0
-1
-2
-3
-4
-5
0
10
20
30
40
50
60
70
80
90
100
110
Time (min)

c)

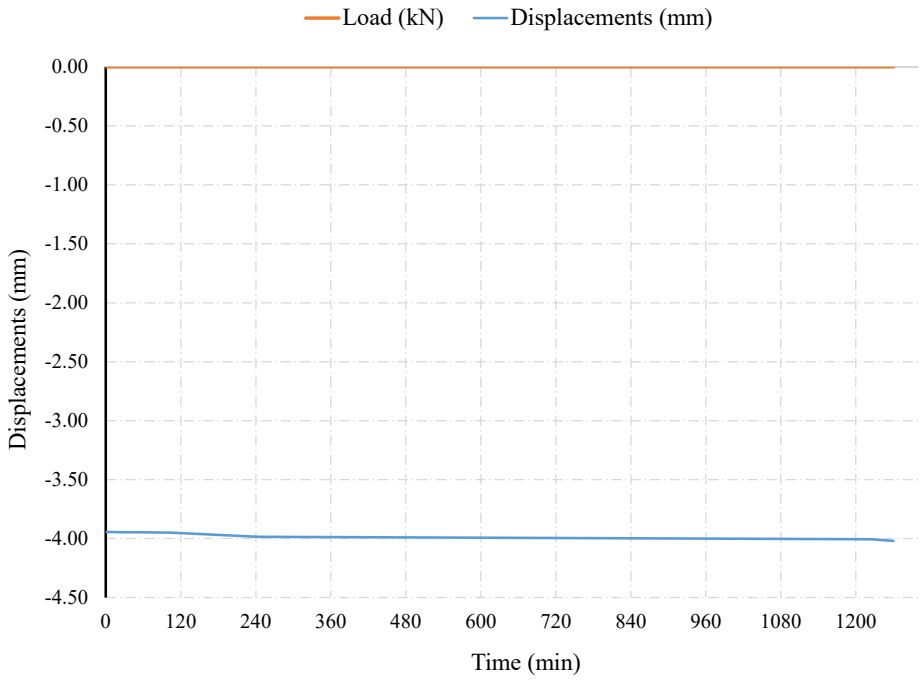
Load (kN)
Displacements (mm)
Displacements (mm)
0.00
-0.50
-1.00
-1.50
-2.00
-2.50
-3.00
-3.50
-4.00
-4.50
0
120
240
360
480
600
720
840
960
1080
1200
Time (min)

d)

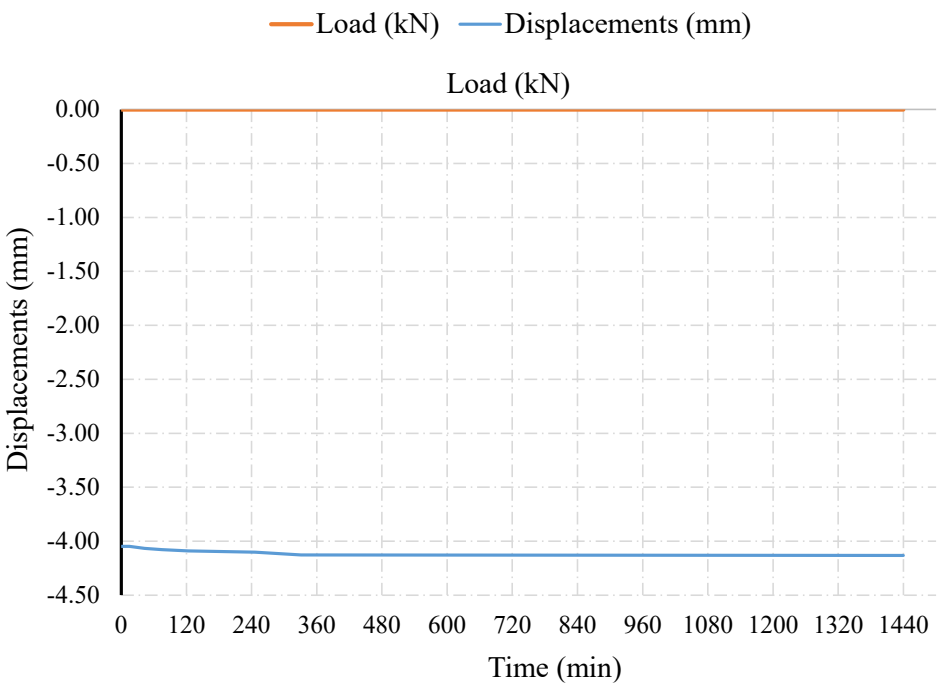
Load (kN)
Displacements (mm)
Load (kN)
Displacements (mm)
0.00
-0.50
-1.00
-1.50
-2.00
-2.50
-3.00
-3.50
-4.00
-4.50
0
120
240
360
480
600
720
840
960
1080
1200
1320
1440
Time (min)

e)

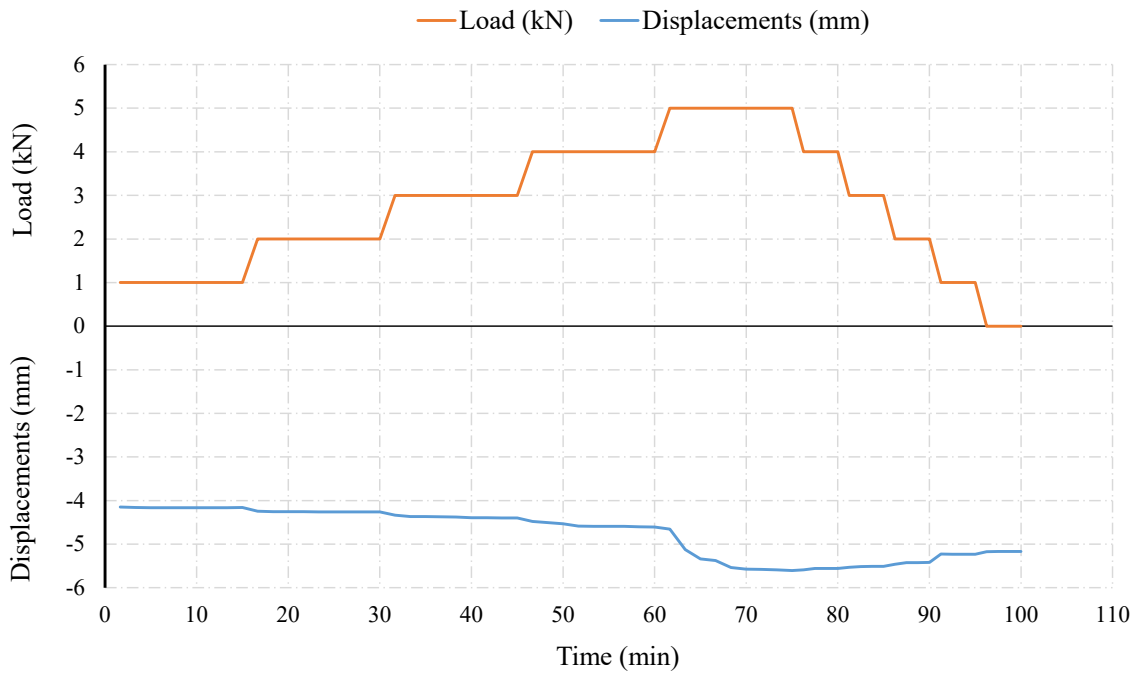
Load (kN)
Displacements (mm)
Load (kN)
Displacements (mm)
6
5
4
3
2
1
0
-1
-2
-3
-4
-5
-6
0
10
20
30
40
50
60
70
80
90
100
110
Time (min)

f)

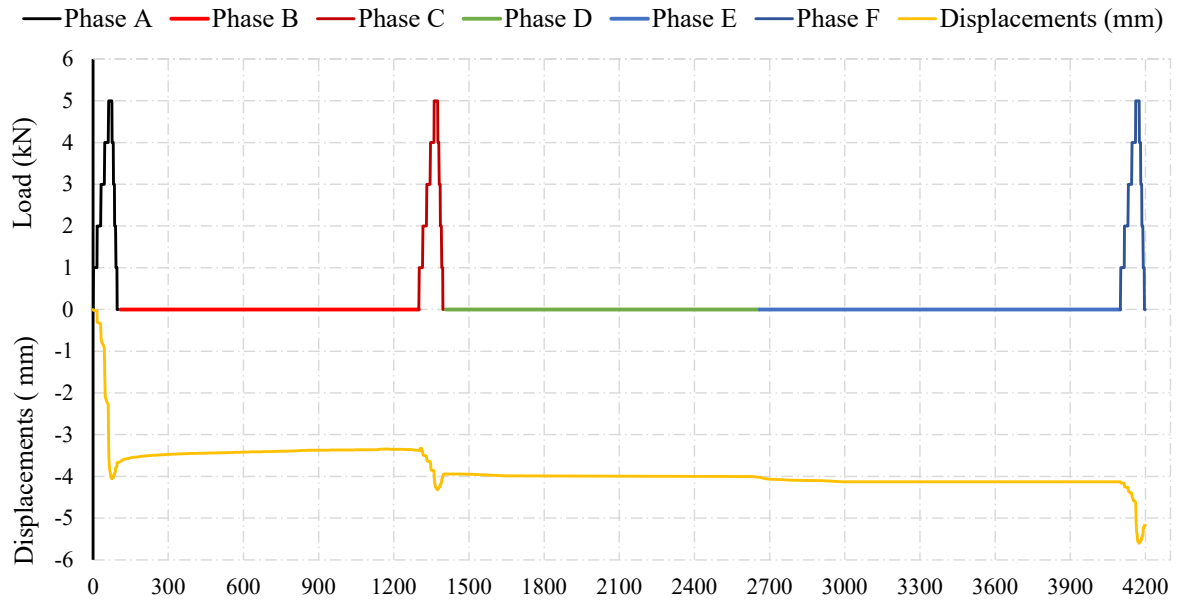

g)

Figure 43. Pile head total displacement-time responses obtained from the experimental model for the testing phases: a) Phase A (mechanical loading); b) Phase B (heating); c) Phase C (mechanical loading under sustained heating); d) Phase D (recovery); e) Phase E (cooling); f) Phase F (mechanical loading under sustained cooling), and g) combined response for Phases A-F.

The measured vertical displacements of the pile head during Phase are presented in Figure 43a to Figure *43*g. As the load increased, the pile exhibited a consistent and relatively linear downward displacement trend, with a total settlement of approximately 4.03 mm at the peak load of 5 kN. The displacement response indicates that the pile remained in the elastic regime, with no evidence of abrupt or non-recoverable deformation. During the unloading stage, a partial recovery of the displacement was observed. However, the pile did not return entirely to its original position, revealing a residual settlement of approximately 3.66 mm. This residual displacement may be attributed to minor soil rearrangement or plastic deformations in the soil-pile interaction zone. The response aligns well with expectations for vertically loaded energy piles embedded in compacted granular or cohesive soil media. This initial mechanical response provides a critical baseline for evaluating the effects of subsequent thermal and thermo-mechanical phases, allowing for an accurate comparison of displacement magnitudes and stiffness variations due to thermal activation.

The resulting vertical displacement of the pile head over time for Phase B is presented in Figure 43b. A gradual upward movement was observed, indicating thermally induced expansion of the pile. The displacement trend shows smooth and progressive behavior, with a total upward movement of approximately 0.32 mm recorded over the entire heating duration. This displacement response is primarily attributed to the thermal expansion of the concrete pile material, as well as thermally induced changes in the stress regime at the soil-pile interface. Despite the absence of mechanical load, the pile experienced minor but measurable displacements, emphasizing the significance of thermal effects in the performance of energy piles. It is worth noting that the magnitude of the thermal-induced movement was significantly smaller compared to the displacements observed during mechanical loading (Phase A), which

is consistent with previous findings in the literature. This phase serves as a critical reference for assessing the thermo-mechanical coupling effects evaluated in subsequent phases.

The recorded results for vertical displacements and applied load during Phase C, which shows a combined loading scenario, are illustrated in Figure 43c. As the mechanical load increased in 1 kN increments up to a maximum of 5 kN, a corresponding increase in downward displacement was observed. The total settlement reached a value of approximately 4.32 mm, which is slightly larger than the maximum displacement observed during Phase A (mechanical loading alone). Upon unloading, the pile exhibited partial elastic recovery, resulting in a residual settlement of around 0.6 mm, marginally higher than the residual displacement recorded in the isothermal loading condition. The slightly amplified displacements under the same load regime, when subjected to sustained thermal conditions, suggest a softening effect induced by the elevated temperature on the pile-soil interaction. This behavior can be attributed to thermally induced reductions in soil stiffness and potential changes in interface friction characteristics. The outcome of Phase C confirms the coupling between thermal and mechanical phenomena in energy piles and highlights the importance of considering temperature effects in geotechnical design involving thermo-active foundations.

As shown in Figure 43d, the vertical displacement trend during Phase D (recovery phase), the vertical displacement trend is characterized by a slow and minor downward movement, with a total recovery displacement of approximately 0.1 mm. The absence of applied loads confirms that this rebound is attributable to delayed elastic recovery and minor stress relaxation within the pile-soil system. The limited magnitude of recovery further reinforces that the majority of the deformation accumulated during the previous thermo-mechanical loading phases (Phases A to C) is largely irreversible, likely resulting from plastic strains and particle rearrangement within the soil. Additionally, the near-stabilized trend at the end of this phase indicates that the system approached a new equilibrium state under unloaded conditions. This phase is crucial in understanding the long-term mechanical behavior of energy piles and provides insight into the extent of residual deformation that remains even after complete removal of operational loads. It highlights the importance of accounting for irreversible settlements and post-loading recovery behavior in the performance assessment of thermo-active foundation systems.

Figure 43e presents the vertical displacement of the pile head throughout the cooling period, Phase E. As shown, a subtle and gradual downward movement was recorded, with the total additional settlement reaching approximately 4.13 mm. This behavior is consistent with the thermally induced contraction of the concrete pile as its temperature decreased relative to the previously elevated temperature maintained in earlier phases. The small magnitude of displacement highlights that thermal contraction, in isolation, exerts a modest influence on overall settlement. However, its cumulative effect in the context of prior thermal expansion and mechanical loading may contribute to long-term behavior and potential irreversible displacements. Furthermore, the result suggests a reduced stiffness recovery of the surrounding soil matrix when transitioning from elevated to lower thermal states. Overall, this phase emphasizes the importance of evaluating both heating and cooling cycles in the operational performance of energy piles, particularly for applications involving frequent temperature fluctuations such as seasonal thermal energy storage systems.

The recorded data during Phase F for pile head displacements and applied load are presented in Figure 43f. Compared to previous loading phases, the displacements observed in Phase F were the largest, with the total vertical settlement reaching approximately 5.6 mm at peak load. Following unloading, the system showed partial recovery, with a residual settlement of about 5.16 mm, indicating a more pronounced plastic response under combined mechanical and cooling effects. The greater displacement compared to the previous mechanical (Phase A) and thermo-mechanical (Phase C) phases suggests that the cooling-induced contraction of the pile and surrounding soil might have reduced interface friction or soil stiffness. Cooling typically induces shrinkage in concrete and can lead to increased relative movement between the pile and soil. Additionally, changes in pore water pressures and suction conditions in fine-grained soils under low temperatures may contribute to the observed behavior. This phase highlights the importance of accounting for low-temperature mechanical performance in the design of energy geostructures, particularly in climates where thermal cycles may include prolonged cooling. The amplified displacements observed here suggest a nonlinear and temperature-dependent interaction between thermal and mechanical loading effects.

The experimental campaign was structured into six phases to assess the thermo-mechanical behavior of a geothermal pile. Phase A established the baseline mechanical response under monotonic loading, with a maximum displacement of ~4.06 mm and a residual settlement of 3.66 mm. Phase B introduced heating at 45 °C without mechanical load, causing a small upward movement (~0.32 mm) due to thermal expansion. In Phase C, mechanical loading was repeated under sustained heating, resulting in increased settlement (~4.32 mm) and residual displacement (~3.94 mm), indicating reduced soil stiffness at elevated temperatures. Phase D involved no applied loads and showed minor recovery (~0.1 mm), while Phase E applied cooling at 10 °C, leading to slight additional settlement (~0.13 mm) due to thermal contraction. Phase F combined mechanical loading with cooling and produced the largest total displacement (~5.6 mm) and residual settlement (~5.16 mm), highlighting the significant influence of temperature on pile-soil interaction. Overall, the results confirm that both heating and cooling cycles affect the mechanical behavior of energy piles and must be accounted for in their design.

4.3.3. Pore pressure

The evolution of pore water pressure during the six experimental phases is presented in Figure 44, based on measurements from five sensors strategically positioned at different depths and lateral distances from the geothermal pile (see sensor layout in Figure 29). These results reflect the coupled hydro-thermal-mechanical interactions occurring in the soil mass throughout the test.

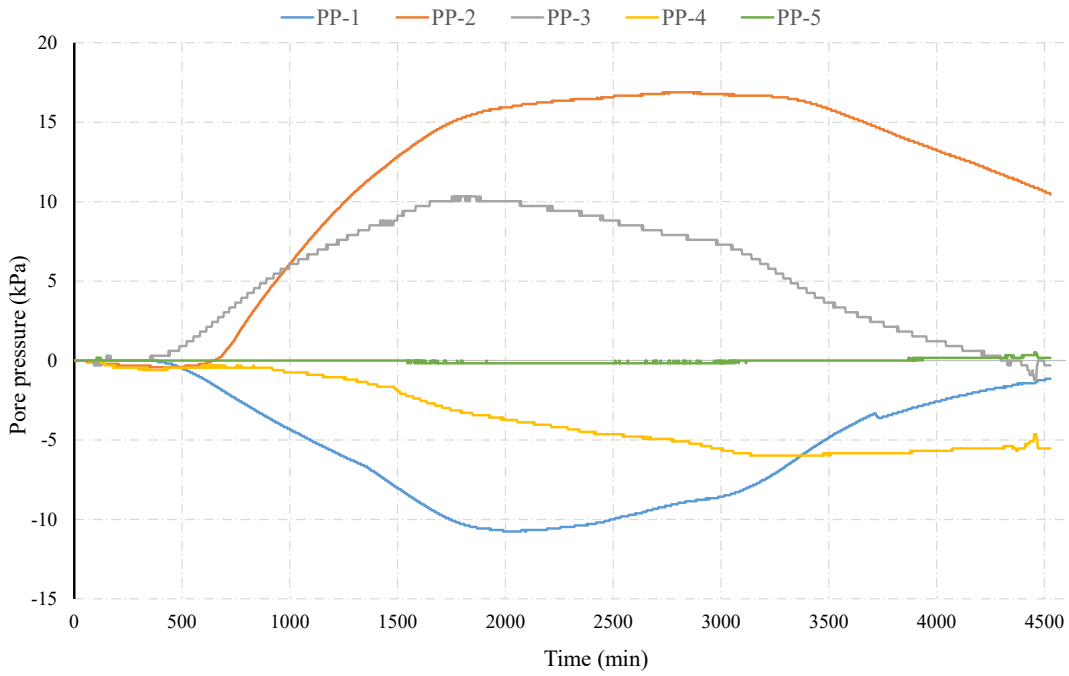

Figure 44. Diagram of pore pressure changes

During Phase A (mechanical loading), pore pressure remained nearly unchanged, confirming the drained behavior of the soil under the applied loading rate. A significant response was observed in Phase B (heating), where sensors closest to the pile (e.g., Serie 2 and Serie 3) recorded a noticeable increase in pore pressure, peaking at approximately 16-17 kPa and 10-11 kPa, respectively. This can be attributed to thermal expansion of pore water and reduced water viscosity, enhancing flow toward zones of lower pressure. In contrast, sensors positioned farther from the pile (Serie 1 and Serie 4) recorded a decrease in pore pressure, indicating suction generation possibly due to water migration or thermally driven desaturation effects. Sensor Series 5 showed minimal change, suggesting it was located in a neutral thermal-hydraulic zone. In Phase C, the continued heating with concurrent mechanical loading resulted in a stabilization or plateau in the pressure values, reflecting the soil's adjustment to steady thermal gradients and limited mechanical influence on pore pressure. During Phase D (recovery with no loading), pressures began to relax: positive pressures gradually dissipated, and negative pressures slightly recovered, indicating the system's return toward equilibrium. Cooling in Phase E induced inverse behavior; positive pore pressures began to drop, while suctions (negative values) started to reduce, reflecting thermal contraction and potential water inflow. Finally, Phase F, which involved mechanical loading under sustained cooling, produced minor changes, mainly maintaining the general trend of dissipation and stabilization. These results emphasize the sensitivity of pore pressure to temperature gradients and sensor location, with distinct behaviors observed between thermally active and remote zones. The data validates the need for considering thermal-hydraulic coupling in energy pile design, especially when predicting excess pore pressure and suction that could influence pile-soil interaction and effective stress conditions.

4.3.4. Total pressure

The evolution of total pressure within the soil mass, monitored by embedded pressure cells at five positions (Figure 29), is presented in Figure 45 across all six experimental phases (A-F). These results reflect the combined effects of mechanical and thermal loads on the stress distribution within the soil, including both induced stresses and soil-structure interaction mechanisms.

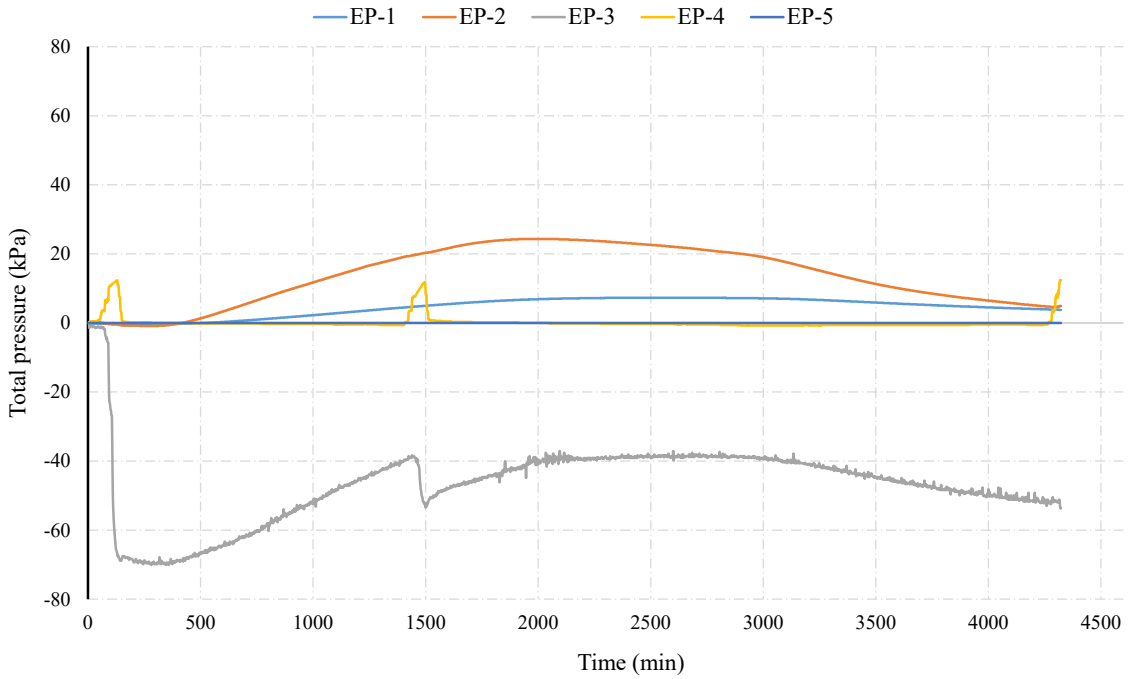

Figure 45. Diagram of total pressure changes

During Phase A (mechanical loading), total pressure values remained close to zero or showed only minor increases, indicating that the applied vertical load was primarily transferred through the pile and minimally distributed laterally into the surrounding soil. The onset of Phase B (heating at 45 °C) marked a significant increase in total pressure at sensors close to the pile (e.g., Serie 2 and Serie 1), reaching peaks of 25-30 kPa, attributed to the thermal expansion of the concrete and adjacent soil. Conversely, Series 3, located deeper or possibly at the base, exhibited a sharp negative pressure (dropping to ~60 kPa), possibly due to thermal contraction or local redistribution of stresses at the pile toe. In Phase C, with heating sustained and mechanical loading reapplied, the pressure values either stabilized or slightly increased depending on their proximity to the load path. Notably, Series 2 maintained elevated pressure levels, highlighting the intensified stress transfer in thermally softened zones. Phase D (no loading) showed gradual pressure relaxation, especially in the previously over-pressurized zones. During cooling in Phase E, a general decrease in total pressures was observed across all sensors, consistent with the contraction of the pile and surrounding soil, which reduced lateral stress. Finally, Phase F, involving mechanical loading under cooling, showed a secondary rise in pressure at some sensors (e.g., Serie 1 and Serie 2), though less pronounced than in Phase C, likely due to stiffer soil behavior at lower temperatures and reduced thermal influence. Overall, the results confirm that total pressure distribution is highly sensitive to both temperature-induced volumetric changes and mechanical boundary conditions, and varies with depth and

radial distance from the pile. These findings emphasize the necessity of accounting for coupled thermal-mechanical effects in the design of energy piles, particularly in assessing load transfer mechanisms and stress mobilization within the soil.

4.3.5. Suction

The variation of matric suction during the six loading phases is illustrated in Figure 46, based on measurements from five sensors distributed around the geothermal pile, as shown in Figure 29. These measurements reflect the dynamic hydro-mechanical behavior of the unsaturated soil in response to thermal and mechanical changes introduced during the experiment.

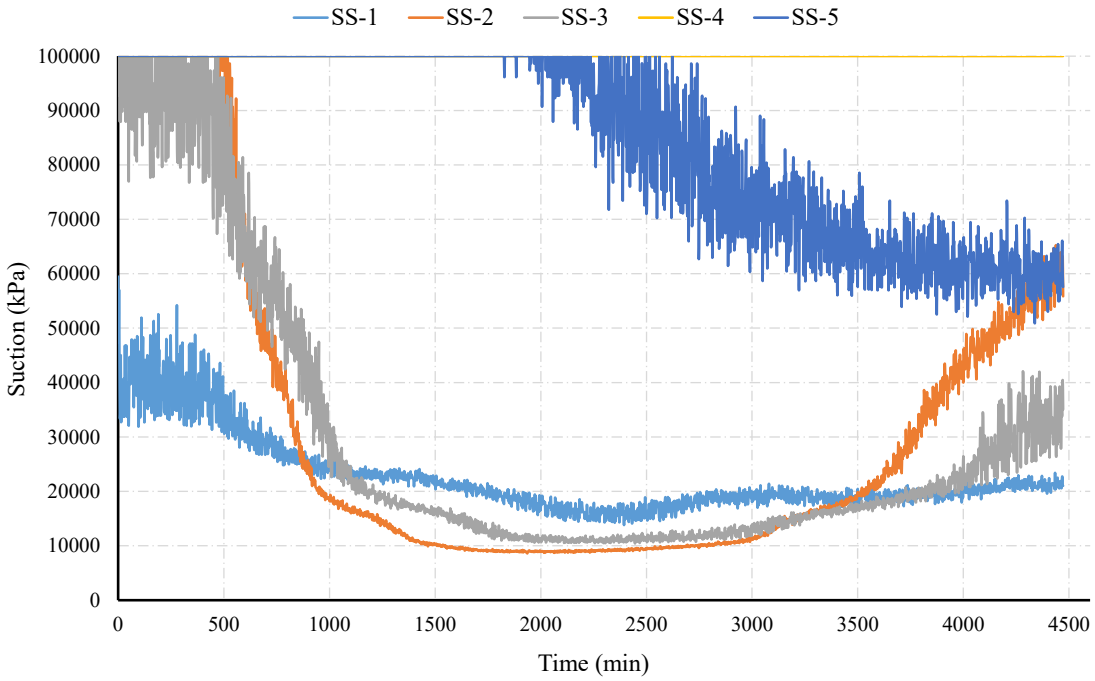

Figure 46. Diagram of suction changes

During Phase A (mechanical loading), suction values remained largely unchanged across all sensors, indicating a negligible influence of short-term loading on soil moisture redistribution. A significant shift occurred in Phase B (heating), where sensors closer to the pile (e.g., Serie 2 and Serie 3) exhibited a rapid and pronounced decrease in suction, falling from initial values around 90-100 kPa to near or below 10 kPa. This trend is attributed to the thermal expansion of pore water, increased vapor pressure, and potential local condensation effects near the heat source, which collectively enhance water availability and reduce matric suction. Sensors farther from the heat-affected zone (e.g., Series 4) maintained nearly constant values, highlighting the spatial dependency of the thermal influence. In Phase C, with heating sustained and mechanical loading applied, suction values remained relatively stable at their reduced levels, suggesting that thermal effects remained dominant over mechanical influences. Phase D (no loading) showed a plateau in suction behavior, with only minor fluctuations, indicating a temporary stabilization of the soil-water retention regime. During Phase E (cooling), suction values began to recover gradually across all responsive sensors, especially in Series 1 and Series 2, reflecting thermal contraction and moisture redistribution toward equilibrium. The recovery continued in Phase F during mechanical loading under cooling, although suction levels did not return to initial values, suggesting some hysteresis in the soil-water retention behavior. Overall, the

results underscore the significant influence of temperature changes on suction dynamics in unsaturated soils. The observed reduction during heating and partial recovery during cooling confirm the strong coupling between thermal and hydraulic fields in the soil matrix surrounding energy piles. These effects are significant for interpreting effective stress changes and understanding long-term hydro-mechanical stability under cyclic thermal operations.

4.3.6. Strains

The axial strain development within the model pile during the experimental program was monitored using electrical resistance strain gauges installed on the longitudinal reinforcement bars, as illustrated in Figure 29. The instrumentation layout was designed to capture the thermo-mechanical response of the pile under different loading and thermal phases, as described in the testing procedure (Phases A-F). During post-processing and quality assessment of the recorded data, it was observed that only the Stain gauge no. 3 provided a continuous, stable, and physically consistent strain response throughout the entire duration of the experiment. Consequently, the strain measurements from strain gauge number 3 were selected as representative for the interpretation of the pile behavior under combined mechanical and thermal loading conditions.

The strain responses recorded by the remaining channels were affected by instrumentation-related disturbances, which limited their suitability for reliable interpretation. These disturbances are attributed to a combination of factors commonly encountered in long-duration thermo-mechanical laboratory testing, including:

- partial loss of bonding between strain gauges and reinforcement bars due to thermal cycling,
- signal drift and electrical noise caused by prolonged exposure to elevated temperatures,
- localized damage to sensor wiring during installation, concreting, or handling, and
- sensitivity of certain gauges to moisture ingress and temperature gradients within the pile cross-section.

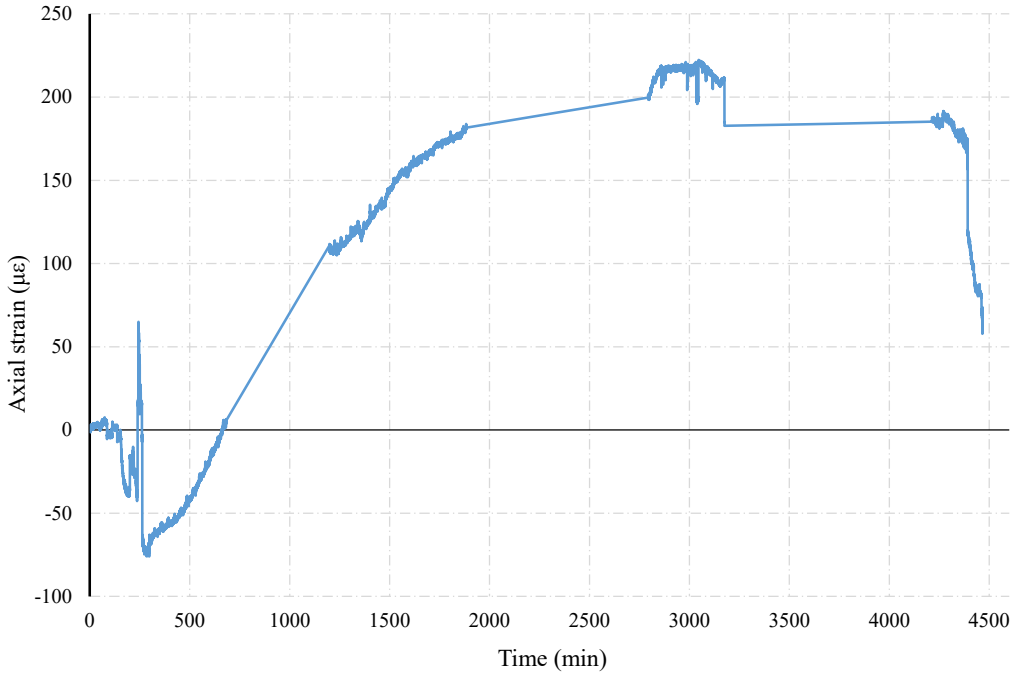

Figure 47. Axial strain-time response during the thermo-mechanical testing phases

In contrast, the strain gauge no. 3 exhibited a coherent and reproducible strain evolution, clearly reflecting the different testing phases. As shown in Figure Y, the strain response captures:

- the elastic strain accumulation during the initial mechanical loading phase (Phase A),
- progressive thermally induced strains during heating (Phase B),
- the combined thermo-mechanical response under sustained temperature and mechanical cycling (Phase C),
- partial strain recovery during the unloading and recovery phase (Phase D),
- strain redistribution during cooling (Phase E), and
- the final mechanical response under reduced temperature conditions (Phase F).

The observed strain trends are physically consistent with the expected behaviour of geothermally active piles, where temperature variations induce axial strains due to restrained thermal expansion and contraction, superimposed on mechanically induced strains from applied axial loads.

5. NUMERICAL MODELLING

The numerical modelling was carried out in PLAXIS 2D using the axisymmetric option, which is appropriate for representing the cylindrical geometry of a single geothermal pile. The model domain was defined with dimensions of x=1.0 m in the radial direction and y=1.5 m in the vertical direction, ensuring sufficient boundary distance to minimize boundary effects. The pile was modelled with a diameter of 0.15 m and a length of 1.0 m, corresponding directly to the geometry of the laboratory-scale experimental pile. To capture the stress-strain and thermal behavior with high accuracy, the mesh was generated using the fine element distribution, providing adequate refinement around the pile-soil interface where the most significant gradients were expected.

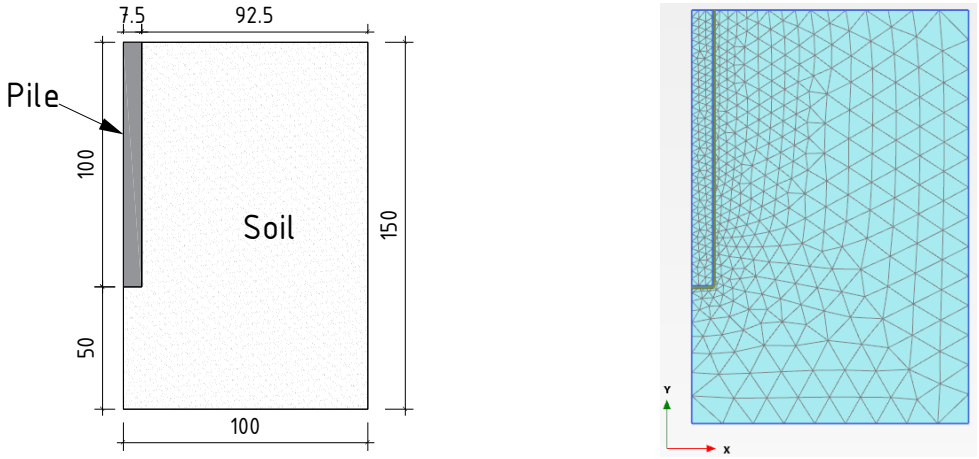

Figure 48. Two-dimensional axisymmetric PLAXIS model of the pile-soil system, illustrating the adopted geometry and finite element discretization

5.1. Material properties and material models

For the numerical model, two distinct material sets were defined: one for the pile (concrete) and another for the soil (silty sand). The pile was represented using a Linear Elastic model with non-porous drainage conditions.

The surrounding soil was modelled as silty sand, using the Hardening Soil Small (HSsmall) constitutive model with drained behavior. The HS small model is an advanced extension of the Hardening Soil model, explicitly developed to capture the stiffness dependency at very small strains. In conventional soil models such as Mohr-Coulomb, the stiffness is treated as constant, which often leads to unrealistic predictions for small deformations typical of laboratory-scale or serviceability problems. By contrast, the HSsmall (strain) model introduces the small-strain shear stiffness $G_{0,\,ref}$ and a decay function controlled by the strain threshold parameter $\gamma_{0.7}$, allowing for a gradual reduction of stiffness with increasing strain. This behavior is highly consistent with experimental evidence on granular soils, where the initial stiffness at very small strains is significantly higher than the secant stiffness at working load levels.

For the present study, the choice of HSsmall was motivated by two key factors:

- Consistency with the physical model: the laboratory-scale pile tests induced relatively small strains in the surrounding silty sand. A model that incorporates stiffness degradation at small strain levels was therefore essential to reflect the observed soil response accurately.
- Improved realism over simpler models: compared to Mohr-Coulomb, which assumes perfectly plastic behavior with a single stiffness value, HSsmall better represents the non-linear stress-strain relationship and the effect of cyclic or thermo-mechanical loading typical of geothermal applications. This enabled a more reliable simulation of both the mechanical and thermal phases of the experiments.

Table 12. Material properties

Parameters	Unit	Pile (Concrete)	Soil (Silty-sand)
General			
Model		Linear Elastic - LE	HS small
Unsaturated unit weight	kN/m^3	25.00	14.60
Mechanical			
Young's modulus/Oedometric modulus E/E_{oed}	kN/m^2	$31.5x10^6$	$9x10^3$
Poisson's ratio	-	0.15	0.20
Cohesion	kN/m^2	-	3.00
Friction angle	°	-	33.00
Thermal			
Volumetric heat capacity	kJ/t/°C	850.00	1100.00
Thermal conductivity	kW/m/°C	$1.96x10^{-3}$	$0.75 x10^{-3}$
Density	t/m^3	2.60	1.70
Thermal expansion	1/°C	$0.07x10^{-3}$	$0.03\ 0^{-3}$

5.2. Staged construction and loading phases

The thermo-mechanical behavior of the geothermal pile was investigated through a sequence of six main loading phases (A-F), reproducing the laboratory-scale experimental program (Figure 40). In the numerical model, each of these phases was subdivided into smaller calculation steps, resulting in a total of 33 subphases in PLAXIS. This staged construction strategy allowed the model to accurately replicate the incremental application of mechanical and thermal loads, as well as the intermediate recovery periods.

Phase A (Mechanical loading/unloading): The pile was subjected to stepwise vertical loading up to 5 kN. The load was applied in increments of 1 kN every 15 minutes, followed by a full unloading sequence where each decrement lasted 5 minutes. In the model, this process was represented by 10 subphases (A1-A10), ensuring that both the progressive loading and unloading were captured.

Phase B (Heating only): After the first mechanical cycle, a thermal load (heating) was applied to the pile without mechanical stress. This stage simulated the geothermal activation of the pile under heating temperature input.

Phase C (Mechanical loading during heating): With the heating maintained constant, the pile was once again subjected to incremental mechanical loading and unloading under the same timing conditions as Phase A (1 kN/15 min for loading, 5 min per unloading step). This ensured consistency with the experimental coupled thermo-mechanical cycle.

Phase D (Recovery): In this phase, no thermal or mechanical load was applied, allowing the soil-pile system to relax and replicate the recovery observed in the physical experiment.

Phase E (Cooling only): The pile was then subjected to a cooling load without mechanical loading, simulating heat extraction and the resulting soil temperature decrease.

Phase F (Mechanical loading during cooling): Finally, while the cooling load was kept constant, the pile underwent another sequence of incremental mechanical loading and unloading, following the same rate as in Phases A and C. Subphases F1-F10 were defined to represent each increment and reduction in this final coupled stage.

Overall, the staged construction procedure with 33 calculation phases provided a detailed representation of the experiment, ensuring that the load increments, load durations, heating, cooling, and recovery processes were faithfully mirrored in the numerical simulations.

Table 13. Loading phases

Phase	Loading type	Time interval	Specifics
Initial phase	Gravity loading	-	-
Phase A1 to A10	Mechanical load	100 minutes (1.67 hours)	Loading increments 1 kN/15 minutes and unloading increments 1 kN/5 minutes
Phase B	Thermal load Heating up to 45°C	1200 minutes (20 hours)	Fully coupled flow-deformation. Temperature: time-dependent function from the previous phase
Phase C1 to C10	Thermal (heating) + Mechanical load	100 minutes (1.67 hours)	Loading increments 1 kN/15 minutes and unloading increments 1 kN/5 minutes Temperature: steady state from the previous phase
Phase D	No load on the pile	1260 minutes (21 hours)	No thermal or mechanical load was applied. Recovery phase
Phase E	Thermal load Cooling up to 10°C	1440 minutes (24 hours)	Fully coupled flow-deformation. Temperature: time-dependent function from the previous phase
Phase F1 to F10	Thermal (cooling) + Mechanical load	100 minutes (1.67 hours)	Loading increments 1 kN/15 minutes and unloading increments 1 kN/5 minutes Temperature: steady state from the previous phase

5.3. Numerical modelling outputs

In the numerical simulations, the analysis focused on the temperature distribution within the pile and the surrounding soil, as well as the resulting vertical deformations (settlements) of the pile. These response parameters were selected to allow direct comparison with the corresponding measurements obtained from the laboratory tests. The staged construction and loading procedure adopted in the numerical model closely followed the experimental testing sequence, thereby ensuring consistency between the physical and numerical investigations.

5.3.1. Temperature in the pile and the surrounding soil

To ensure direct comparability with the experimental investigation, temperature results were extracted at locations corresponding to the positions of the thermocouple sensors used in the laboratory setup. The spatial arrangement of the monitoring points in the numerical model was therefore defined in accordance with the experimental instrumentation layout, both along the pile length and within the adjacent soil domain. This consistent definition of observation points allows a meaningful comparison between numerical predictions and experimentally measured temperature responses under the applied thermal and thermo-mechanical loading conditions.

Figure 49a - Figure *49*f presents the numerically obtained temperature distributions within the geothermally active pile and the surrounding soil at the end of each loading and thermal phase defined in the experimental program (Phases A-F). The output times correspond exactly to the completion of each phase, ensuring consistency between the imposed thermal boundary conditions and the extracted numerical results. For each phase, the contour plots illustrate the spatial evolution of temperature, including the maximum and minimum values reached within the computational domain, allowing direct interpretation of heat transfer mechanisms during heating, recovery, and cooling.

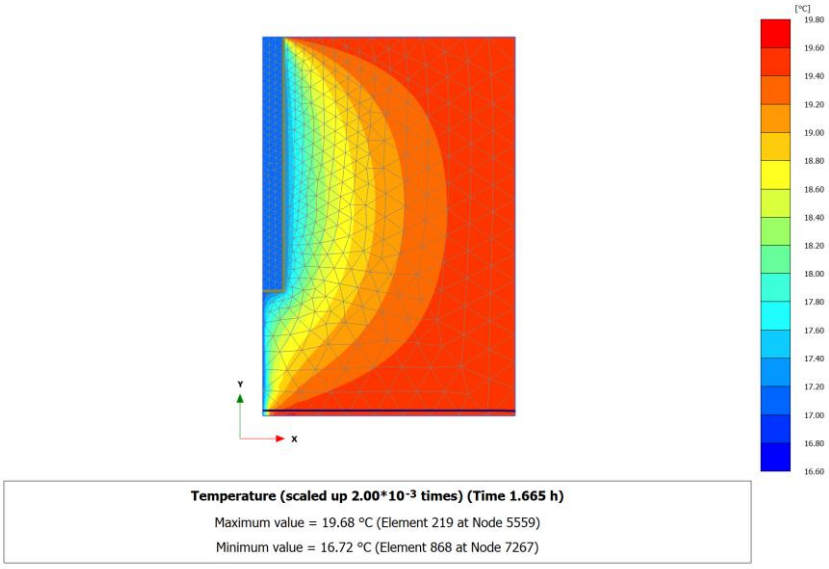

a)

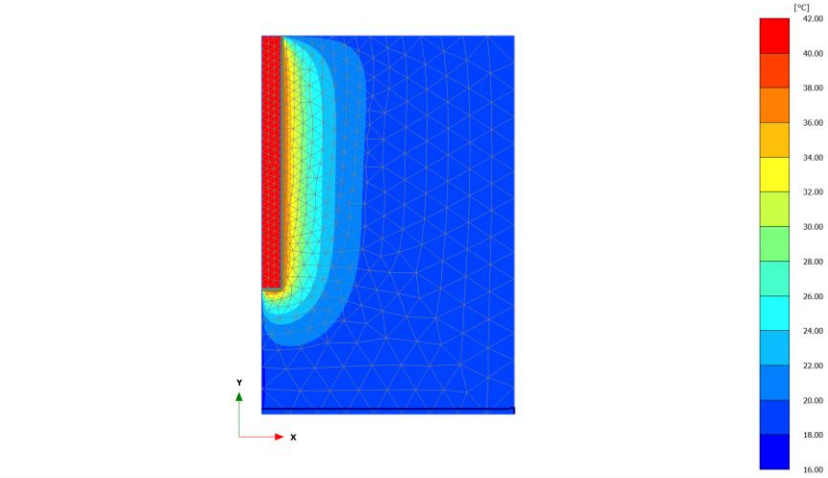

Temperature (scaled up 1.00*10-3 times) (Time 21.67 h)

Maximum value = 41.62 °C (Element 830 at Node 371)

Minimum value = 17.31 °C (Element 344 at Node 5884)

b)

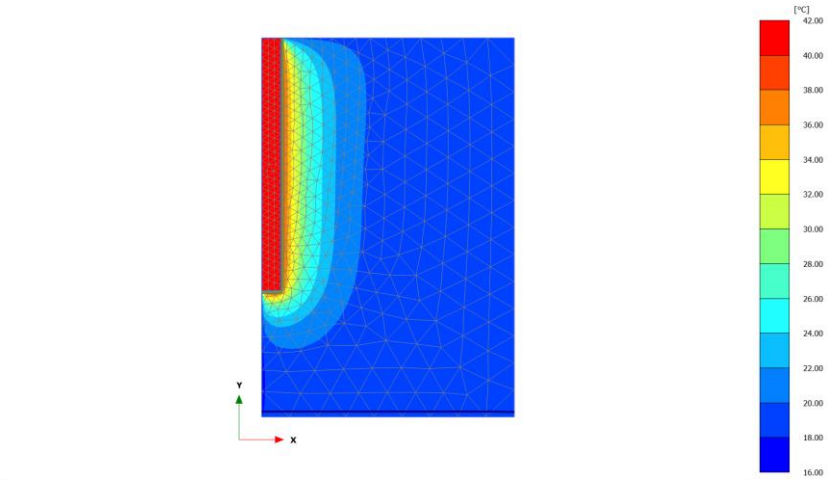

Temperature (scaled up 1.00*10-3 times) (Time 23.33 h)

Maximum value = 41.62 °C (Element 830 at Node 371)

Minimum value = 17.31 °C (Element 344 at Node 5884)

c)

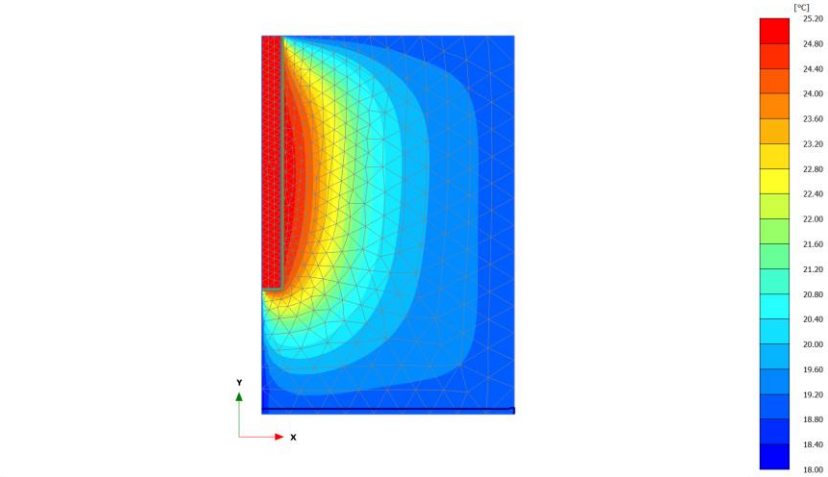

Temperature (scaled up 2.00*10^{-3} times) (Time 44.33 h)

Maximum value = 25.18 °C (Element 830 at Node 371)

Minimum value = 18.22 °C (Element 228 at Node 5568)

d)

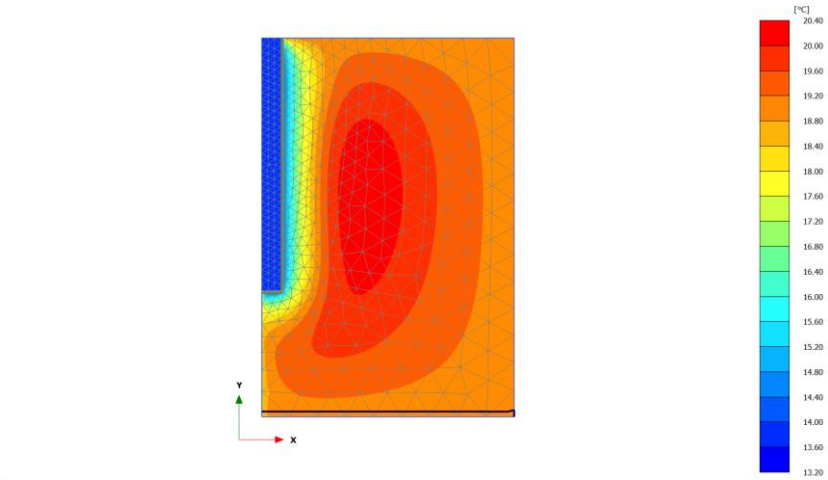

Temperature (scaled up 2.00*10^{-3} times) (Time 68.33 h)

Maximum value = 20.31 °C (Element 468 at Node 4259)

Minimum value = 13.49 °C (Element 830 at Node 371)

e)

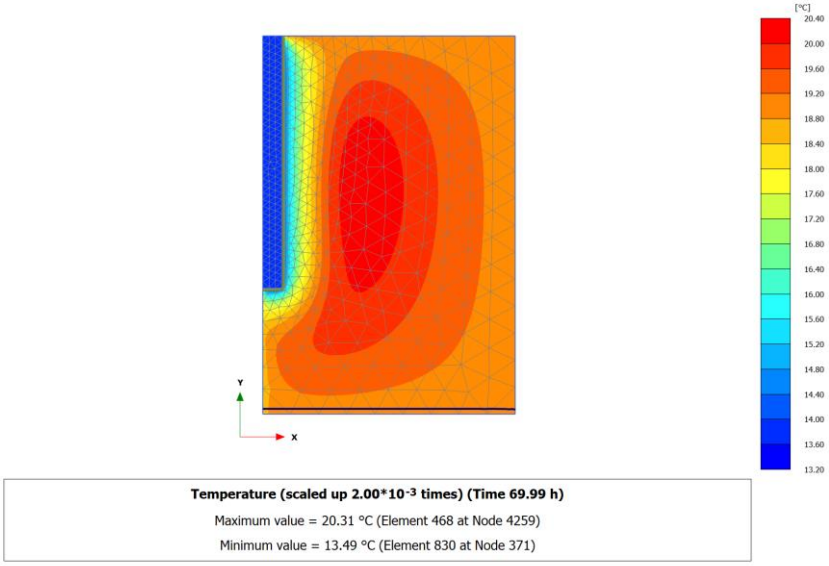

f)

Figure 49. PLAXIS 2D temperature contours (°C) showing the temperature distribution in the pile and surrounding soil at the end of each testing phase: a) Phase A; b) Phase B (heating); c) Phase C (loading under heating); d) Phase D (recovery); e) Phase E (cooling), and f) Phase F (loading under cooling)

At the end of Phase A, the temperature field remains nearly uniform, with temperatures ranging approximately between 16.7 °C and 19.7 °C. These values indicate that the pile-soil system remains close to its initial thermal equilibrium, confirming that mechanical loading alone does not induce any significant thermal disturbance before the application of heating.

After sustained heating at 45 °C (Phase B), a pronounced increase in pile temperature is observed. The numerical results show a maximum temperature of approximately 41.6 °C within the pile, while the minimum temperature in the far-field soil remains around 17.3 °C. A clear radial temperature gradient develops, demonstrating conductive heat transfer from the pile toward the surrounding soil mass.

At the end of Phase C, during which mechanical loading was applied while heating was maintained, the temperature distribution remains largely unchanged compared to Phase B. The pile temperature continues to reach approximately 41.6 °C, with minimum soil temperatures remaining close to 17.3 °C. This confirms that the applied mechanical loading does not significantly affect the thermal field, which is governed primarily by sustained thermal input.

Following the recovery phase (Phase D), the maximum temperature in the pile decreases to approximately 25.2 °C, while the minimum temperature in the soil is about 18.2 °C. The reduction in peak temperature and the smoother thermal gradients indicate gradual heat dissipation from the pile into the surrounding soil once active heating is discontinued.

At the end of the cooling phase (Phase E), the temperature field shows a clear inversion of the thermal gradient. The pile temperature drops to a minimum of approximately 13.9 °C, while the surrounding soil reaches temperatures up to 20.3 °C. This confirms the effectiveness of the cooling process and highlights the pile's ability to extract heat from the adjacent soil.

The final temperature distribution at the end of Phase F indicates that the cooling-induced thermal field is preserved during mechanical loading. The pile remains cooler than the surrounding soil, with temperature values similar to those observed at the end of Phase E (minimum around 13.9 °C and maximum around 20.3 °C). This further confirms that mechanical loading has a negligible influence on the temperature evolution compared to thermal boundary conditions.

Based on the experimental setup shown in Figure 29, the numerical model developed in PLAXIS 2D reproduces the same geometry, sensor locations, and thermal loading history applied during the laboratory testing program. Using the numerical output results obtained for all testing phases (A-F), temperature-time diagrams were derived for representative locations within the pile body and the surrounding soil. The pile temperature was calculated as the average value of thermocouples T1-T3, while the soil temperature evolution was evaluated using averaged values from three rows of sensors: T4-T6 (first row), T7-T9 (second row), and T10-T12 (third row). This approach enables the assessment of both the temporal and spatial attenuation of temperature with increasing distance from the pile axis during the heating, recovery, and cooling phases.

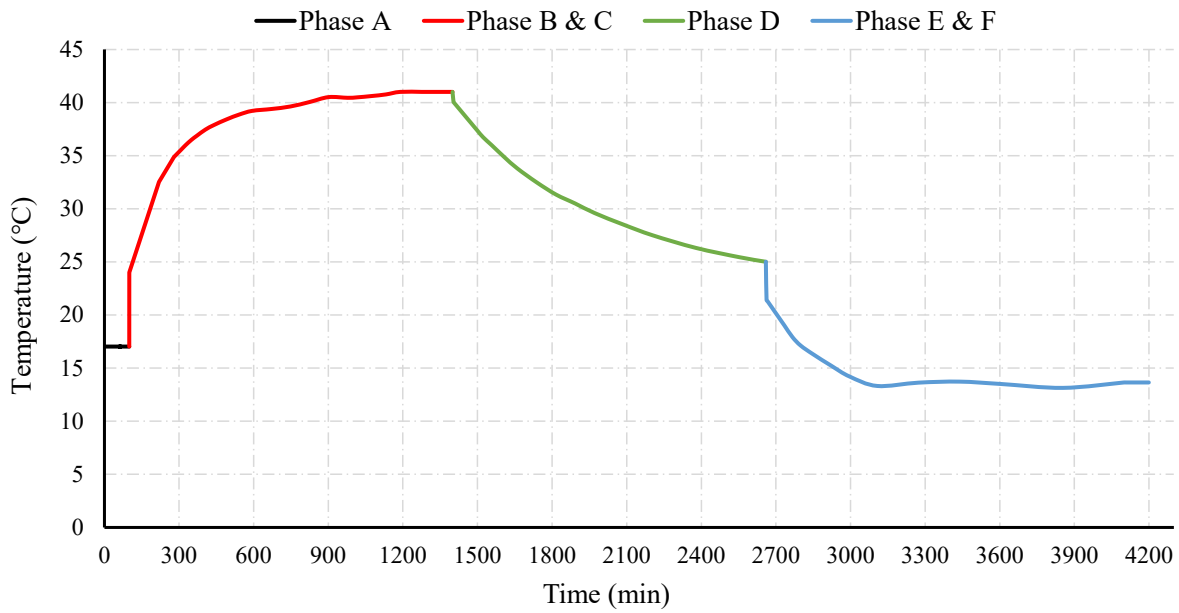

a)

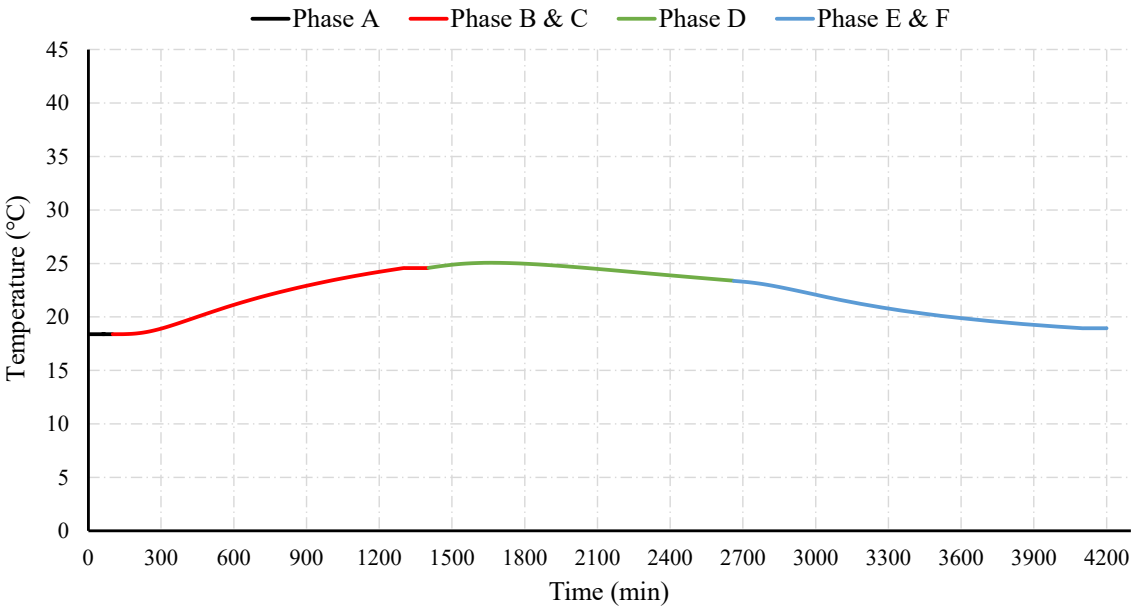
Phase A
Phase B & C
Phase D
Phase E & F
Temperature (°C)
0
5
10
15
20
25
30
35
40
45
0
300
600
900
1200
1500
1800
2100
2400
2700
3000
3300
3600
3900
4200
Time (min)

b)

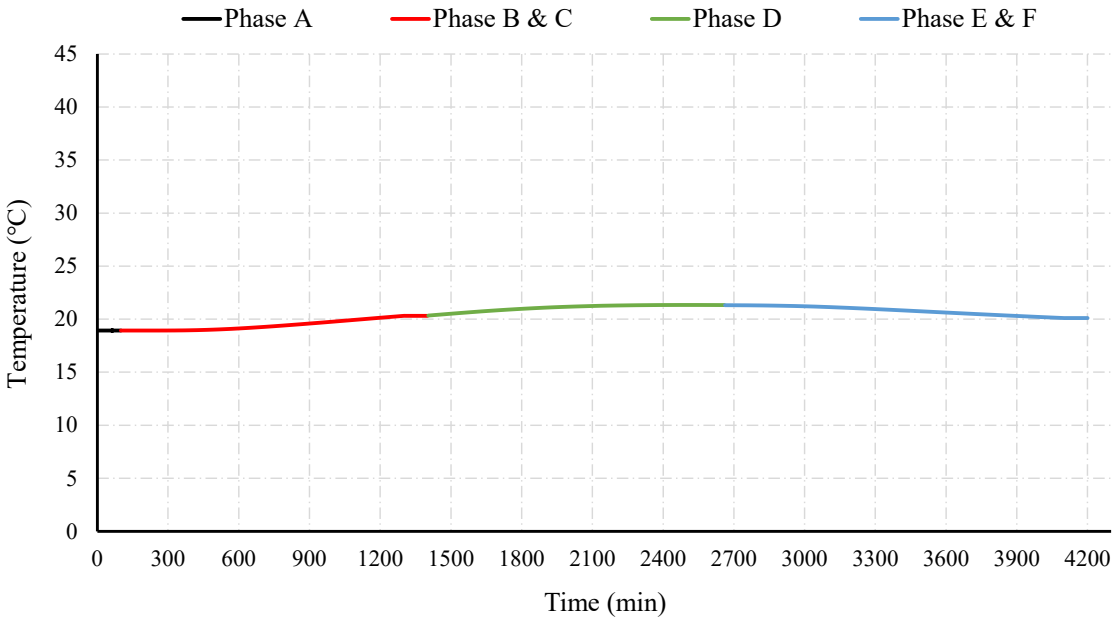
Phase A
Phase B & C
Phase D
Phase E & F
Temperature (°C)
0
5
10
15
20
25
30
35
40
45
0
300
600
900
1200
1500
1800
2100
2400
2700
3000
3300
3600
3900
4200
Time (min)

c)

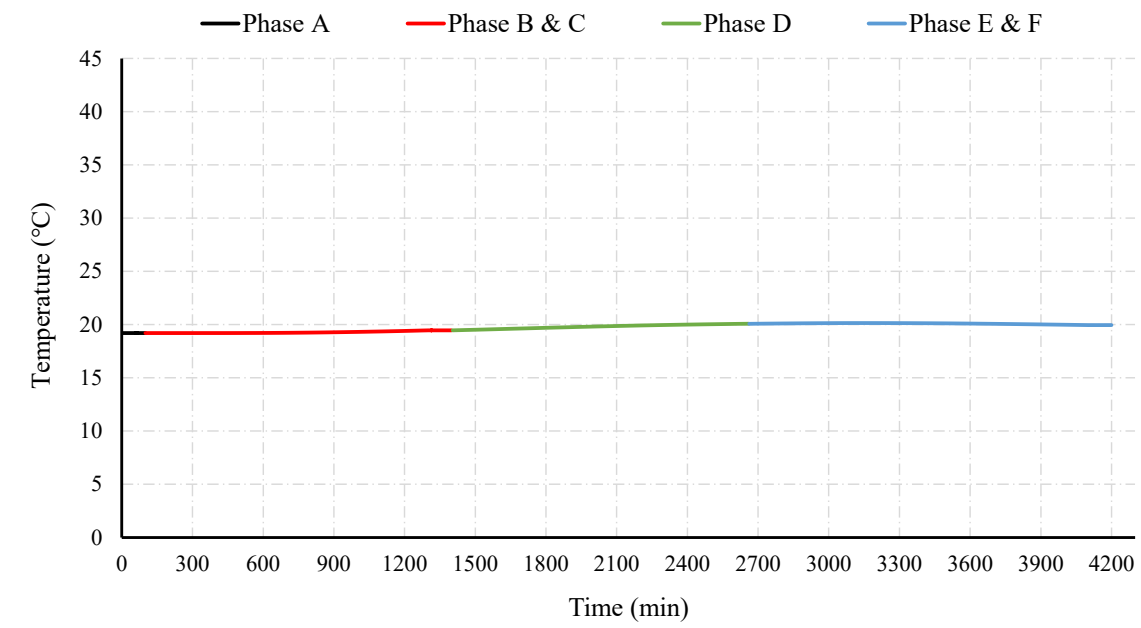

d)

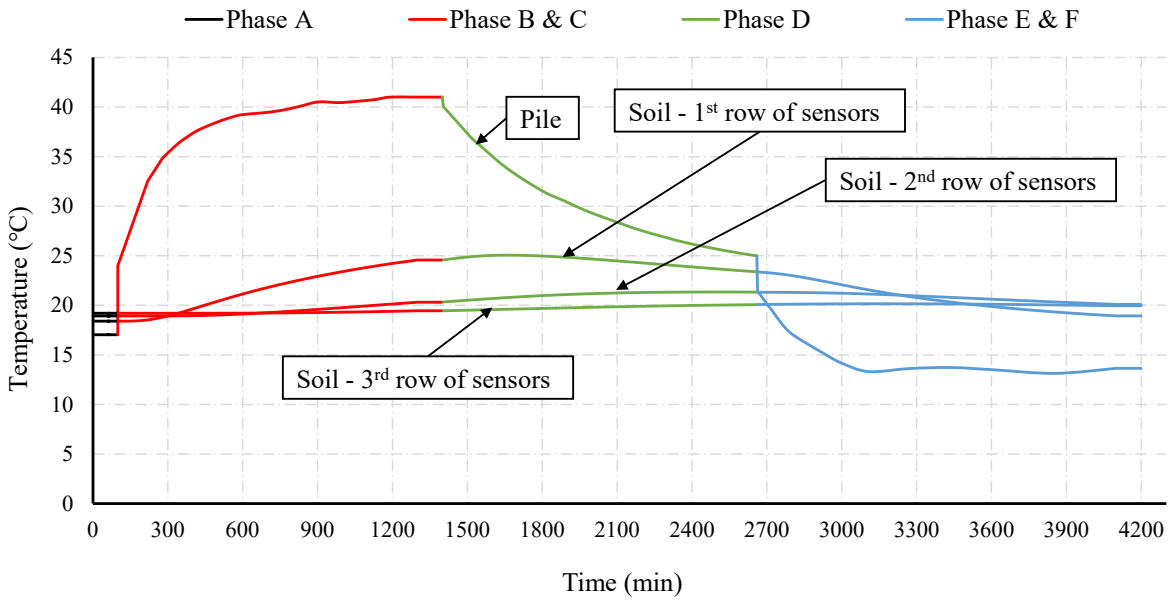

e)

Figure 50. Temperature changes in the pile and the surrounding soil due to thermal effects applied to the pile in the numerical model. a) Pile; b) 1st row of sensors in the soil; c) 2nd row of sensors in the soil; d) 3rd row of sensors in the soil, and e) pile and surrounding soil

The temperature-time diagram for the pile body shows a rapid temperature increase during Phases B and C, corresponding to the imposed heating at 45°C. The pile temperature rises sharply at the onset of heating and gradually approaches a quasi-steady value, reflecting the dominant role of the pile as the primary heat source. During Phase D, a clear temperature decay is observed as heat dissipates into the surrounding soil following termination of active heating. In Phases E and F, the temperature decreases further due to active cooling, stabilizing at a lower level, which confirms the pile's capacity to both inject and extract heat depending on the imposed thermal boundary conditions.

The temperature response of the first row of soil sensors, located closest to the pile, follows a similar trend to that observed within the pile but with reduced magnitude and delayed response. During the heating phases, the soil temperature increases gradually, indicating conductive heat transfer from the pile into the surrounding ground. Peak temperatures remain significantly lower than those within the pile, highlighting the attenuation of thermal energy with radial distance. During recovery and cooling phases, the temperature decreases smoothly, demonstrating the soil's thermal buffering capacity and gradual dissipation of stored heat.

At the second row of sensors, the temperature variations are further attenuated compared to the first row. The heating phases result in a modest temperature increase, with a slower rate of change and lower peak values. This behavior reflects the increased distance from the pile and the resulting reduction in heat flux. During the recovery and cooling phases, temperature changes remain gradual and limited in amplitude, indicating that thermal influence at this distance is primarily governed by long-term conduction rather than direct thermal input.

The temperature-time diagram for the third row of soil sensors shows minimal temperature variation throughout all testing phases. Only slight increases are observed during heating, while recovery and cooling phases produce negligible changes. This confirms that the thermal influence zone of the pile is spatially limited and that, at greater distances, the soil remains close to its initial thermal condition. Such behavior is consistent with expected conductive heat transfer mechanisms in low-permeability soil media.

5.3.2. Vertical displacements

Figure 51a - Figure *51*f present the numerical results of vertical displacements of the pile-soil system obtained from the PLAXIS 2D analysis. Vertical displacements were evaluated at the pile head, consistent with the experimental measurements. The subsequent figures illustrate the displacement fields at characteristic stages of the testing program (A5, B, C, D, E, and F5), allowing evaluation of the interaction effects from the mechanical loading and thermally induced expansion or contraction of the pile.

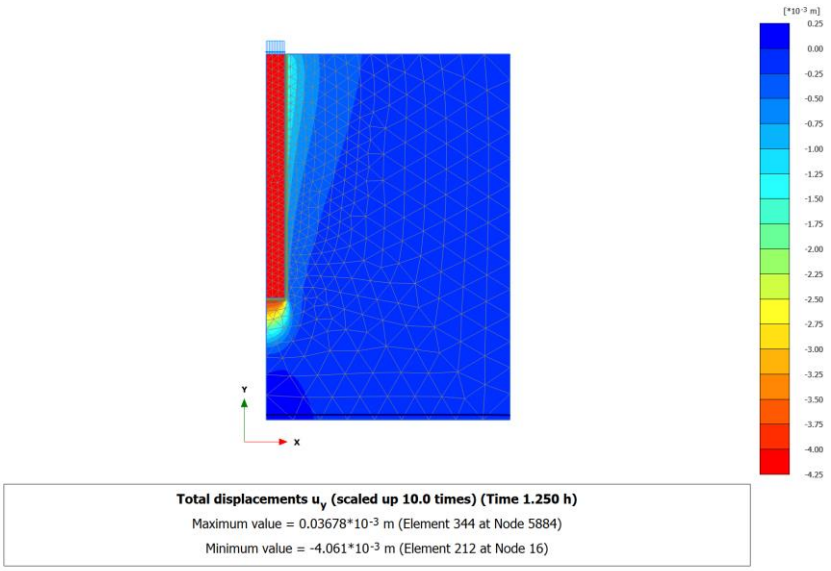

a)

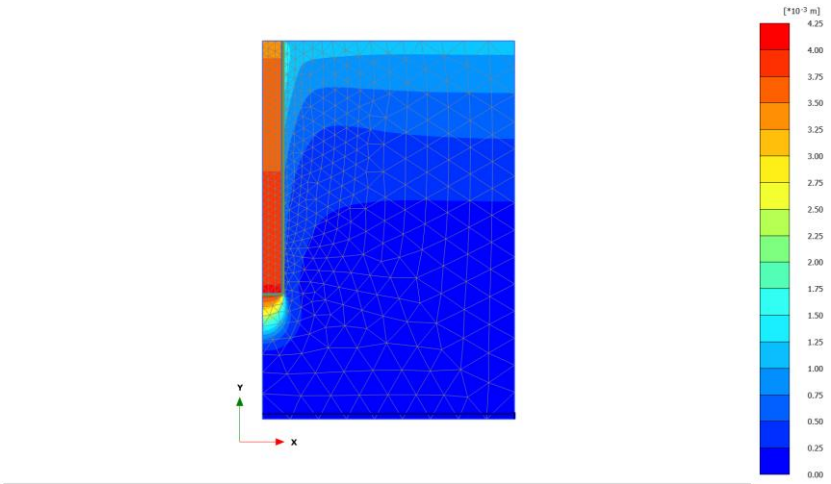

Total displacements |u| (scaled up 10.0 times) (Time 21.67 h)
Maximum value = 4.019*10-3 m (Element 215 at Node 7207)

b)

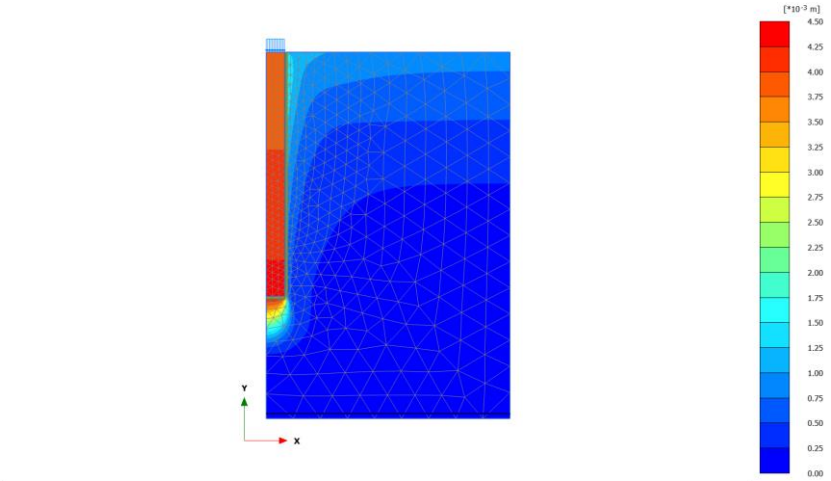

Total displacements |u| (scaled up 10.0 times) (Time 22.92 h)
Maximum value = 4.333*10-3 m (Element 215 at Node 7207)

c)

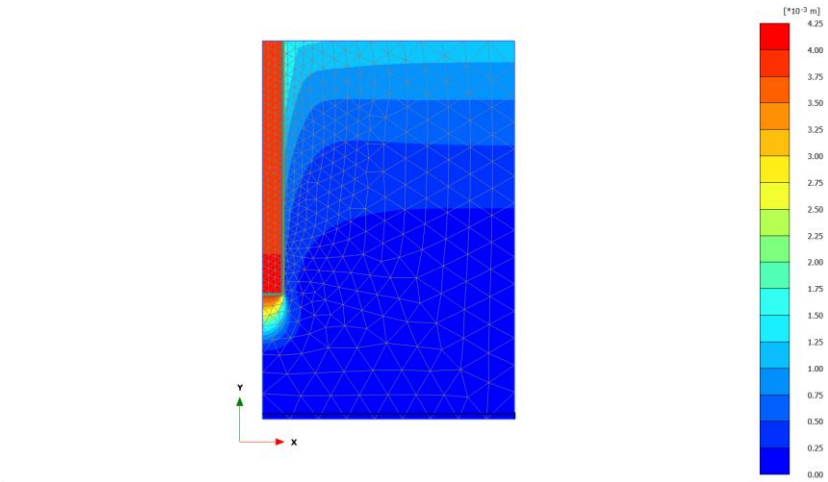

Total displacements |u| (scaled up 10.0 times) (Time 44.33 h)
Maximum value = 4.038*10-3 m (Element 820 at Node 7197)

d)

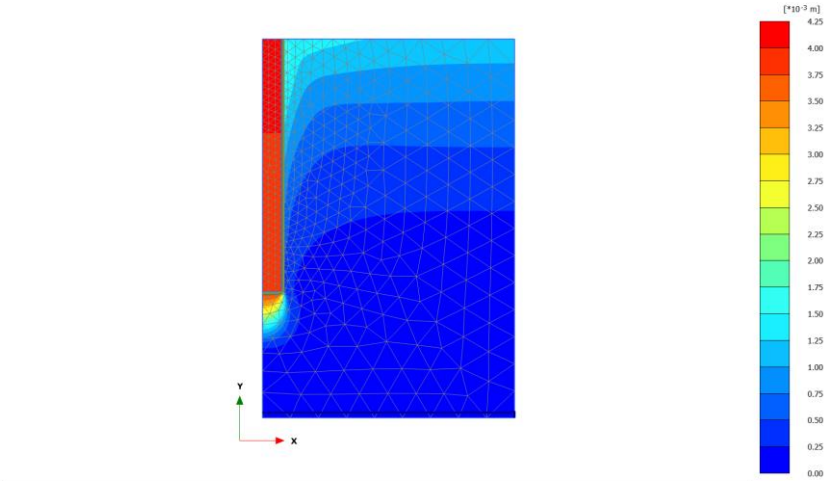

Total displacements |u| (scaled up 10.0 times) (Time 68.33 h)
Maximum value = 4.029*10-3 m (Element 212 at Node 16)

e)

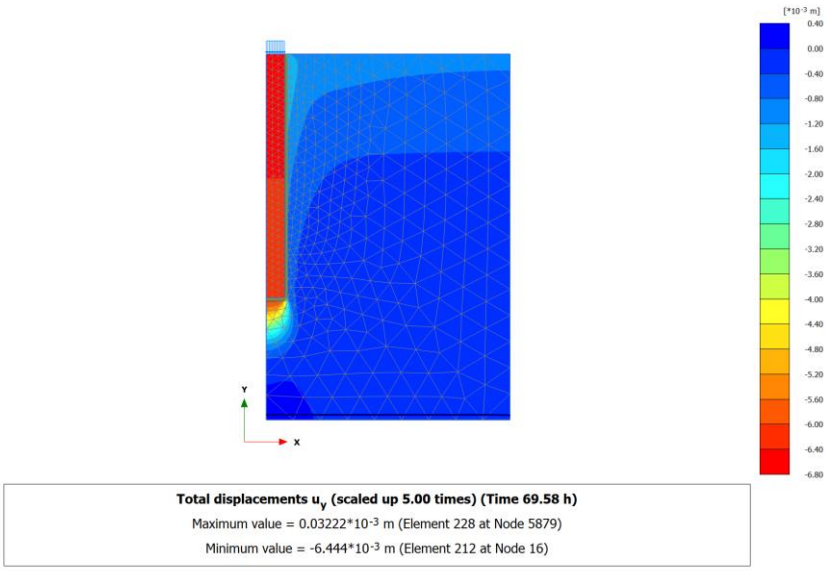

f)

Figure 51. PLAXIS 2D total displacement contours of the pile-soil system at characteristic testing phases: a) Phase A5 (maximum mechanical loading); b) Phase B (heating); c) Phase C (maximum mechanical loading under sustained heating); d) Phase D (recovery); e) Phase E (cooling), and f) Phase F5 (maximum mechanical loading under sustained cooling)

Figure 51a shows the vertical displacement field at the end of Phase A5, maximum mechanical load during Phase A, corresponding to mechanical loading under ambient thermal conditions. The pile exhibits downward displacement concentrated along the shaft and at the pile tip, with the maximum settlement occurring at the pile head, consistent with conventional axial pile behavior. This state represents the reference condition before the application of thermal loading.

The displacement field at the end of Phase B, shown in Figure 51b, indicates a reduction in downward displacement at the pile head compared to Phase A5. This response is attributed to thermal expansion of the pile during heating, which induces upward axial strain and partially counteracts the mechanically induced settlement. Although the surrounding soil exhibits smooth displacement redistribution, the dominant effect at the pile head is the decrease in settlement caused by pile expansion.

Figure 51c presents the displacement field at the end of Phase C5-maximum mechanical loading, while heating was sustained. Compared to Phase B, the pile head displacement increases again due to the superposition of mechanical loading on the thermally expanded pile. Nevertheless, the displacement remains lower than that observed in Phase A5, confirming that thermal expansion continues to offset part of the mechanically induced settlement.

At the end of the recovery phase (Phase D), shown in Figure 51d, a gradual increase in downward displacement at the pile-head is observed as the pile cools and thermal expansion diminishes. This behavior reflects partial loss of thermally induced uplift, while residual displacements persist due to irreversible soil deformation accumulated during previous loading phases.

Figure 51e illustrates the displacement field at the end of Phase E, corresponding to active cooling of the pile. The pile undergoes thermal contraction, resulting in increased downward

displacement at the pile head. This phase highlights the reversal of the thermal effect observed during heating, with cooling enhancing settlement relative to the recovery phase.

The final displacement field, shown in Figure 51f, corresponds to Phase F5-maximum mechanical loading of Phase F, in which mechanical loading was applied under sustained cooling conditions. The pile head displacement increases further due to the combined effect of mechanical loading and thermal contraction. The results indicate that while thermal effects significantly modify the displacement response, mechanical loading remains the dominant contributor to the overall pile settlement.

Figure 52a - Figure *52*g present the numerically obtained pile head total displacement-time responses for the geothermally active pile during testing Phases A to F. Vertical displacements were measured at the pile top, in accordance with the experimental measurement location. Each figure illustrates the pile response during an individual loading or thermal phase, while the final figure combines all phases to provide a comprehensive view of the pile's thermo-mechanical behavior. The applied axial load history is shown together with the displacement response, allowing direct interpretation of the interaction between mechanical loading, heating, recovery, and cooling effects.

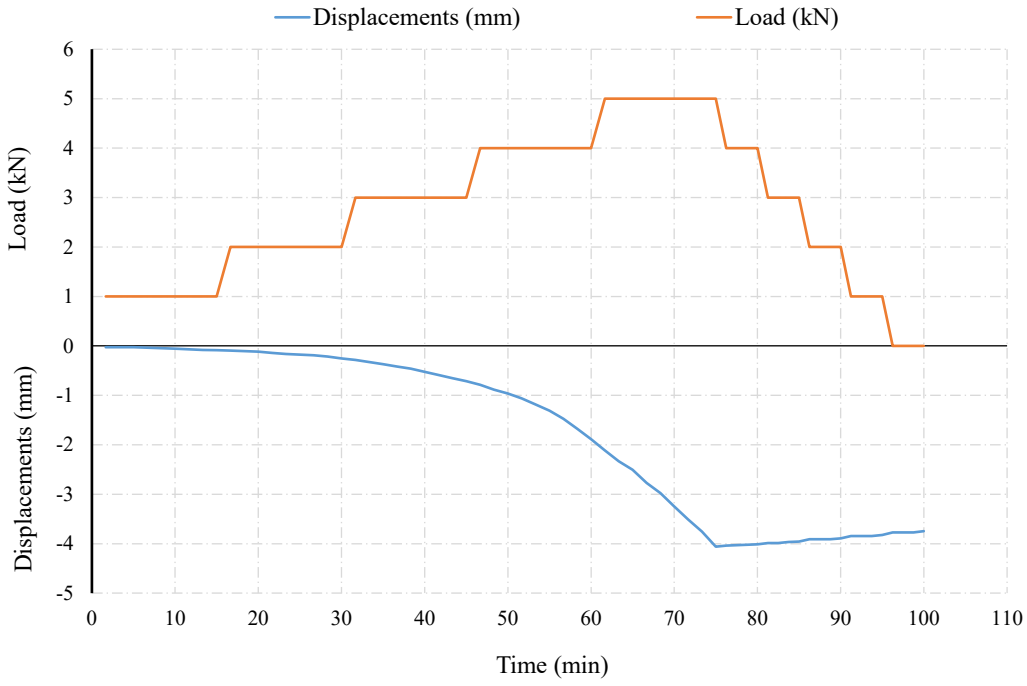

a)

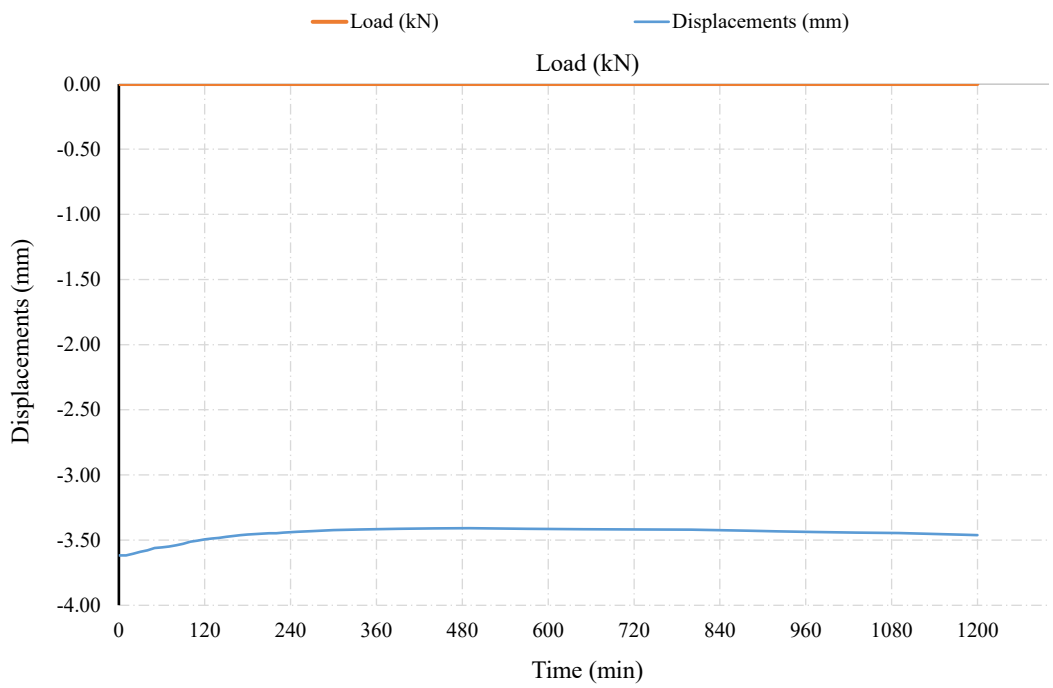
Load (kN)
Displacements (mm)
Load (kN)
0.00
-0.50
-1.00
-1.50
-2.00
-2.50
-3.00
-3.50
-4.00
Displacements (mm)
0
120
240
360
480
600
720
840
960
1080
1200
Time (min)

b)

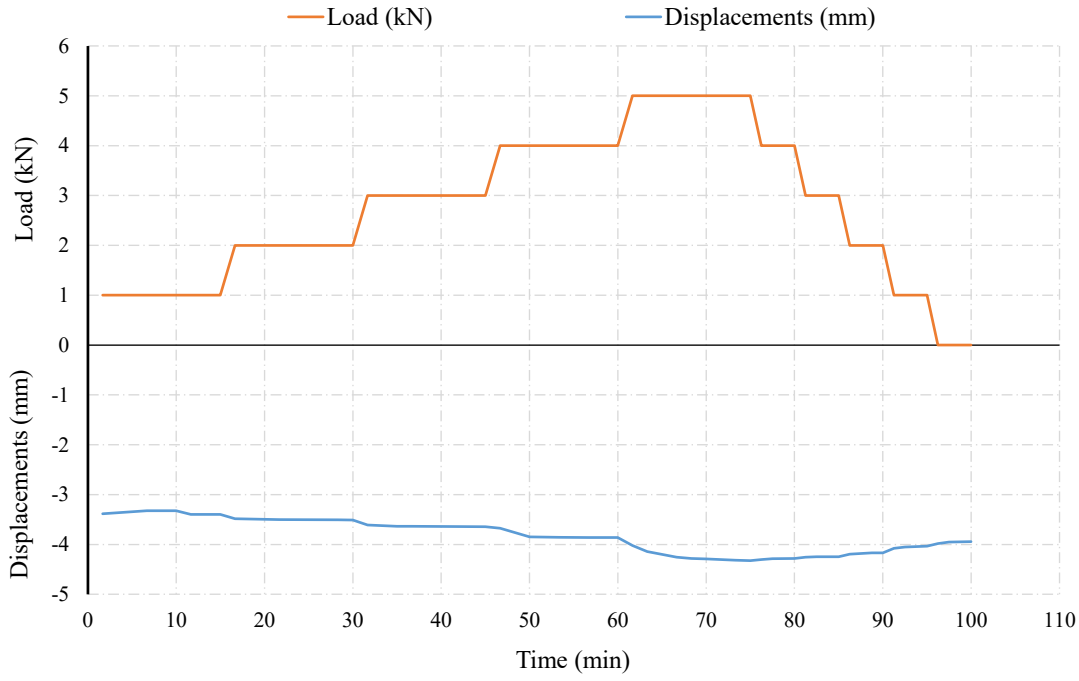
Load (kN)
Displacements (mm)
6
5
4
3
2
1
0
-1
-2
-3
-4
-5
Load (kN)
Displacements (mm)
0
10
20
30
40
50
60
70
80
90
100
110
Time (min)

c)

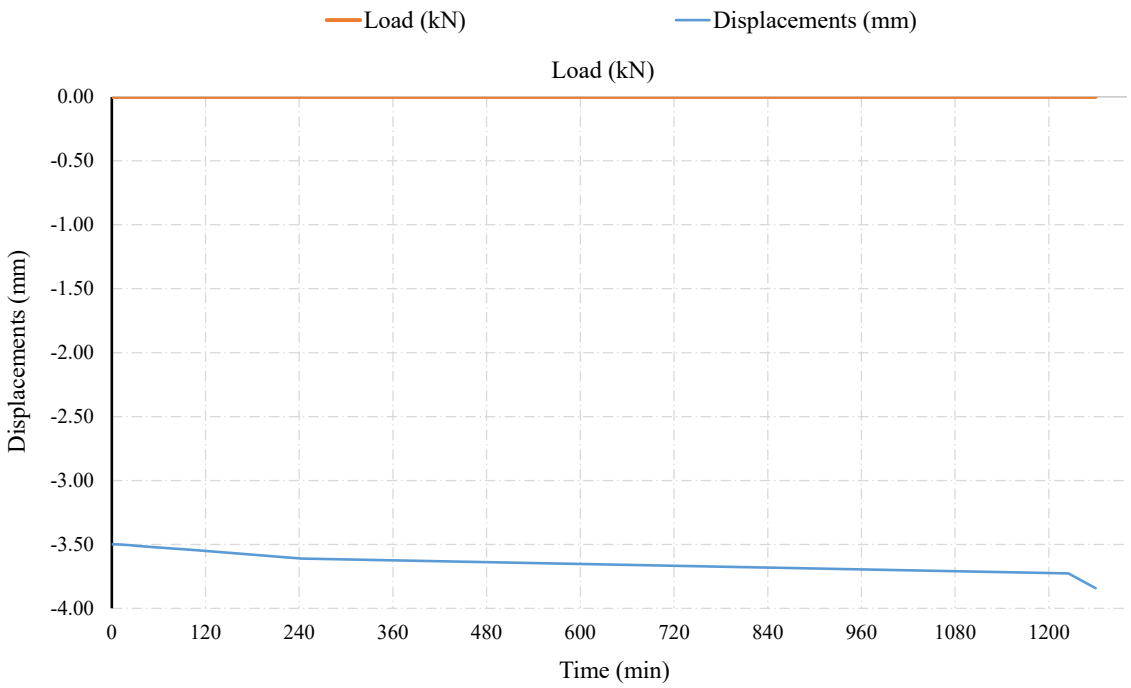
Load (kN)
Displacements (mm)
Load (kN)
0.00
-0.50
-1.00
-1.50
-2.00
-2.50
-3.00
-3.50
-4.00
Displacements (mm)
0
120
240
360
480
600
720
840
960
1080
1200
Time (min)

d)

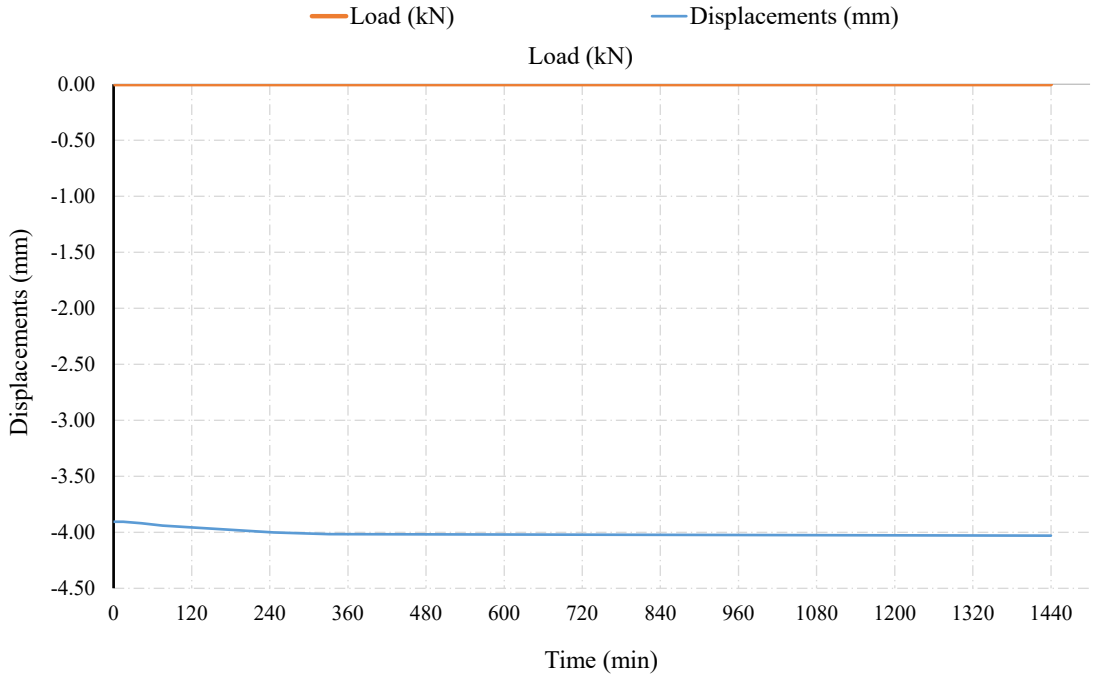
Load (kN)
Displacements (mm)
Load (kN)
0.00
-0.50
-1.00
-1.50
-2.00
-2.50
-3.00
-3.50
-4.00
-4.50
Displacements (mm)
0
120
240
360
480
600
720
840
960
1080
1200
1320
1440
Time (min)

e)

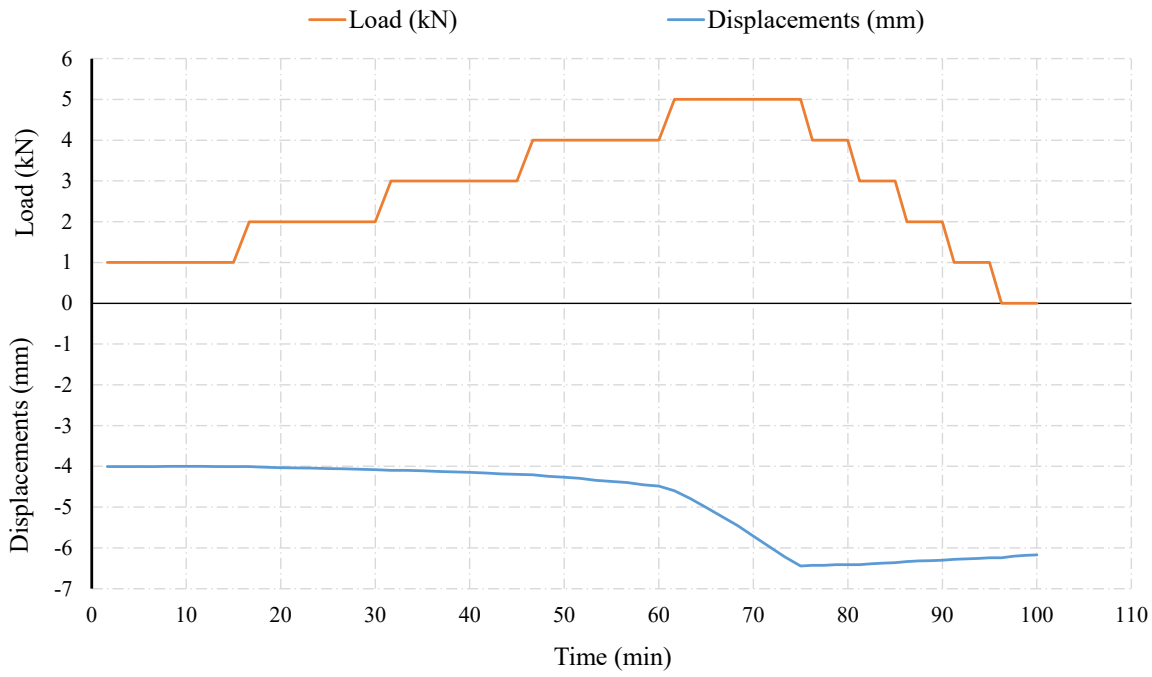

f)

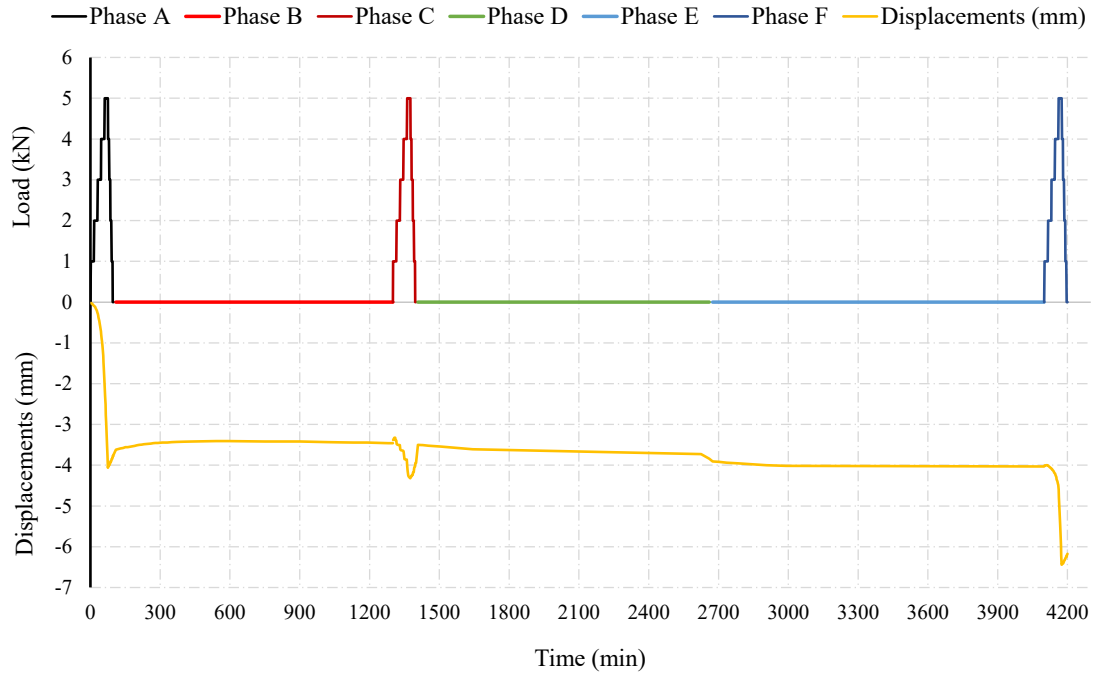

g)

Figure 52. Pile head total displacement-time responses obtained from the PLAXIS 2D numerical model for the testing phases: (a) Phase A (mechanical loading), (b) Phase B (heating), (c) Phase C (mechanical loading under sustained heating), (d) Phase D (recovery), (e) Phase E (cooling), (f) Phase F (mechanical loading under sustained cooling), and (g) combined response for Phases A-F.

Figure 52a shows the pile head displacement during Phase A, which consists of stepwise mechanical loading and unloading under ambient thermal conditions. The displacement increases progressively with increasing load, indicating conventional axial pile settlement behavior. Partial recovery is observed during unloading; however, residual displacement

remains, reflecting irreversible soil deformation. This response establishes the mechanical reference state before thermal activation.

The displacement-time response during Phase B is shown in Figure 52b. In the absence of mechanical loading, the pile head displacement decreases in magnitude (uplift) as heating progresses. This behavior is attributed to thermal expansion of the pile, which counteracts the previously accumulated mechanical settlement. The displacement stabilizes toward the end of the heating phase, indicating a quasi-steady thermal state.

Figure 52c presents the pile head displacement during Phase C, where mechanical loading is applied while heating is maintained. Compared to Phase A, the displacement response shows reduced settlement for the same load levels, confirming the continued influence of thermal expansion. The combined effect of mechanical loading and sustained heating results in a moderated settlement response relative to purely mechanical conditions.

The displacement evolution during the recovery phase (Phase D) is shown in Figure 52d. With both mechanical and thermal loads removed, a gradual increase in downward displacement is observed. This behavior reflects thermal dissipation and contraction of the pile, leading to partial loss of the thermally induced uplift. The slow rate of displacement change indicates time-dependent redistribution of stresses within the pile-soil system.

Figure 52e shows the pile head displacement during active cooling. The displacement increases further in the downward direction due to thermal contraction of the pile, which amplifies settlement. The response remains smooth and continuous, demonstrating stable pile-soil interaction during cooling and confirming the reversibility of thermal strains relative to heating.

The displacement-time response during Phase F is presented in Figure 52f. Mechanical loading applied under sustained cooling leads to the largest settlement values observed during the testing program. The combined effect of axial load and thermal contraction governs the pile response, indicating that cooling enhances mechanically induced displacements.

Figure 52g summarizes the pile head displacement over the entire testing sequence. The plot clearly highlights the alternating influence of mechanical loading, thermal expansion during heating, partial recovery, and enhanced settlement during cooling. The results demonstrate that thermal effects significantly modify pile head displacements, while mechanical loading remains the primary driver of permanent settlement. This combined response provides a consistent basis for comparison with experimental measurements and supports the interpretation of thermo-mechanical pile behavior.

6. RESULTS AND DISCUSSIONS

This chapter presents and discusses the results obtained within the framework of this doctoral research, which investigates the thermo-mechanical behavior of geothermally active piles through a combined experimental and numerical approach. A special emphasis is placed on the interpretation of the experimental results, which constitute the core contribution of this thesis, while the numerical analysis is used to support, interpret, and validate the observed physical behavior. The experimental program involved laboratory-scale testing of a model pile subjected to controlled mechanical loading, thermal loading, and combined thermo-mechanical actions. Throughout the testing, key response parameters were continuously monitored, including the evolution of temperature within the pile and in the surrounding soil, as well as vertical displacements measured at the pile-head. The adopted loading scheme enabled the isolation and assessment of individual and coupled effects of mechanical and thermal actions on pile behavior. In parallel, a numerical finite element model was developed to replicate the experimental conditions as precisely as possible. The numerical simulations were performed using the same geometric configuration, material properties, boundary conditions, and loading sequence as those adopted in the laboratory tests. Output results were extracted at locations corresponding to the experimental measurement points, allowing for a direct and meaningful comparison between experimental observations and numerical predictions. The comparative analysis shows that the numerical results are in very close agreement with the experimental observations for both temperature evolution and vertical pile deformations. The trends, magnitudes, and temporal development of the responses are consistently captured by the numerical model, with only minor deviations observed in certain phases. The differences are within acceptable limits and primarily attributed to modelling simplifications, boundary effects, and inherent experimental uncertainties, rather than to fundamental discrepancies in the underlying thermo-mechanical behavior. The discussion in this chapter focuses on two principal aspects of the pile response: (i) temperature changes within the pile and the surrounding soil, and (ii) vertical deformations of the pile induced by mechanical and thermal loading. For each aspect, the experimental results are first analyzed and interpreted, followed by a comparative discussion with the corresponding numerical results. The chapter aims to provide a comprehensive understanding of the thermo-mechanical behavior of geothermally active piles and to assess the capability of numerical models to reliably reproduce experimentally observed responses under combined loading conditions.

6.1. Temperature in the pile and the surrounding soil

A detailed comparison between the experimentally measured and numerically predicted temperature changes in the pile and surrounding soil during the entire testing duration is presented. The comparison is performed for all loading phases (A-F) at all measurement locations, including the pile and the three rows of soil sensors installed at increasing radial distances from the pile shaft. The numerical results were extracted at locations corresponding exactly to the positions of the experimental temperature sensors, allowing for a direct and meaningful comparison. This approach enables an assessment of the reliability of the numerical model to reproduce both the magnitude and temporal evolution of temperature changes

observed during the experimental program. Overall, the comparison demonstrates a very close agreement between experimental and numerical results. The numerical model successfully captures the main thermal trends, peak temperatures, and cooling behaviour in both the pile and the surrounding soil. Minor differences are observed in specific phases or sensor rows that are limited in magnitude and attributed to experimental uncertainties, boundary effects, and model simplifications, rather than to differences in the governing thermal mechanisms.

Figure 53 presents the comparison between experimentally measured and numerically predicted temperature changes within the pile for all loading phases. During the heating phases (B and C), a rapid temperature increase is observed, followed by a stabilization period, which is accurately reproduced by the numerical model. The peak pile temperature and the rate of temperature increase show very close agreement between the two approaches.

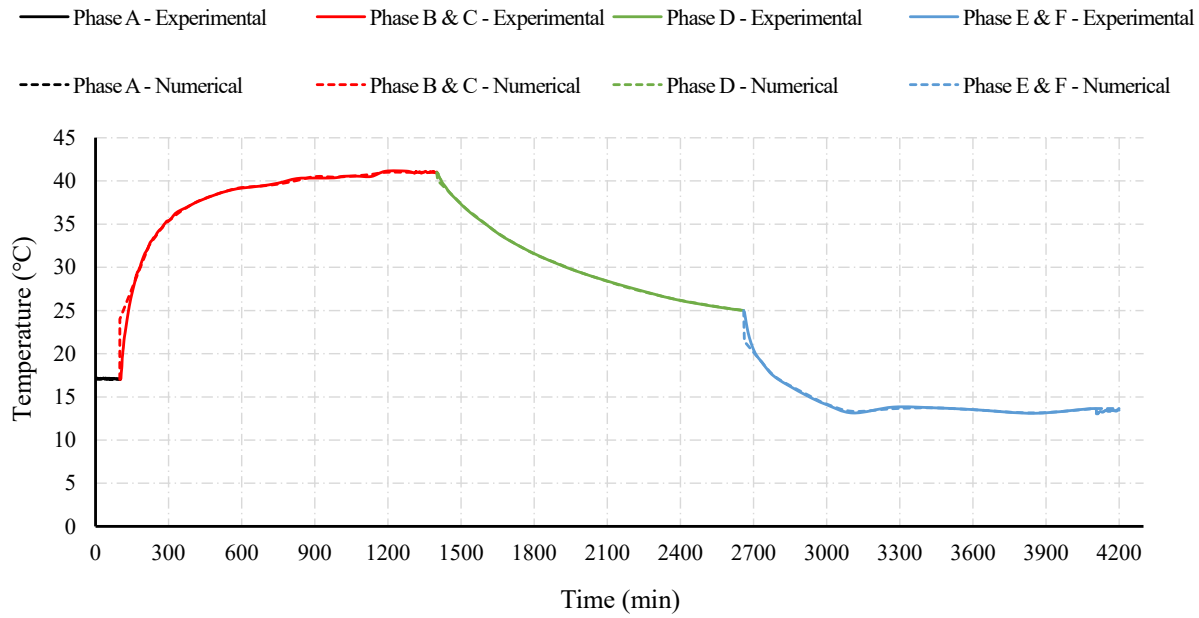

Figure 53. Temperature changes in the pile: experimental vs numerical

During the cooling phase (Phase D), both experimental and numerical results exhibit a gradual temperature decrease, indicating controlled heat dissipation from the pile to the surrounding soil. The subsequent phases (E and F) show further temperature reduction and stabilization at a lower level. Overall, the numerical model captures both the magnitude and the temporal evolution of the pile temperature with high accuracy, confirming its ability to represent heat transfer within the pile material.

Figure 54 illustrates the temperature evolution in the first row of soil sensors, located closest to the pile shaft. Compared to the pile, the temperature increase in the surrounding soil is more gradual and attenuated, reflecting the thermal diffusion process from the pile into the soil.

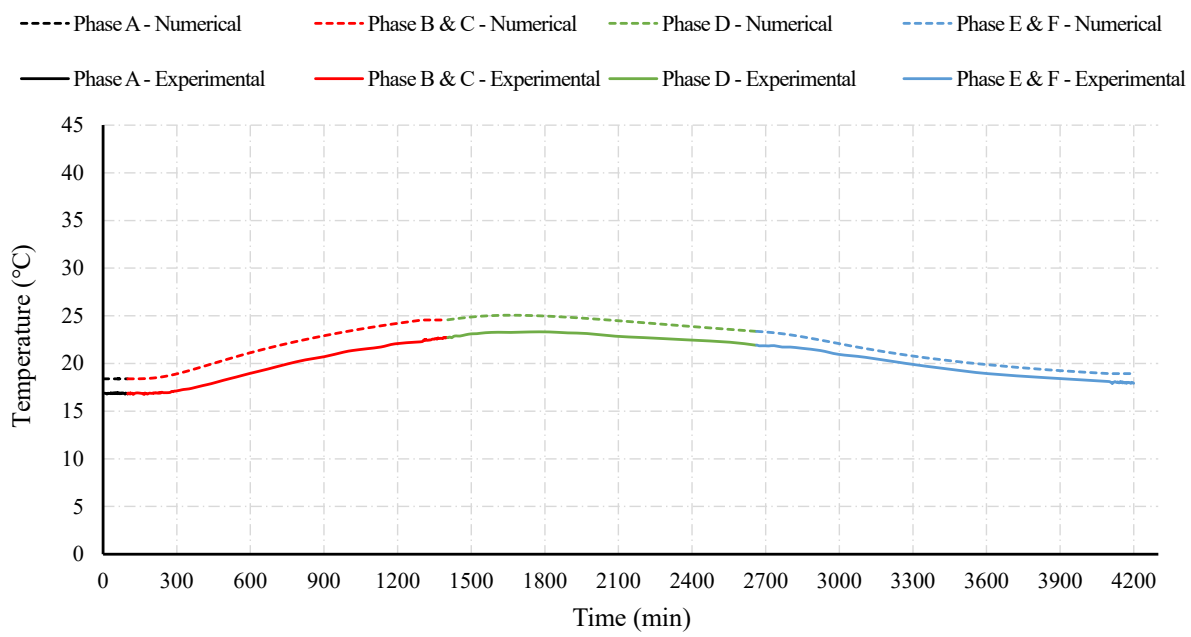

Figure 54. Temperature changes of the first row of soil sensors: experimental vs numerical

The numerical results closely follow the experimental measurements throughout all phases, reproducing the delayed temperature rise during heating and the smooth temperature decay during cooling. Slight differences in peak temperature values are observed; however, the overall agreement remains very good, indicating that the numerical model accurately captures heat transfer at the pile-soil interface.

Figure 55 shows the comparison of temperature changes recorded in the second row of soil sensors, located at a greater radial distance from the pile. As expected, the temperature variations are smaller and develop more slowly compared to the first row, demonstrating the attenuation of thermal effects with increasing distance from the pile.

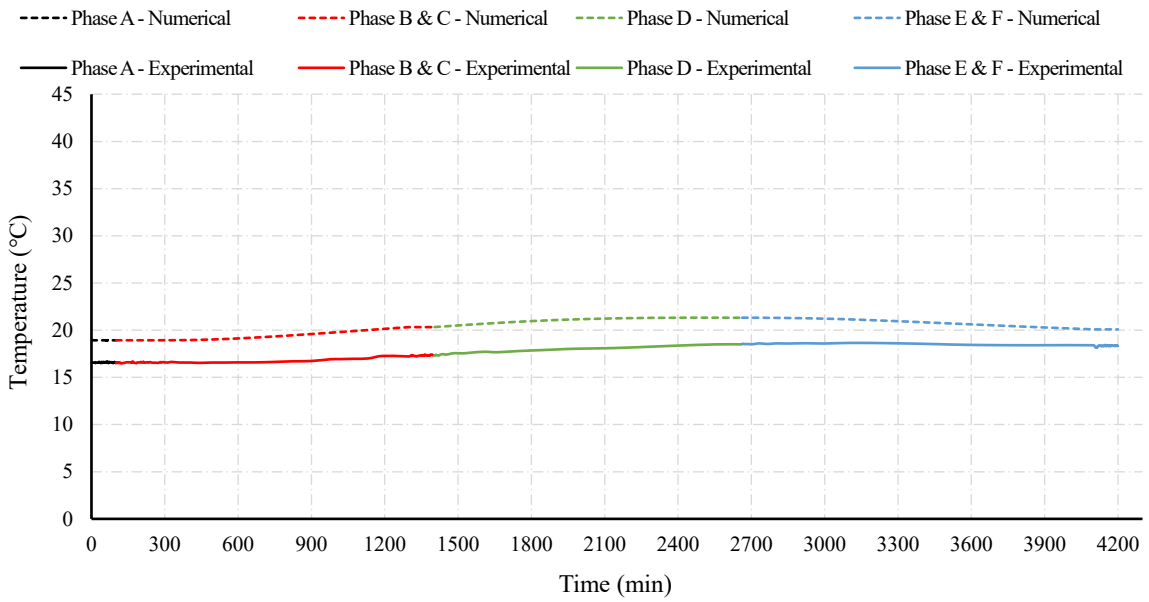

Figure 55. Temperature changes of the second row of soil sensors: experimental vs numerical

The numerical predictions are in close agreement with the experimental data, successfully reproducing both the gradual temperature increase during the heating phases and the stabilization behaviour during cooling. The consistency between experimental and numerical trends confirms that the numerical model effectively represents radial heat propagation through the soil mass.

Figure 56 presents the temperature evolution in the third row of soil sensors, representing the furthest measurement points from the pile. The recorded temperature changes are relatively small, indicating limited thermal influence at this distance.

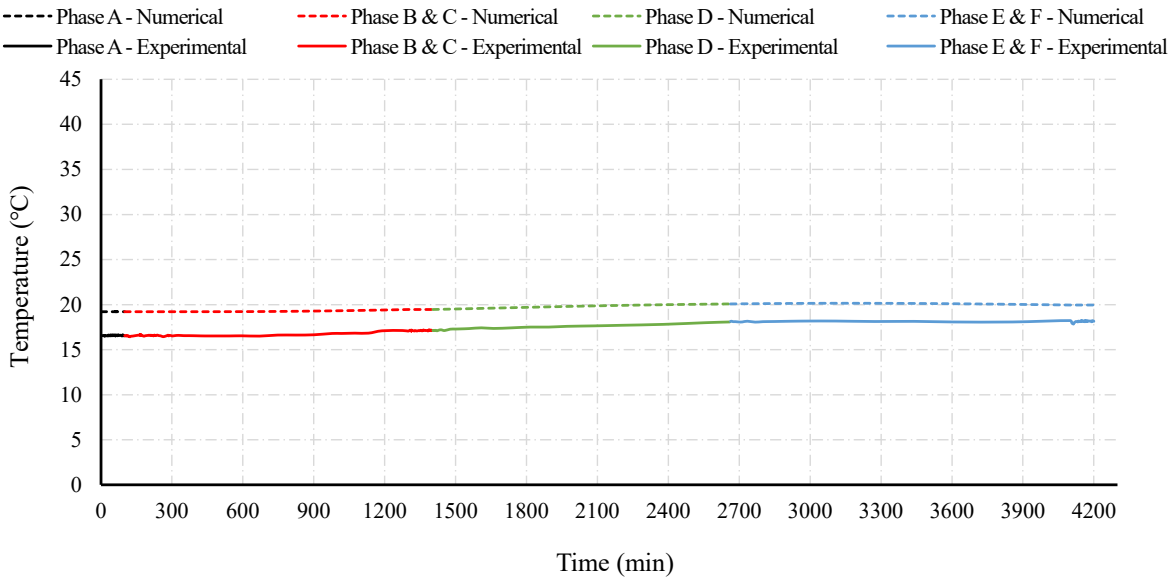

Figure 56. Temperature changes of the third row of soil sensors: experimental vs numerical

Both experimental and numerical results exhibit similar temperature levels and trends, with minimal deviations throughout the testing period. The numerical model slightly overestimates temperatures in some phases; however, these differences remain small and do not affect the overall interpretation. The results confirm that thermal effects diminish significantly with increasing radial distance from the pile.

Figure 57 provides a comprehensive comparison of temperature changes in the pile and in all three rows of soil sensors for both experimental and numerical results. The figure clearly illustrates the strong thermal gradient between the pile and the surrounding soil, as well as the progressive attenuation of temperature variations with increasing distance from the pile.

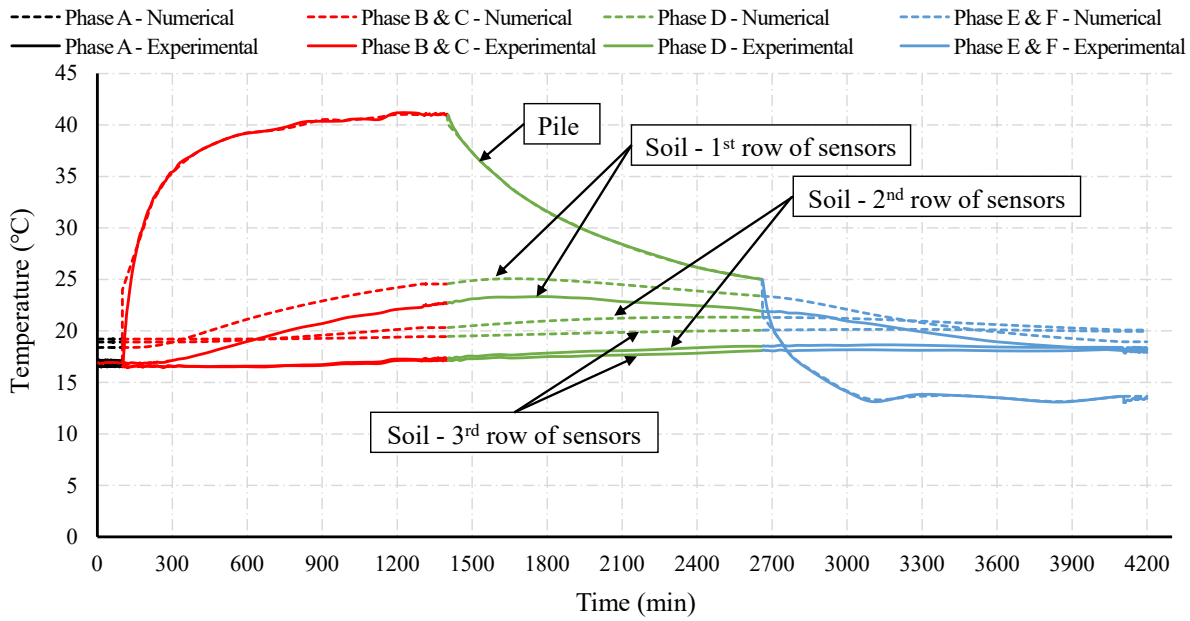

Figure 57. Temperature changes in the pile and surrounding soil: experimental vs numerical

The numerical model reproduces the overall thermal response with very good accuracy across all measurement locations. The close agreement observed in the pile and in each soil sensor row demonstrates the robustness of the numerical modelling approach and its suitability for simulating thermo-active pile behavior under combined thermal loading conditions.

Overall, the comparison of the temperature changes in the pile and the surrounding soil demonstrates a very close agreement between experimental measurements and numerical predictions across all loading phases and sensor locations. The numerical model successfully reproduces the magnitude, temporal evolution, and spatial attenuation of temperature variations observed during the experimental program, including the rapid temperature increase in the pile during heating, the delayed thermal response in the surrounding soil, and the progressive reduction of thermal influence with increasing radial distance from the pile. Minor discrepancies identified in certain phases or sensor rows remain limited and can be reasonably attributed to experimental uncertainties, boundary conditions, and idealizations inherent to the numerical modelling approach. Nevertheless, these differences do not affect the overall interpretation of the results. The consistency observed between experimental and numerical results confirms that the the reliability of the numerical model for simulating heat transfer mechanisms in geothermally active piles.

To complement the graphical comparison of temperature-time responses presented in the preceding figures, a quantitative comparison between experimental and numerical temperature results is provided in Table 14 - Table *17*. The tables summarize the temperatures recorded in the pile and in each row of soil sensors for the end of relevant loading phases, including initial conditions, heating, recovery, and cooling stages. The reported values are extracted directly from the corresponding experimental and numerical curves at identical measurement locations, allowing a consistent assessment of the level of agreement between the two approaches. The percentage difference is calculated with respect to the experimental values and is used as an

indicator of the accuracy of the numerical model in reproducing the observed thermal behaviour.

Table 14. Comparison of pile temperature: Experimental vs Numerical

Phase	Thermal loading condition	Experimental temperature by the end of each phase, T (°C)	Numerical temperature by the end of each phase T (°C)	Temperature difference (%)
A	No thermal load	17.02	17.03	0.06
B & C	Heating	41.05	41.0	0.12
D	Recovery phase	25.0	25.0	0.0
E & F	Cooling	13.45	13.65	1.47

Table 15. Comparison of soil temperature - 1st row of sensors: Experimental vs Numerical

Phase	Thermal loading condition	Experimental temperature by the end of each phase, T (°C)	Numerical temperature by the end of each phase, T (°C)	Temperature difference (%)
A	No thermal load	16.80	18.39	8.65
B & C	Heating	22.7	24.57	7.61
D	Recovery phase	21.92	23.38	6.24
E & F	Cooling	17.92	18.94	5.39

Table 16. Comparison of soil temperature - 2nd row of sensors: Experimental vs Numerical

Phase	Thermal loading condition	Experimental temperature by the end of each phase, T (°C)	Numerical temperature by the end of each phase, T (°C)	Temperature difference (%)
A	No thermal load	16.52	18.92	12.68
B & C	Heating	17.35	20.32	14.62
D	Recovery phase	18.50	21.32	13.22
E & F	Cooling	18.32	20.09	8.81

Table 17. Comparison of soil temperature - 3rd row of sensors: Experimental vs Numerical

Phase	Thermal loading condition	Experimental temperature by the end of each phase, T (°C)	Numerical temperature by the end of each phase, T (°C)	Temperature difference (%)
A	No thermal load	16.55	19.21	13.85
B & C	Heating	17.13	19.46	11.97
D	Recovery phase	18.08	20.07	9.92
E & F	Cooling	18.13	19.95	9.12

The quantitative comparison confirms the observations drawn from the graphical results, demonstrating an excellent agreement between experimental and numerical temperatures within the pile, with differences generally remaining negligible. In the surrounding soil, slightly larger discrepancies are observed, increasing with radial distance from the pile, which is consistent with the increased sensitivity of soil temperature fields to boundary conditions, material heterogeneity, and heat transfer assumptions adopted in the numerical model. Nevertheless, the overall level of agreement remains satisfactory for all sensor rows and loading phases. These results confirm that the numerical model reliably captures the governing heat transfer mechanisms in geothermally active piles and provides a robust basis for interpreting the thermo-mechanical response discussed in subsequent sections.

6.2. Vertical displacements

This sub-chapter presents a comparative analysis of the vertical displacements measured at the pile head during the experimental program and those predicted by the numerical model. The comparison is carried out for all loading phases (A-F), considering both mechanical and combined thermo-mechanical loading conditions. Vertical displacements were continuously monitored at the pile head throughout the testing duration, allowing the evolution of settlements to be evaluated as a function of applied load, thermal actions, and time. The numerical results were extracted at the pile head location corresponding to the experimental measurement point, ensuring consistency between the two approaches. The discussion focuses on the magnitude and development of vertical displacements during each loading phase, as well as on the ability of the numerical model to reproduce experimentally observed trends. Overall, the experimental and numerical results show very close agreement, with minor deviations attributed to modelling idealizations, soil-structure interaction effects, and experimental uncertainties.

Figure 58 shows the comparison of vertical pile head displacements during Phase A, which corresponds to the initial mechanical loading stage. Both experimental and numerical results indicate a gradual increase in settlement with increasing applied load.

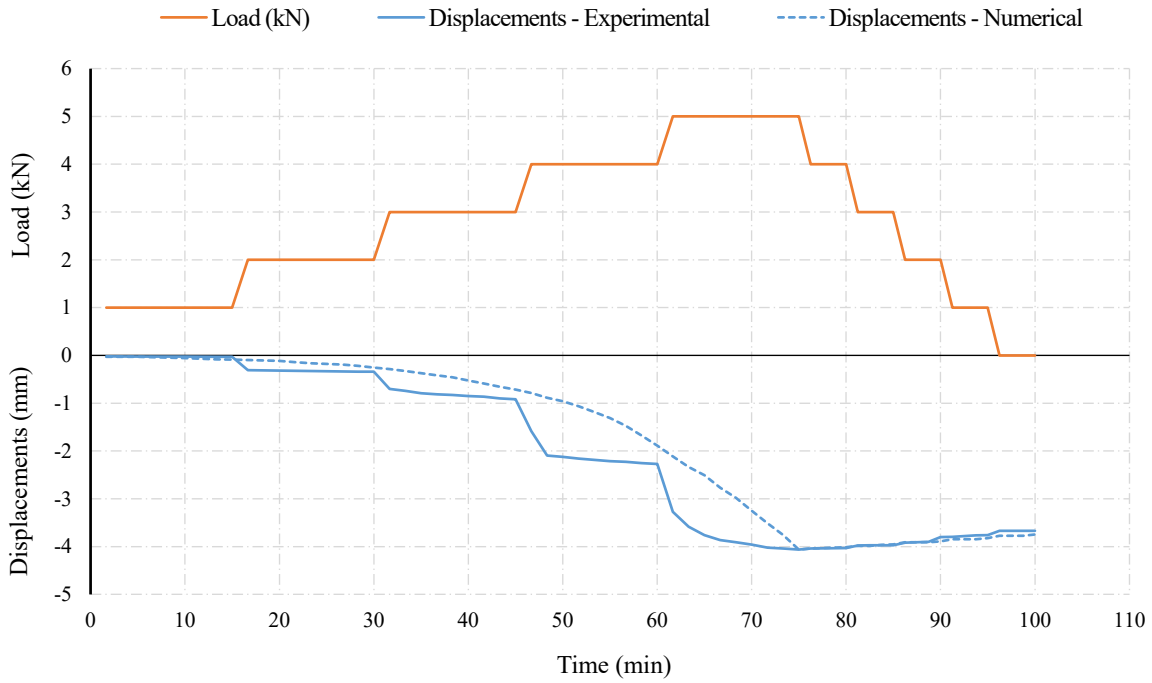

Figure 58. Phase A: pile head displacements, experimental vs numerical

The numerical model closely follows the experimental response, capturing both the magnitude of displacements and their incremental development. The small differences observed at higher load levels are minor and are likely related to simplifications in modelling the initial stiffness of the soil-pile system. Overall, the agreement confirms that the numerical model adequately represents the mechanical response of the pile under axial loading.

Figure 59 presents the pile head displacement behavior during Phase B, characterized by sustained loading over an extended period. The experimental results show a gradual increase in settlement with time, indicating time-dependent deformation of the soil-pile system.

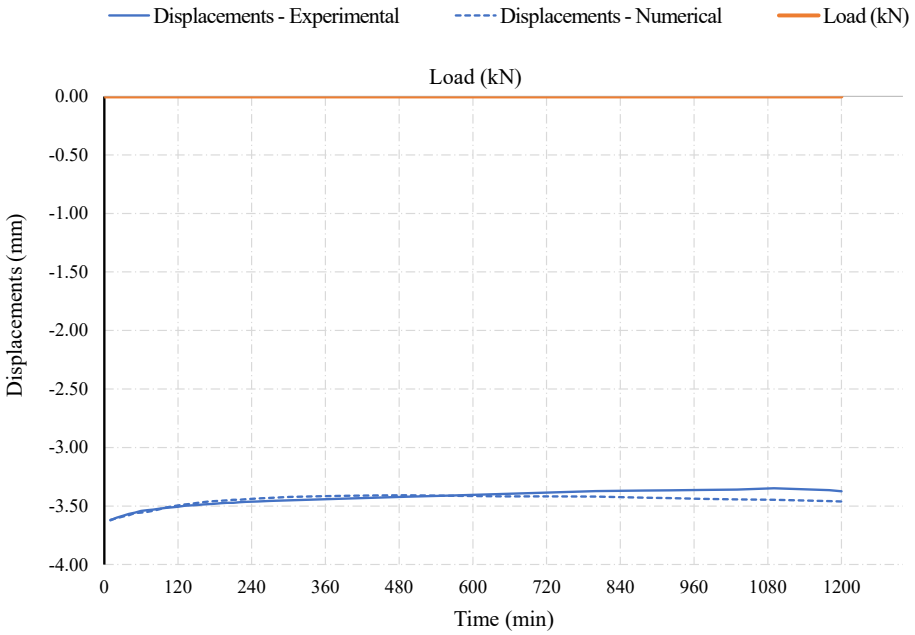

Figure 59. Phase B: pile head displacements, experimental vs numerical

The numerical predictions reproduce the general trend and magnitude of displacement development with good accuracy. Slight differences in the rate of settlement accumulation can be observed; however, the overall agreement remains very good, demonstrating that the numerical model is capable of simulating time-dependent displacement behaviour under constant load conditions.

Figure 60 illustrates the vertical displacement response of the pile head during Phase C, which corresponds to combined mechanical loading and heating. In this phase, the pile is subjected simultaneously to an increase in axial load and thermal activation, allowing the coupled thermo-mechanical behaviour to be evaluated.

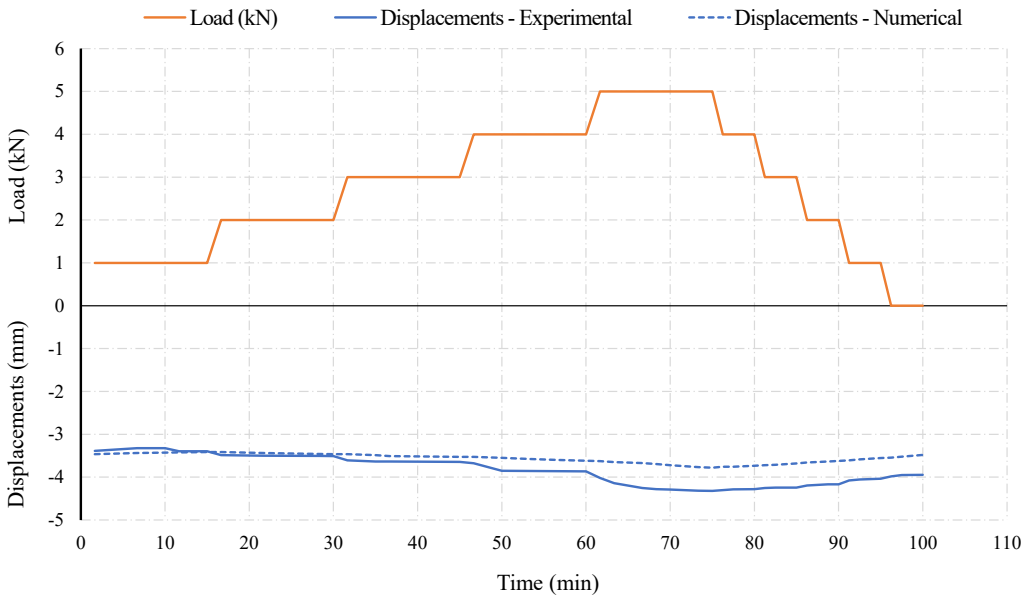

Figure 60. Phase C: pile head displacements, experimental vs numerical

The experimental results show that the rate of settlement development is reduced compared to purely mechanical loading phases, indicating the counteracting effect of thermally induced pile expansion against mechanically induced compression. This interaction results in a moderated displacement response despite the applied load increment. The numerical model successfully reproduces this coupled behaviour, capturing both the magnitude and the temporal evolution of vertical displacements observed experimentally. The close agreement between experimental and numerical results confirms that the thermo-mechanical interaction mechanisms are adequately represented in the numerical analysis.

Figure 61 presents the pile head displacement behaviour during Phase D, which represents a recovery phase where no mechanical load or thermal action is applied to the pile. This phase allows the assessment of displacement recovery and time-dependent behaviour of the soil-pile system following combined thermo-mechanical loading.

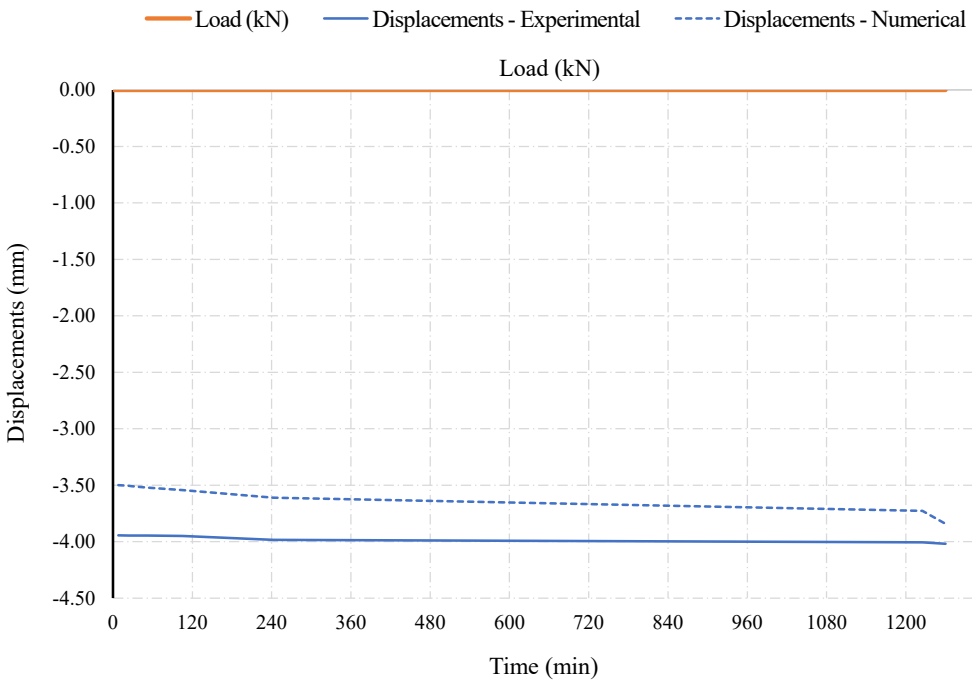

Figure 61. Phase D: pile head displacements, experimental vs numerical

Both experimental and numerical results indicate a stabilization of vertical displacements, accompanied by a slight recovery towards smaller settlement values. This response reflects the partial reversibility of deformations induced during previous loading phases, as well as stress redistribution within the surrounding soil. The numerical predictions closely follow the experimental trend during the recovery period, demonstrating the model's capability to simulate unloading and relaxation effects in the absence of external actions. Minor differences between the two curves remain limited and do not affect the overall interpretation of the recovery behaviour.

Figure 62 presents the vertical displacement response of the pile head during Phase E, which corresponds to the cooling phase. In this phase, thermal loading is applied in the form of cooling, while no additional mechanical load is imposed on the pile.

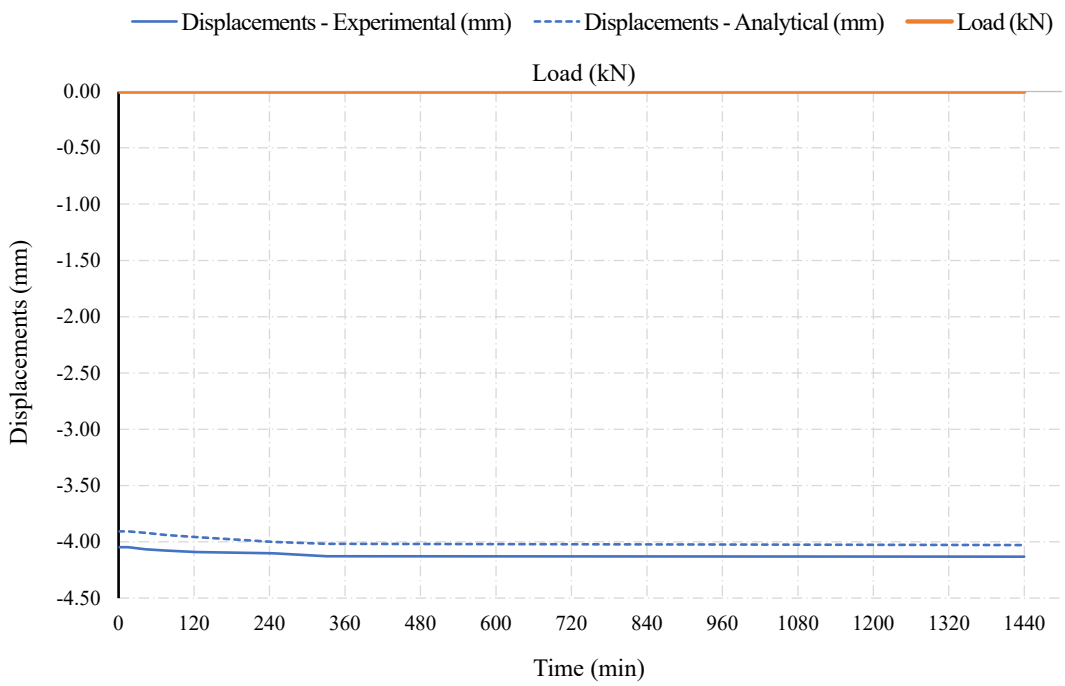

Figure 62. Phase E: pile head displacements, experimental vs numerical

The experimental results show an increase in downward displacement during cooling, which can be attributed to thermally induced contraction of the pile. This behaviour highlights the reversal of the beneficial expansion effects observed during heating phases and confirms the sensitivity of pile head displacements to thermal actions. The numerical model captures this response with good accuracy, reproducing both the magnitude and the trend of displacement development during cooling. Minor differences between experimental and numerical results are limited and may be related to idealizations in thermal boundary conditions and heat exchange mechanisms. Overall, the close agreement confirms the ability of the numerical model to simulate thermally induced contraction effects in geothermally active piles.

Figure 63 illustrates the pile head displacement behaviour during Phase F, during which cooling is applied simultaneously with mechanical loading. This phase represents the most critical loading condition, as thermally induced contraction and mechanically induced compression act in the same direction.

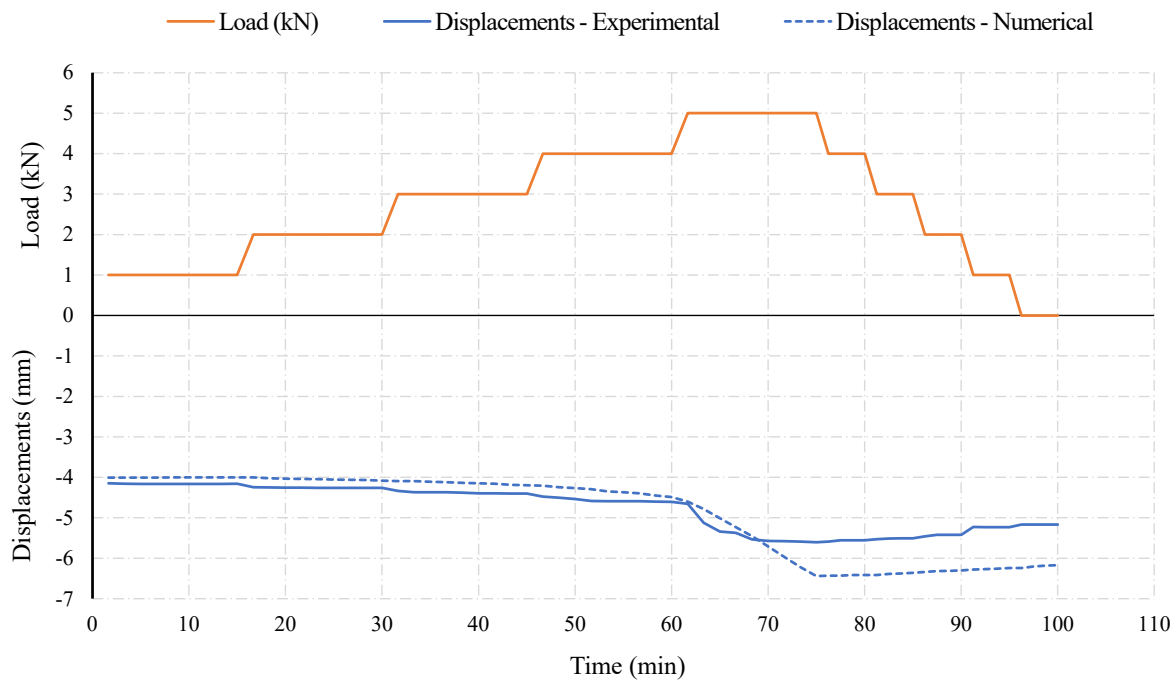

Figure 63. Phase F: pile head displacements, experimental vs numerical

The experimental results indicate a pronounced increase in settlement during this phase, reflecting the combined effect of axial load and pile contraction. The cumulative nature of these actions leads to the largest displacement recorded during the entire testing programme. The numerical predictions closely follow the experimental response, capturing both the magnitude and temporal evolution of settlements under combined mechanical and cooling loads. Although slightly larger deviations can be observed compared to other phases, the overall agreement remains very good. This confirms that the numerical model is capable of predicting unfavorable thermo-mechanical interaction scenarios relevant for the design of geothermally active piles.

Figure 64 presents a combined comparison of pile head displacements for all loading phases. The figure clearly illustrates the cumulative development of settlements during mechanical loading phases, the influence of thermal actions in reducing displacement during heating, and the partial reversibility observed during unloading and cooling.

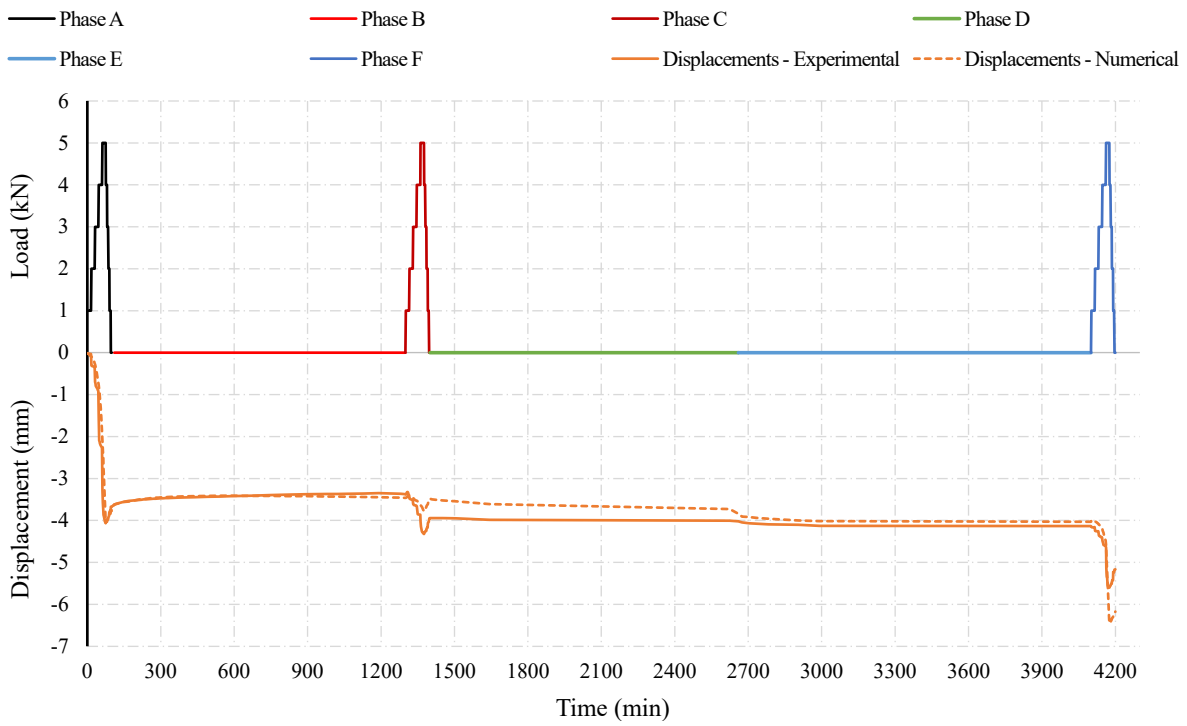

Figure 64. Physical vs Numerical displacement response for Phases A-F

The numerical results closely follow the experimental displacement history throughout the entire testing period. The consistency between the two approaches confirms that the numerical model reliably captures both mechanical and thermo-mechanical displacement behaviour of the pile, providing confidence in its applicability for simulating geothermally active pile systems.

Overall, the close agreement observed between experimental measurements and numerical predictions across all loading phases confirms the robustness of the numerical modelling approach and its suitability for analyzing vertical displacement behaviour of geothermally active piles under combined mechanical and thermal actions.

Table 18 summarizes the comparison of maximum vertical displacements obtained from the experimental tests and numerical simulations for each loading phase (A-F). The results show a very high level of consistency, with differences generally within ±5%

Table 18. Comparison of vertical displacements: Experimental vs Numerical

Phase	Loading condition	Experimental U_{max} displacement (mm)	Numerical U_{max} displacement (mm)	Displacement difference (%)
A	Mechanical loading-unloading	-4	-3.8	5
B	Heating only	-3.5	-3.4	2.9
C	Mechanical + Heating	-4.5	-4.3	4.4
D	Recovery (no load)	-4	-4	0
E	Cooling only	-4.2	-4.1	2.4
F	Mechanical + Cooling	-5.6	-6.3	11

The largest displacement occurred in Phase F (mechanical loading under cooling), where both experimental and numerical results indicated significantly higher settlements compared to Phases A and C, confirming the stronger influence of cooling on pile behaviour. The smallest

deviations are observed in the recovery phase (D), where both approaches recorded stable displacement values. Overall, the table demonstrates that the numerical model successfully reproduced the experimental pile settlement behaviour across all thermo-mechanical loading conditions.

7. SUMMARY, CONCLUSIONS, AND DESIGN RECOMMENDATIONS

7.1. Summary of the Research

This research investigates the thermo-mechanical behavior and structural response of geothermally active piles through a combined program of laboratory-scale experimental testing and numerical modeling. The primary motivation was to broaden the understanding of how thermal actions associated with geothermal operation interact with mechanical loading and to use it for the validation of modelling procedures. Finally, all the conclusions are used to produce design recommendations for the energy geostructures. A controlled laboratory-scale physical model of a single pile embedded in soil was tested under a phased loading programme with mechanical loading and unloading, heating, cooling, combined thermo-mechanical loading, and recovery phases. The experimental setup was instrumented to record the multi-physical response of the pile-soil system. Measurements included temperature evolution in the pile and surrounding soil, pile head vertical displacements, pore water pressure, total soil pressure, soil suction, and axial strains within the pile. This extensive instrumentation enabled detailed observation and interpretation of coupled thermo-mechanical mechanisms governing pile behaviour. Although a broad range of response parameters was monitored during the experimental programme, the thesis places special emphasis on temperature changes and pile - head vertical displacements. These quantities represent the most direct indicators of the global thermo-mechanical response and serviceability performance of geothermally active piles. The remaining measurements (of pore pressure, total pressure, suction, and pile strains) were used to support the interpretation of the observed behaviour and to ensure consistency of the experimental observations, but they were not analyzed exhaustively to maintain a clear focus on the primary objectives of the research. In parallel to the experimental programme, a numerical model was developed using the finite element method to reproduce the laboratory conditions as closely as possible. The numerical model has the same geometry, loading sequence, and material properties as the experimental setup, enabling direct comparison between measured and simulated responses. Numerical outputs were extracted at locations corresponding to the experimental instrumentation, allowing systematic validation of the modelling approach. The results obtained from the experimental investigation and numerical simulations were compared and discussed in detail, with particular attention given to the evolution of temperature in the pile and surrounding soil, the development of pile-head vertical displacements under different loading phases, and the influence of combined mechanical and thermal actions. The validated numerical model was subsequently used as a basis for interpreting the observed behaviour and for proposing design-oriented recommendations relevant to geothermally active piles.

7.2. Main Conclusions

Based on experimental observations, numerical analyses, and their comparative interpretation, the following main conclusions can be drawn.

7.2.1. Experimental Investigations

- The thermal response of the soil-pile system is characterized by a strong temperature gradient between the pile and the surrounding soil, with temperature variations attenuating rapidly with increasing radial distance from the pile shaft. This confirms that the thermal influence zone of a geothermally active pile is concentrated near the pile and governed primarily by heat conduction mechanisms.
- Heating and cooling cycles induce measurable axial deformation of the pile, which directly influences pile-head vertical displacements. Heating results in thermally induced pile expansion that can partially counteract mechanically induced settlements, whereas cooling leads to pile contraction and increased settlement.
- Combined thermo-mechanical loading phases demonstrate that thermal and mechanical actions interact in a non-negligible manner, producing displacement responses that differ from those observed under purely mechanical loading. This highlights the necessity of considering coupled effects in the assessment of serviceability behaviour of energy piles.
- During the recovery phase without applied mechanical or thermal loading, the pile exhibits certain reversibility of pile-head displacements, indicating that a portion of the thermo-mechanically induced deformation is recoverable, while residual settlements remain due to soil-structure interaction and stress redistribution.
- Measurements of the pore pressure, total soil pressure, suction, and axial strains within the pile confirm that thermal loading affects stress transfer mechanisms at the pile-soil interface and within the surrounding soil mass, supporting the interpretations derived from temperature and displacement observations.

7.2.2. Conclusions from numerical modelling and validation

The HSsmall finite element model can successfully reproduce the temperature evolution in the pile and surrounding soil for all loading phases, including heating, recovery, and cooling. Agreement between experimental and numerical results is particularly high within the pile, while slightly larger deviations occur in the surrounding soil, increasing with distance from the pile shaft.

Numerically predicted pile-head vertical displacements very closely follow the experimentally measured trends across all loading phases. The model captures cumulative settlement during mechanical loading, moderated displacement response during heating, and increased settlement during cooling and combined mechanical-cooling phases.

The most unfavorable displacement response is associated with combined mechanical loading and cooling, during which thermally induced contraction and mechanical compression act in the same direction. This phase governs the maximum settlement demand and is therefore critical for design considerations.

Minor differences between experimental and numerical results are attributed to modelling idealizations, boundary conditions, and inherent experimental uncertainties rather than to fundamental limitations of the modelling approach.

Overall, it can be concluded that the validated numerical modelling framework provides a reliable tool for analyzing thermo-mechanical behaviour of geothermally active piles and for

supporting parametric studies and design-oriented assessments beyond the specific experimental configuration investigated.

A quantitative comparison between experimental measurements and numerical predictions demonstrates a high level of agreement for both thermal and mechanical responses of the pile-soil system. For pile temperatures, differences between experimental and numerical results at the end of each loading phase are very small, generally remaining below 1.5%, while soil temperature predictions exhibit slightly larger deviations, typically in the range of 5-14%, with increasing discrepancy observed at greater radial distances from the pile shaft. These differences are attributed primarily to modelling idealizations and uncertainties in soil thermal properties and boundary conditions. Similarly, numerically predicted pile head vertical displacements closely match experimental values, with differences generally below 5% for most loading phases. The largest deviation, of approximately 11%, occurs during the combined mechanical loading and cooling phase, which represents the most unfavorable condition due to the superposition of mechanical compression and thermally induced contraction. Despite these minor discrepancies, the numerical model reliably captures both the magnitude and evolution of temperature changes and vertical displacements, confirming its suitability for analyzing the thermo-mechanical behavior and serviceability performance of geothermally active piles.

7.3. Design recommendations for geothermally active piles

Based on the experimental findings and the validated numerical modelling presented in this thesis, design-oriented recommendations are proposed for geothermally active piles subjected to combined mechanical and thermal actions. These recommendations are formulated in accordance with the reliability-based safety format of EN 1990 and the principles adopted in EN 1997 (second-generation Eurocode 7), while recognizing that current standards do not explicitly address thermo-mechanical effects in energy geostructures.

Thermal actions in geothermally active piles are classified as variable indirect actions, which induce stresses and deformations through restrained thermal strains rather than being applied directly as external forces. Unlike conventional environmental thermal actions, the magnitude of thermal loading in energy piles is primarily governed by the operational control of the geothermal system and is therefore bounded within a predefined temperature range.

Experimental observations and numerical validation performed in this research demonstrate a high degree of reproducibility of thermally induced effects. In particular, pile temperatures are reproduced numerically with very small deviations, while pile head vertical displacements are captured with differences that remain generally below 5%, reaching higher values only under the most unfavorable combined mechanical-cooling conditions. These findings indicate that the uncertainty associated with the thermal action itself is moderate, and that the dominant sources of uncertainty are related to soil thermal properties, soil-pile interaction, and modelling idealizations rather than to the magnitude of the imposed temperature change.

7.3.1. Classification of thermal actions

Thermal actions induced by heating and cooling cycles in geothermally active piles should be treated as variable actions associated with the operational conditions of the geothermal system.

Thermal actions are neither permanent nor accidental in nature but occur repeatedly within a controlled temperature range governed by system design and building demand.

7.3.2. Partial factor for thermal variable actions (ULS)

Within the Eurocode framework, this level of uncertainty justifies the adoption of a dedicated partial factor for thermal-induced effects consistent with the reliability level required for variable indirect actions with moderate uncertainty, while still providing an adequate margin of safety for ultimate limit state verification. Accordingly, a partial factor:

$$\gamma_T = 1.2$$

is recommended for thermally induced axial forces, stresses, or displacement demands in ULS combinations. This value reflects the controlled and operational nature of thermal loading in energy piles, while accounting for modelling and parameter uncertainties identified in the experimental-numerical comparison. This factor may be applied to thermally induced axial force, stress, or displacement when thermal actions are included in ULS combinations.

7.3.3. Combination factors for thermal action (SLS)

For serviceability limit state verification, EN 1990 introduces combination factors to define representative values of variable actions based on their probability of occurrence and duration. Thermal actions in energy piles are cyclic and operational, with a limited likelihood of coinciding with extreme mechanical variable actions and with a demonstrated degree of deformation reversibility during recovery phases. On this basis, the following combination factors are recommended:

- Frequent combination:

$$\psi_{0,T} = 0.6$$

- Quasi-permanent combination:

$$\psi_{2,T} = 0.3$$

These values reflect the reduced probability of sustained extreme thermal operation and are consistent with the partial reversibility of thermally induced deformations observed experimentally.

7.3.4. Correlation between mechanical and thermal actions

Mechanical variable actions and thermal actions may generally be assumed statistically independent for typical building applications, as mechanical loading depends on occupancy and usage, whereas thermal actions depend on geothermal system operation:

$$\rho(Q,T) = 0.0$$

Where operational data or building usage patterns indicate partial coupling between mechanical demand and thermal operation, a conservative correlation coefficient:

$$\rho(Q,T) = 0.3$$

may be adopted to ensure adequate safety.

7.3.5. Applicability and scope

The proposed design factors are derived within the scope of this research and apply to axially loaded energy piles in silty sandy soils subjected to short-term thermal cycling. Engineering judgement is required when extending these recommendations to other soil conditions, long-term cyclic loading, or full-scale applications.

Overall, the results demonstrate that thermal actions associated with geothermal operation can significantly influence the serviceability response of piles and should be explicitly accounted for in design. The recommendations proposed in this chapter provide a rational, Eurocode-consistent basis for the practical integration of geothermal functionality into foundation engineering.

The findings of this thesis are based on laboratory-scale testing of a single pile configuration and short-term thermal cycling. Although the combined experimental and numerical approach provides valuable insight into thermo-mechanical behaviour, further research is required to extend the applicability of the results.

In conclusion, this research demonstrates that thermal actions associated with geothermal operation significantly influence the mechanical behaviour and serviceability performance of geothermally active piles. The combined experimental and numerical approach adopted in this thesis provides clear evidence that thermo-mechanical coupling effects should be explicitly considered in the design of energy piles. The findings and recommendations presented contribute to an-enhanced understanding and provide a rational basis for integration of geothermal functionality and activation of structural elements as an engineering practice.

8. REFERENCES

[1] Brandl, H., 2006. Energy foundations and other thermo-active ground structures. Géotechnique, 56(2), pp.81-122.

[2] McCartney, J.S. and Rosenberg, J.E., 2011. Impact of heat exchange on side shear in thermo-active foundations. In *Geo-Frontiers 2011: Advances in geotechnical engineering* (pp. 488-498).

[3] Amatya, B.L., Soga, K., Bourne-Webb, P.J., Amis, T. and Laloui, L., 2012. Thermo-mechanical behaviour of energy piles. *Géotechnique*, *62*(6), pp.503-519.

[4] Laloui, L., Nuth, M. and Vulliet, L., 2006. Experimental and numerical investigations of the behaviour of a heat exchanger pile. *International journal for numerical and analytical methods in geomechanics*, *30*(8), pp.763-781.

[5] Bourne-Webb, P.J., Amatya, B., Soga, K., Amis, T., Davidson, C. and Payne, P., 2009. Energy pile test at Lambeth College, London: geotechnical and thermodynamic aspects of pile response to heat cycles. *Géotechnique*, *59*(3), pp.237-248.

[6] Murphy, K.D., McCartney, J.S., and Henry, K.S., 2014. Thermo-mechanical characterization of a full-scale energy foundation. In *From soil behavior fundamentals to innovations in geotechnical engineering: honoring Roy E. Olson* (pp. 617-628).

[7] Stewart, M.A. and McCartney, J.S., 2014. Centrifuge modeling of soil-structure interaction in energy foundations. *Journal of Geotechnical and Geoenvironmental Engineering*, *140*(4), p.04013044.

[8] Wu, D., Liu, H.L., Kong, G.Q., and Abuel-Naga, H., 2022. Effect of stress history of saturated clay on engineering behaviour of an energy pile. *Environmental Geotechnics*, *9*(7), pp.490-499.

[9] Laloui, L. and Loria, A.F.R., 2019. *Analysis and design of energy geostructures: theoretical essentials and practical application*. Academic Press.

[10] Bourne-Webb, P., Burlon, S., Javed, S., Kürten, S. and Loveridge, F., 2016. Analysis and design methods for energy geostructures. *Renewable and Sustainable Energy Reviews*, *65*, pp.402-419.

[11] Soga, K. and Rui, Y., 2016. Energy geostructures. In *Advances in ground-source heat pump systems* (pp. 185-221). Woodhead Publishing.

[12] Dai, Q., Zhang, D., and Li, Z., 2023. Mechanical assessment of energy wall in the long term. *Acta Geotechnica*, *18*(1), pp.1-34.

[13] Delerablee, Y., Burlon, S. and Reiffsteck, P., 2020. Long-term assessment of thermal sustainability of thermoactive geostructures. *Environmental Geotechnics*, *7*(4), pp.249-265.

[14] Loveridge, F., 2012. *The thermal performance of foundation piles used as heat exchangers in ground energy systems* (Doctoral dissertation, University of Southampton).

[15] Laloui, L., Moreni, M. and Vulliet, L., 2003. Behavior of a dual-purpose pile as foundation and heat exchanger. Canadian Geotechnical Journal, 40(2), pp.388-402.

[16] Rotta Loria, A.F., 2018. Performance-based design of energy pile foundations. *DFI Journal-The Journal of the Deep Foundations Institute*, *12*(2), pp.94-107.

[17] Fadejev, J., Simson, R., Kurnitski, J. and Haghighat, F., 2017. A review on energy piles design, sizing, and modelling. Energy, 122, pp.390-407.

[18] Mohamad, Z., Fardoun, F., and Meftah, F., 2021. A review on energy piles design, evaluation, and optimization. *Journal of cleaner production*, *292*, p.125802.

[19] Vasilescu, A.R., 2019. *Design and execution of energy piles: Validation by in-situ and laboratory experiments* (Doctoral dissertation, École centrale de Nantes).

[20] EN, B., 1997. 1 (2004), Eurocode 7: Geotechnical design. *Part*, *1*, pp.171.

[21] En, C.E.N., 1992. 1-1: Eurocode 2-Design of concrete structures. *General rules and rules*

[22] Loria, A.F.R., Bocco, M., Garbellini, C., Muttoni, A., and Laloui, L., 2020. The role of thermal loads in the performance-based design of energy piles. *Geomechanics for Energy and the Environment*, *21*, p.100153.

[23] Di Bari, F., 2019. *Performance-based design of energy piles in the framework of Eurocodes* (Doctoral dissertation, Politecnico di Torino).

[24] Rotta Loria, A.F., 2021, January. Analytical Modelling of Energy Geostructures. In *International Conference of the International Association for Computer Methods and Advances in Geomechanics* (pp. 1093-1101). Cham: Springer International Publishing

[25] Caulk, R., Ghazanfari, E. and McCartney, J.S., 2016. Parameterization of a calibrated geothermal energy pile model. *Geomechanics for Energy and the Environment*, *5*, pp.1-15.

[26] Abuel-Naga, H., Raouf, M.I.N., Raouf, A.M. and Nasser, A.G., 2015. Energy piles: current state of knowledge and design challenges. *Environmental Geotechnics*, *2*(4), pp.195-210

[27] Abdelaziz, S. and Ozudogru, T.Y., 2016. Non-uniform thermal strains and stresses in energy piles. *Environmental Geotechnics*, *3*(4), pp.237-252

[28] Bidarmaghz, A. and Narsilio, G.A., 2016. Shallow geothermal energy: emerging convective phenomena in permeable saturated soils. *Géotechnique Letters*, *6*(2), pp.119-123

[29] Laloui, L., Moreni, M. and Vulliet, L., 2003. Comportement d'un pieu bi-fonction, fondation et échangeur de chaleur. *Canadian Geotechnical Journal*, *40*(2), pp.388-402

[30] Mimouni, T., Lei, L. and Laloui, L., 2015. Estimating soil thermal diffusivity with interference analyses. *Acta Geotechnica*, *10*(2), pp.197-208

[31] Loria, A.F.R., Vadrot, A. and Laloui, L., 2017. Effect of non-linear soil deformation on the interaction among energy piles. *Computers and Geotechnics*, *86*, pp.9-20

[32] Sutman, M., Brettmann, T. and Olgun, C.G., 2019. Full-scale in-situ tests on energy piles: Head and base-restraining effects on the structural behaviour of three energy piles. *Geomechanics for Energy and the Environment*, *18*, pp.56-68

[33] Sutman, M., Olgun, C.G. and Laloui, L., 2019. Cyclic load-transfer approach for the analysis of energy piles. *Journal of Geotechnical and Geoenvironmental Engineering*, *145*(1), p.04018101

[34] McCartney, J.S. and Murphy, K.D., 2017. Investigation of potential dragdown/uplift effects on energy piles. *Geomechanics for Energy and the Environment*, *10*, pp.21-28

[35] Murphy, K.D. and McCartney, J.S., 2015. Seasonal response of energy foundations during building operation. *Geotechnical and Geological Engineering*, *33*(2), pp.343-356

[36] McCartney, J.S., Murphy, K.D. and Henry, K.S., 2015. Response of an energy foundation to temperature fluctuations. In *IFCEE 2015* (pp. 1691-1700).

[37] Murphy, K.D., McCartney, J.S. and Henry, K.S., 2015. Evaluation of thermo-mechanical and thermal behavior of full-scale energy foundations. *Acta Geotechnica*, *10*(2), pp.179-195.

[38] Faizal, M., Bouazza, A., Haberfield, C. and McCartney, J.S., 2018. Axial and radial thermal responses of a field-scale energy pile under monotonic and cyclic temperature changes. *Journal of Geotechnical and Geoenvironmental Engineering*, *144*(10), p.04018072

[39] Vieira, A., Alberdi-Pagola, M., Christodoulides, P., Javed, S., Loveridge, F., Nguyen, F., Cecinato, F., Maranha, J., Florides, G., Prodan, I. and Van Lysebetten, G., 2017. Characterisation of ground thermal and thermo-mechanical behaviour for shallow geothermal energy applications. *Energies*, *10*(12), p.2044

[40] Andersland, O.B. and Ladanyi, B., 1994. Frozen Ground. In *An introduction to frozen ground engineering* (pp. 1-22). Boston, MA: Springer US

[41] Ladanyi, B. and Andersland, O., 2004. *Frozen ground engineering* (Vol. 414). Wiley

[42] Andersland, O.B. and Ladanyi, B., 1994. Foundations in frozen soils. In *An introduction to frozen ground engineering* (pp. 182-224). Boston, MA: Springer US

[43] Cousin, B., Loria, A.F.R., Bourget, A., Rognon, F. and Laloui, L., 2019. Energy performance and economic feasibility of energy segmental linings for subway tunnels. *Tunnelling and Underground Space Technology*, *91*, p.102997

[44] Saggu, R. and Chakraborty, T., 2016. Thermomechanical response of geothermal energy pile groups in sand. *International Journal of Geomechanics*, *16*(4), p.04015100.

[45] Abbaszadeh Amirdehi, H. and Shooshpasha, I., 2022. Evaluation of coupled interaction effects caused by the long-term performance of energy piles in a piled raft foundation. *Geotechnical and Geological Engineering*, *40*(10), pp.5153-5180

[46] Cecinato, F. and Salciarini, D., 2022. Energy performance assessment of thermo-active micro-piles via numerical modeling and statistical analysis. *Geomechanics for Energy and the Environment*, *29*, p.100268

[47] Bhartiya, P., Basu, D. and Chakraborty, T., 2021. Nonlinear settlement of piled rafts in sandy soil. *International Journal of Geomechanics*, *21*(11), p.04021214

[48] Ronchi, F., Salciarini, D., Cavalagli, N. and Tamagnini, C., 2018. Thermal response prediction of a prototype Energy Micro-Pile. *Geomechanics for Energy and the Environment*, *16*, pp.64-82

[49] Rotta Loria, A.F. and Laloui, L., 2017. Impact of thermally induced soil deformation on the serviceability of energy pile groups. In *Advances in Laboratory Testing and Modelling of Soils and Shales* (pp. 421-428). Cham: Springer International Publishing

[50] Suryatriyastuti, M.E., Mroueh, H. and Burlon, S., 2014. A load transfer approach for studying the cyclic behavior of thermo-active piles. *Computers and Geotechnics*, *55*, pp.378-391

[51] Saggu, R. and Chakraborty, T., 2023. Effect of Soil State on Load-Displacement of Thermal Piles. *Indian Geotechnical Journal*, *53*(6), pp.1213-1225

[52] Olgun, C.G., Ozudogru, T.Y., Abdelaziz, S.L. and Senol, A., 2015. Long-term performance of heat exchanger piles. *Acta Geotechnica*, *10*(5), pp.553-569

[53] Gawecka, K.A., Taborda, D.M., Potts, D.M., Cui, W., Zdravković, L. and Haji Kasri, M.S., 2017. Numerical modelling of thermo-active piles in London Clay. *Proceedings of the Institution of Civil Engineers-Geotechnical Engineering*, *170*(3), pp.201-219

[54] Cekerevac, C. and Laloui, L., 2004. Experimental study of thermal effects on the mechanical behaviour of a clay. *International journal for numerical and analytical methods in geomechanics*, *28*(3), pp.209-228

[55] Eslami, H., Rosin-Paumier, S., Abdallah, A. and Masrouri, F., 2017. Pressuremeter test parameters of a compacted illitic soil under thermal cycling. *Acta Geotechnica*, *12*(5), pp.1105-1118

[56] Laloui, L. and Di Donna, A. eds., 2013. *Energy geostructures: innovation in underground engineering*. John Wiley & Sons.

[57] Houhou, R. and Laloui, L., 2022. Geomechanics for energy and the environment: Current developments. *Geomechanics for Energy and the Environment*, *32*, p.100345.

[58] McCartney, J.S., Murphy, J.S. and Stewart, M.A., 2013. Thermo-mechanical behavior of energy foundations. In *Proceedings of 18th international conference on soil mechanics and geotechnical engineering, Paris* (pp. 3379-3382).

[59] Loveridge, F., McCartney, J.S., Narsilio, G.A. and Sanchez, M., 2020. Energy geostructures: a review of analysis approaches, in situ testing and model scale experiments. *Geomechanics for Energy and the Environment*, *22*, p.100173.

[60] Hashemi, A., Sutman, M., Medero, G.M. and Buckman, J., 2023. Compressibility and microstructure of kaolin in varying thermo-hydro-mechanical states imposed by energy geostructures. *Engineering Geology*, *324*, p.107248.

[61] Morais, T.D.S.O., Tsuha, C.D.H.C. and Vilar, O.M., 2021. Thermal properties of a tropical unsaturated soil. In *MATEC Web of Conferences* (Vol. 337, p. 01019). EDP Sciences.

[62] Romio, L.C., Zimmer, T., Bremm, T., Buligon, L., Herdies, D.L. and Roberti, D.R., 2022. Influence of different methods to estimate the soil thermal properties from experimental dataset. *Land*, *11*(11), p.1960.

[63] Loveridge, F., 2012. *The thermal performance of foundation piles used as heat exchangers in ground energy systems* (Doctoral dissertation, University of Southampton).

[64] Rees, S.W., Adjali, M.H., Zhou, Z., Davies, M. and Thomas, H.R., 2000. Ground heat transfer effects on the thermal performance of earth-contact structures. *Renewable and Sustainable Energy Reviews*, *4*(3), pp.213-265.

[65] Di Sipio, E. and Bertermann, D., 2018. Thermal properties variations in unconsolidated material for very shallow geothermal application (ITER project). *International Agrophysics*, *32*(2).

[66] Thota, S.K., Vahedifard, F. and McCartney, J.S., 2021. A temperature-dependent model for ultimate bearing capacity of energy piles in unsaturated fine-grained soils. *Journal of Geotechnical and Geoenvironmental Engineering*, *147*(11), p.04021132.

[67] Coccia, C.J.R. and McCartney, J.S., 2016. Thermal volume change of poorly draining soils I: Critical assessment of volume change mechanisms. *Computers and Geotechnics*, *80*, pp.26-40.

[68] Thota, S.K., Cao, T.D., Vahedifard, F. and Ghazanfari, E., 2020, February. An effective stress model for unsaturated soils at elevated temperatures. In *Geo-Congress 2020* (pp. 358-366). Reston, VA: American Society of Civil Engineers.

[69] Dumont, M., Taibi, S., Fleureau, J.M., Abou-Bekr, N. and Saouab, A., 2011. A thermo-hydro-mechanical model for unsaturated soils based on the effective stress concept. *International Journal for Numerical and Analytical Methods in Geomechanics*, *35*(12), pp.1299-1317.

[70] Chen, D., 2016. *Soil structure interaction in energy piles*. University of California, San Diego.

[71] DeJong, J.T., Randolph, M.F., and White, D.J., 2003. Interface load transfer degradation during cyclic loading: a microscale investigation. *Soils and foundations*, *43*(4), pp.81-93.

[72] DeJong, J.T., White, D.J., and Randolph, M.F., 2006. Microscale observation and modeling of soil-structure interface behavior using particle image velocimetry. *Soils and foundations*, *46*(1), pp.15-28.

[73] Amis, T., Bourne-Webb, P., Davidson, C., Amatya, B. and Soga, K., 2008. An investigation into the effects of heating and cooling energy piles whilst under working load at Lambeth College, Clapham Common. In *UK Proceedings 11th Int. Conf. Deep Foundations, Deep Foundation Institute*.

[74] Bourne-Webb, P.J., Bodas Freitas, T.M. and Freitas Assunção, R.M., 2016. Soil-pile thermal interactions in energy foundations. *Géotechnique*, *66*(2), pp.167-171.

[75] Knellwolf, C., Peron, H. and Laloui, L., 2011. Geotechnical analysis of heat exchanger piles. *Journal of Geotechnical and Geoenvironmental Engineering*, *137*(10), pp.890-902.

[76] Bourne-Webb, P.J., Amatya, B. and Soga, K., 2013. A framework for understanding energy pile behaviour. *Proceedings of the Institution of Civil Engineers-Geotechnical Engineering*, *166*(2), pp.170-177.

[77] Yavari, N., Tang, A.M., Pereira, J.M. and Hassen, G., 2014. A simple method for numerical modelling of mechanical behaviour of an energy pile. *Géotechnique Letters*, *4*(2), pp.119-124.

[78] Christodoulides, P., Vieira, A., Lenart, S., Maranha, J., Vidmar, G., Popov, R., Georgiev, A., Aresti, L., and Florides, G., 2020. Reviewing the modeling aspects and practices of shallow geothermal energy systems. *Energies*, *13*(16), p.4273.

[79] Fadejev, J., Simson, R., Kurnitski, J. and Haghighat, F., 2017. A review on energy piles design, sizing, and modelling. *Energy*, *122*, pp.390-407.

[80] Burlon, S., Habert, J., Szymkievicz, F., Suryatriyastuti, M., and Mroueh, H., 2013. Towards a design approach of bearing capacity of thermo-active piles. In *European geothermal congress* (pp. 1-6).

[81] Li, M. and Lai, A.C., 2015. Review of analytical models for heat transfer by vertical ground heat exchangers (GHEs): A perspective of time and space scales. *Applied Energy*, *151*, pp.178-191.

[82] Eskilson, P., 1987. Thermal analysis of heat extraction boreholes.

[83] Zeng, H.Y., Diao, N.R. and Fang, Z.H., 2002. A finite line-source model for boreholes in geothermal heat exchangers. *Heat Transfer-Asian Research: Co-sponsored by the Society of Chemical Engineers of Japan and the Heat Transfer Division of ASME*, *31*(7), pp.558-567.

[84] Man, Y., Yang, H., Diao, N., Liu, J., and Fang, Z., 2010. A new model and analytical solutions for borehole and pile ground heat exchangers. *International Journal of Heat and Mass Transfer*, *53*(13-14), pp.2593-2601.

[85] Javed, S. and Claesson, J., 2011. New analytical and numerical solutions for the short-term analysis of vertical ground heat exchangers. *ASHRAE Transactions*, *117*(1), pp.3-12.

[86] Zhang, W., Yang, H., Lu, L., Cui, P., and Fang, Z., 2014. The research on ring-coil heat transfer models of pile foundation ground heat exchangers in the case of groundwater seepage. *Energy and buildings*, *71*, pp.115-128.

[87] Zhang, W., Yang, H., Lu, L. and Fang, Z., 2013. The analysis on solid cylindrical heat source model of foundation pile ground heat exchangers with groundwater flow. *Energy*, *55*, pp.417-425.

[88] Bandos, T.V., Campos-Celador, Á., López-González, L.M. and Sala-Lizarraga, J.M., 2014. Finite cylinder-source model for energy pile heat exchangers: Effects of thermal storage and vertical temperature variations. *Energy*, *78*, pp.639-648.

[89] Loveridge, F. and Powrie, W., 2014. G-Functions for multiple interacting pile heat exchangers. Energy, 64, pp.747-757.

[90] Zarrella, A., De Carli, M. and Galgaro, A., 2013. Thermal performance of two types of energy foundation pile: Helical pipe and triple U-tube. *Applied Thermal Engineering*, *61*(2), pp.301-310.